

NATURAL SENSITIZERS FOR SOLAR CELL BASED  
ON GEL POLYMER ELECTROLYTES CONTAINING  
IODIDE/TRIIODIDE REDOX COUPLE

MARZIYEH ALINEJAD

FACULTY OF SCIENCE  
UNIVERSITI MALAYA  
KUALA LUMPUR

2022

**NATURAL SENSITIZERS FOR SOLAR CELL BASED  
ON GEL POLYMER ELECTROLYTES CONTAINING  
IODIDE/TRIIODIDE REDOX COUPLE**

**MARZIYEH ALINEJAD**

**DISSERTATION SUBMITTED IN FULFILMENT OF  
THE REQUIREMENTS FOR THE DEGREE OF MASTER  
OF SCIENCE**

**DEPARTMENT OF PHYSICS  
FACULTY OF SCIENCE  
UNIVERSITI MALAYA  
KUALA LUMPUR**

**2022**

**UNIVERSITI MALAYA**  
**ORIGINAL LITERARY WORK DECLARATION**

Name of Candidate: **MARZIYEH ALINEJAD**

Matric No: **SMA170007**

Name of Degree: **MASTER OF SCIENCE**

Title of Dissertation: **NATURAL SENSITIZERS FOR SOLAR CELL BASED ON GEL POLYMER ELECTROLYTES CONTAINING IODIDE/TRIIODIDE REDOX COUPLE**

Field of Study: **PHYSICS**

I do solemnly and sincerely declare that:

- (1) I am the sole author/writer of this Work;
- (2) This Work is original.
- (3) Any use of any work in which copyright exists was done by way of fair dealing and for permitted purposes and any excerpt or extract from, or reference to or reproduction of any copyright work has been disclosed expressly and sufficiently and the title of the Work and its authorship have been acknowledged in this Work;
- (4) I do not have any actual knowledge nor do I ought reasonably to know that the making of this work constitutes an infringement of any copyright work;
- (5) I hereby assign all and every rights in the copyright to this Work to the University of Malaya ("UM"), who henceforth shall be owner of the copyright in this Work and that any reproduction or use in any form or by any means whatsoever is prohibited without the written consent of UM having been first had and obtained;
- (6) I am fully aware that if in the course of making this Work, I have infringed any copyright whether intentionally or otherwise, I may be subject to legal action or any other action as may be determined by UM.

Candidate's Signature

Date:

Subscribed and solemnly declared before,

Witness's Signature

Date:

Name:

Designation:

# NATURAL SENSITIZERS FOR SOLAR CELL BASED ON GEL POLYMER ELECTROLYTES CONTAINING IODIDE/TRIIODIDE REDOX COUPLE

## ABSTRACT

Polyvinyl alcohol (PVA) based gel polymer electrolytes (GPEs) containing iodide/triiodide have been prepared. Two types of solvents namely dimethylformamide (DMF) and dimethyl sulfoxide (DMSO) have been used in the preparation of the GPEs. The GPEs are (i) DMF/PVA/KI/I<sub>2</sub>, (ii) DMF/PVA/KI/I<sub>2</sub>/4-tert-butylpyridine (TBP), (iii) DMSO/PVA/KI/I<sub>2</sub> and, (iv) DMSO/PVA/KI/I<sub>2</sub>/TBP. The ionic conductivity of GPEs at different temperatures have been determined from the electrochemical impedance spectroscopy (EIS) measurement. X-ray diffraction (XRD) and Fourier-transform infrared spectroscopy (FTIR) have been performed to analyze the structural properties of the GPEs. All GPEs have been tested for dye-sensitized solar cell (DSSC) with natural sensitizers extracted from different natural sources namely blackberry, blueberry, raspberry and saffron. DSSCs have been characterized with  $J-V$  measurement, EIS, Intensity-modulated photocurrent spectroscopy (IMPS), and Intensity-modulated photovoltage spectroscopy (IMVS). The GPEs without TBP shows the ionic conductivity of  $(14.05 \pm 3.50) \text{ mS cm}^{-1}$  for DMF GPE and  $(2.45 \pm 1.51) \text{ mS cm}^{-1}$  for DMSO GPE. The addition of TBP does not improve the ionic conductivity of the GPE with  $(11.99 \pm 6.84) \text{ mS cm}^{-1}$  for DMF GPE and  $(2.98 \pm 1.35) \text{ mS cm}^{-1}$  for DMSO GPE. DSSCs have been fabricated by sandwiching GPE in between photoanode and platinum counter electrode. The photoanode has been prepared by coating two layers of TiO<sub>2</sub> on fluorine doped tin oxide (FTO) substrate via doctor blade method and sensitized with natural sensitizer. DMF/PVA/KI/I<sub>2</sub>/TBP GPE exhibit the best performance in DSSC with anthocyanin dye system. The best performance of DSSC can be explained via the charges transfer

resistance, electron transfer time and electron recombination time from the EIS, IMPS and IMVS data respectively.

**Keywords:** 4-tert-butylpyridine (TBP); Dye-sensitized solar cells; Gel polymer electrolytes; Natural dye sensitizers.

Universiti Malaya

**PEMEKA SEMULAJADI UNTUK SEL SOLAR BERASASKAN ELEKTROLIT  
GEL POLIMER YANG MENGANDUNGI PASANGAN REDOX  
IODIDE/TRIIODIDE**

**ABSTRAK**

Polivinil alkohol (PVA) berasas gel polymer elektrolit (GPEs) yang mengandungi iodide/triiodide telah disediakan. Dua jenis pelarut iaitu dimethylformamide (DMF) dan dimethyl sulfoxide (DMSO) telah digunakan dalam penyediaan GPE. GPE itu adalah (i) DMF/PVA/KI/I<sub>2</sub>, (ii) DMF/PVA/KI/I<sub>2</sub>/4-tert-butylpyridine (TBP), (iii) DMSO/PVA/KI/I<sub>2</sub> dan (iv) DMSO/PVA/KI/I<sub>2</sub>/TBP. Kekonduksian ionic GPE pada suhu yang berbeza telah ditentukan daripada pengukuran spektroskopi impedans electrokimia (EIS). Belauan X-ray (XRD) dan spektroskopi transformasi inframerah-Fourier (FTIR) telah dijalankan untuk menganalisa pencirikan struktur semua GPE. Kesemua GPEs telah diuji di dalam pencilup sel suria terpeka (DSSC) dengan pemeka semulajadi diekstrak dari sumber semulajadi iaitu buah beri hitam, beri biru, raspberi dan kunyit. DSSC telah dicirikan dengan pengukuran  $J-V$ , EIS, spektroskopi keamatan-termodulat arus foto (IMPS) dan keamatan-termodulat voltan foto (IMVS). GPEs tanpa TBP menunjukkan nilai kekonduksian ionik ( $14.05 \pm 3.50$ ) mS cm<sup>-1</sup> untuk DMF GPE dan ( $2.45 \pm 1.51$ ) mS cm<sup>-1</sup> untuk DMSO GPE. Penambahan TBP dalam GPE tidak mempertingkatkan kekonduksian GPE dengan ( $11.99 \pm 6.84$ ) mS cm<sup>-1</sup> untuk DMF GPE dan ( $2.98 \pm 1.35$ ) mS cm<sup>-1</sup> untuk DMSO GPE. DSSC telah difabrikasi dengan mengapitkan GPE diantara fotoanod dan platinum elektrod. Fotoanod telah disediakan dengan menyalut dua lapisan TiO<sub>2</sub> pada fluorine doped tin oxide (FTO) substrat melalui kaedah “doctor blade” dan dipekakan dengan pemeka semulajadi. DMF/PVA/KI/I<sub>2</sub>/TBP GPE menunjukkan prestasi terbaik dalam DSSC dengan system pemeka anthocyanin. Prestasi terbaik yang

ditunjukkan oleh DSSC boleh dijelaskan melalui rintangan pemindahan cas, masa pemindahan elektron dan masa pembangunan semula elektron didapati EIS, IMPS dan IMVS data.

**Kata kunci:** 4-tert-butilpiridina(TBP); suria terpeka pewarna; gel elektrolit polimer; pemeka pewarna semula jadi.

Universiti Malaya

## ACKNOWLEDGEMENTS

Foremost, I would like to express my sincere appreciation and gratitude to my former supervisor Professor Dr. Abdul Kariem Bin Hj Mohd Arof who has provided me the opportunity and conducive environment to undertake this study. Under his supervision, I have built the confidence to pursue my master study with patience and optimism.

Also, I would like to sincerely thank to my supervisors, Dr. Mohd Hamdi Bin Ali @ Buraidah for his constant guidance, support, and encouragement throughout this journey, which I could not have found a better supervisor for this journey.

Besides, I would like to thank the Universit Malaya and Ministry of Higher Education for providing me financial support, through IPPP grants, and the opportunity to conduct such valuable research during my studies. I wish also to thank all the supporting staff and technicians in the department of physics.

Finally, I dedicate this work to my dear parents for their endless love and encouragement & my dear husband for his unlimited love and support.

## TABLE OF CONTENTS

<b>ABSTRACT</b> .....	<b>iii</b>
<b>ABSTRAK</b> .....	<b>v</b>
<b>ACKNOWLEDGEMENTS</b> .....	<b>vii</b>
<b>TABLE OF CONTENT</b> .....	<b>viii</b>
<b>LIST OF FIGURES</b> .....	<b>xii</b>
<b>LIST OF TABLES</b> .....	<b>xv</b>
<b>LIST OF SYMBOLS AND ABBREVIATIONS</b> .....	<b>xvi</b>
<b>CHAPTER 1: INTRODUCTION</b> .....	<b>1</b>
1.1 Background .....	1
1.2 Problem statement .....	2
1.3 Research objectives .....	2
1.4 Scope and limitations of the study.....	3
1.5 Thesis organization.....	3
<b>CHAPTER 2: LITERATURE REVIEW</b> .....	<b>5</b>
2.1 Introduction.....	5
2.2 Solar cell.....	5
2.3 Dye- sensitized solar cells.....	6
2.3.1 Main component of the DSSC.....	6
2.3.2 Working principle of DSSCs.....	7
2.4 Electrolyte.....	9
2.4.1 Liquid electrolyte (LE).....	9
2.4.2 Solid polymer electrolyte (SPE).....	10
2.4.3 Gel polymer electrolyte (GPE).....	11
2.4.3.1 tert-Butylpyridine (TBP).....	12

2.4.3.2	Dimethylformamide (DMF).....	12
2.4.3.3	Dimethyl sulfoxide (DMSO).....	13
2.5	Counter electrode (CE).....	14
2.6	Photoanode.....	15
2.6.1	Fluorine doped Tin Oxide (FTO) Glass Substrate.....	15
2.6.2	Mesoporous Titanium dioxide (TiO <sub>2</sub> ) nanoparticles film.....	15
2.6.3	Dyes.....	16
2.7	Natural dyes as photosensitizer.....	18
2.7.1	Dye preparation.....	22
2.7.2	Blackberry.....	24
2.7.3	Blueberry.....	25
2.7.4	Dragon fruit.....	27
2.7.5	Raspberry.....	28
2.7.6	Saffron.....	30
2.7.7	Anthocyanin.....	32
2.7.8	Carotenoid.....	33
2.8	Summary of the chapter.....	34
	<b>CHAPTER 3: RESEARCH METHODOLOGY.....</b>	<b>36</b>
3.1	Introduction.....	36
3.2	Materials.....	36
3.3	Preparation of the dyes.....	38
3.3.1	Drying process.....	38
3.3.2	Dye extraction.....	38
3.4	Preparation of gel polymer electrolytes.....	39
3.5	Preparation of photoanode.....	39

3.5.1	Cleaning process of FTO glasses.....	39
3.5.2	Preparation of conductive layers of TiO <sub>2</sub> (photoanode).....	40
3.5.3	Sensitizing of the photoanode.....	40
3.6	Preparation of Pt counter electrode (Cathode).....	40
3.7	DSSCs fabrication.....	41
3.8	Characterization.....	41
3.8.1	Characterization of gel polymer electrolyte.....	41
3.8.1.1	Ionic Conductivity.....	42
3.8.1.2	X-Ray Diffractometer (XRD).....	42
3.8.1.3	FTIR.....	42
3.8.2	Characterization of DSSCs.....	42
3.8.3	Photovoltaic characteristics.....	43
3.8.4	Electrochemical impedance spectroscopy (EIS).....	45
3.8.5	IMPS/IMVS.....	45
3.9	Safety aspects.....	48
3.10	Summary of the chapter.....	48
<b>CHAPTER 4: RESULTS AND DISCUSSION.....</b>		<b>49</b>
4.1	Ionic conductivity of the selected gel polymer electrolytes.....	49
4.2	Fourier-transform infrared spectroscopy (FTIR) of the selected electrolytes...	52
4.3	Characterization of the electrolyte: X-ray diffraction (XRD) studies.....	53
4.4	DSSCs performance analyses of Blackberry.....	54
4.4.1	Photovoltaic (J-V) characteristics.....	54
4.4.2	Electrical impedance spectroscopy (EIS).....	56
4.4.3	IMPS and IMVS study of photovoltaic cells.....	58
4.5	DSSCs performance analyses of Blueberry.....	60

4.5.1	Photovoltaic (J-V) characteristics.....	60
4.5.2	Electrical impedance spectroscopy (EIS).....	61
4.5.3	IMPS and IMVS study of photovoltaic cells.....	63
4.6	DSSCs performance analyses of Raspberry.....	65
4.6.1	Photovoltaic (J-V) characteristics.....	65
4.6.2	Electrical impedance spectroscopy (EIS).....	66
4.6.3	IMPS and IMVS study of photovoltaic cells.....	67
4.7	DSSCs performance analyses of Saffron.....	69
4.7.1	Photovoltaic (J-V) characteristics.....	69
4.7.2	Electrical impedance spectroscopy (EIS).....	70
4.7.3	IMPS and IMVS study of photovoltaic cells.....	71
4.8	Summary of chapter .....	73
<b>CHAPTER 5: CONCLUSION.....</b>		<b>75</b>
<b>REFERENCES.....</b>		<b>77</b>
<b>LIST OF PUBLICATIONS AND PAPERS PRESENTED.....</b>		<b>94</b>

## LIST OF FIGURES

Figure 2.1	: Schematic figure of p-n junction.....	6
Figure 2.2	: The structure of a dye sensitized solar cell.....	7
Figure 2.3	: Schematic diagram of a working DSSCs.....	7
Figure 2.4	: Schematic of the chemical structure of Dimethylformamide (DMF).....	13
Figure 2.5	: Schematic of the chemical structure of Dimethyl sulfoxide (DMSO)..	14
Figure 2.6	: Organogram of natural pigments extracted from different fruits, flowers, seeds, leaves, and vegetables.....	20
Figure 2.7	: Fresh blackberry fruit.....	24
Figure 2.8	: Chemical structure of Blackberry Flavonoid and Anthocyanin.....	25
Figure 2.9	: Chemical Structure of Blueberry Anthocyanin and Flavonoid.....	26
Figure 2.10	: Fresh Blueberry fruit.....	27
Figure 2.11	: Fresh dragon fruit.....	27
Figure 2.12	: Chemical structure of Dragon Betanin.....	28
Figure 2.13	: Fresh Raspberry fruit.....	29
Figure 2.14	: Chemical structure of Anthocyanin and Ellagitannin of Raspberry.....	29
Figure 2.15	: Saffron flower's structure.....	30
Figure 2.16	: The structure of Crocetin, Safranal, Crocin, and Picrocrocin of saffron.....	31
Figure 2.17	: Fresh saffron stigma.....	32
Figure 2.18	: Structure of anthocyanin pigments and the binding between anthocyanin molecule and TiO <sub>2</sub> particle.....	33
Figure 2.19	: Several carotenoids with different functional group.....	34
Figure 3.1	: Methodology flowchart of this research.....	37
Figure 3.2	: Image of the assembled DSSCs.....	41
Figure 3.3	: Solar simulator with reference cell positioned for testing.....	43

Figure 3.4	: Illustration of J-V characteristics of a solar cell. Blue line: measured current-voltage curve. Red line: area of $V_{OC} * J_{SC}$ . Green line: area of $V_{max} * J_{max}$ .....	44
Figure 3.5	: Sketch of the light signal focused on a DSSC during IMPS and IMVS.....	45
Figure 3.6	: I-V curves of a DSC showing the regions covered by EIS, IMPS, and IMVS.....	47
Figure 4.1	: Bulk resistance from the Cole-Cole plot of real and imaginary $R_s$ .....	50
Figure 4.2	: Log conductivity of the gel polymer electrolytes.....	51
Figure 4.3	: FTIR spectra recorded between 0 and 4000 $cm^{-1}$ for gel polymers electrolytes (A, and C) and samples containing TBP additive (B, and D).....	53
Figure 4.4	: The XRD pattern of the gel polymer electrolyte A, B, C and D.....	54
Figure 4.5	: Blackberry J-V Curves of photovoltaic cells with different GPEs.....	55
Figure 4.6	: The Nyquist plots of EIS for the blackberry fabricated photovoltaic cells with different GPEs.....	57
Figure 4.7	: IMPS plot for the DDSCs based blackberry dye with different GPEs..	58
Figure 4.8	: IMVS plot for the DDSCs based blackberry dye with different GPEs..	59
Figure 4.9	: Blueberry J-V curves of photovoltaic cells with different GPEs.....	60
Figure 4.10	: The Nyquist plots of EIS for the blueberry fabricated photovoltaic cells with different GPEs.....	62
Figure 4.11	: IMPS Nyquist type plot for the blueberry fabricated photovoltaic cells with different GPEs.....	63
Figure 4.12	: IMVS Nyquist type plot for the blueberry fabricated photovoltaic cells with different GPEs.....	64
Figure 4.13	: Raspberry J-V curves of photovoltaic cells with different GPEs.....	65
Figure 4.14	: The Nyquist plots of EIS for the raspberry fabricated photovoltaic cells with different GPEs.....	67
Figure 4.15	: IMPS Nyquist type plot for the raspberry fabricated photovoltaic cells with different GPEs.....	68
Figure 4.16	: IMVS Nyquist type plot for the blueberry fabricated photovoltaic cells with different GPEs.....	68

Figure 4.17 : Saffron J-V curves of photovoltaic cells with different GPEs.....	70
Figure 4.18 : The Nyquist plots of EIS for the saffron fabricated photovoltaic cells with different GPEs.....	71
Figure 4.19 : IMPS Nyquist type plot for the saffron fabricated photovoltaic cells with different GPEs.....	72
Figure 4.20 : IMVS Nyquist type plot for the saffron fabricated photovoltaic cells with different GPEs.....	73

Universiti Malaya

## LIST OF TABLES

Table 2.1	: DSSCs with liquid electrolytes.....	9
Table 2.2	: DSSCs with solid polymer electrolytes.....	10
Table 2.3	: DSSCs with gel polymer electrolytes using synthetic dyes.....	11
Table 2.4	: Photovoltaic performance of DSSC utilizing various natural dyes as photosensitizer.....	21
Table 3.1	: Time and weight of the fruits before and after drying.....	38
Table 3.2	: The composition of GPEs.....	39
Table 4.1	: Conductivity of gel polymer electrolytes in different temperatures....	51
Table 4.2	: Photovoltaic parameters of Blackberry with different GPEs.....	55
Table 4.3	: Rp value of DSSCs using blackberry dyes.....	58
Table 4.4	: The parameters obtained from IMPS and IMVS experiments for the DSSCs using blackberry dye with different GPEs.....	60
Table 4.5	: Photovoltaic parameters of Blueberry with different GPEs.....	61
Table 4.6	: Rp value of DSSCs using blueberry dye.....	63
Table 4.7	: The parameters obtained from IMPS and IMVS experiments for the DSSCs using blueberry dye with different GPEs.....	65
Table 4.8	: Photovoltaic parameters of raspberry with different GPEs.....	66
Table 4.9	: Rp value of DSSCs using raspberry dye with different GPEs.....	67
Table 4.10	: The parameters obtained from IMPS and IMVS experiments for the DSSCs using rapberry dye with different GPEs.....	69
Table 4.11	: Photovoltaic parameters of raspberry with different GPEs.....	70
Table 4.12	: EIS parameters of fabricated DSSCs for saffron dye with different GPEs.....	71
Table 4.13	: The parameters obtained from IMPS and IMVS experiments for the DSSCs using saffron dye with different GPEs.....	73

## LIST OF SYMBOLS AND ABBREVIATIONS

CS28	:	[RuL <sub>1</sub> L <sub>2</sub> (NCS) <sub>2</sub> ] (CS27), [RuL <sub>1</sub> L <sub>3</sub> (NCS) <sub>2</sub> ]
CYC-B1	:	Ruthenium with an alkyl bithiophene group
CYC-B3	:	Ruthenium with an alkyl bithiophene (less than B1) group
DMSO	:	Dimethyl sulfoxide
DMF	:	Dimethylformamide
DMPII	:	1,2-dimethyl-3-propylimidazolium iodide
DSSCs	:	Dye sensitized solar cells
GPE	:	Gel polymer electrolyte
HOMO	:	Highest occupied molecular orbitals
LUMO	:	Lowest unoccupied molecular orbital
MD-153	:	4-[9,9-bis(n-alkyl) fluorene-2-yl]-1,2,3,3a,4,8b-hexahydrocyclopent[b]-indole-7-carbaldehyde and [3-(11-carboxyundecyl)4-oxo-2-thioxo-5-thiazolidinylidene]-4-oxo-3-thiazolidine acetic acid
MePN	:	N-methylpyridoxine
N3	:	Cis-bis(isothiocyanato)bis(2,2'-bipyridyl-4,4'-dicarboxylato) ruthenium (II)
N719	:	Cis-di(thiocyanato)bis (2,2' -bipyridyl-4,4' - dicarboxylate) ruthenium (II)
N945	:	Bu <sub>4</sub> N [Ru (Hdcbpy)(L1) (NCS) <sub>2</sub> ]
NMBI	:	N-methylbenzimidazole
PAN	:	Polyacrylonitrile
PMII	:	Plasmepsin II
Ru535	:	Ru (4,4'-dicarboxy-2,2'- bipyridine) <sub>2</sub> (NCS) <sub>2</sub> (Ru535)
SWCNT	:	Single-Walled Carbon Nanotube
TBP	:	4. tert-Butyl pyridine
TPAR3	:	Triphenylamine

Z907	:	Cis-Bis(isothiocyanato)(2,2'-bipyridyl-4,4'-dicarboxylato) (4,4'-di-nonyl-2'-bipyridyl) ruthenium (II)
Z910	:	Ru(dcbpy)(dmsbpy)(NCS) <sub>2</sub>
ZNO needle	:	Zinc nitrate
BMII	:	1-butyl-3-methylimidazolium iodide

Universiti Malaya

## CHAPTER 1: INTRODUCTION

### 1.1 Background

Increasing energy crisis and environmental concerns through fossil fuel and its depletion reserve have led to very intense research on sustainable and renewable energy sources (Nastasi *et al.* 2022) such as tidal power, solar thermal, biomass, hydropower, and solar energy (J.-H. Kim *et al.* 2022).

Photovoltaic cell is a device that convert solar energy which is photon into electricity. The first practical photovoltaic cell has been designed at Bell Laboratories in 1954 (Dewan and Yadav 2021). The first generation of the solar cells which have been commercialized are based on the crystalline silicon materials. The fabrication process was expensive and using toxic chemicals to obtained high purified silicon. The second generation of the solar cells are based on thin film technology such as cadmium telluride and cadmium indium gallium. This type of solar cells is cheaper and using less materials but also less efficiency as compared to the first generation. The solar cells that using sensitizer as light absorption such as quantum dot sensitized solar cell (QDSSC) and dye sensitized solar cell (DSSCs) are considered as the third generations of solar cells and exhibits a potential to be higher efficiency than the second generation while having low cost in fabrication (Mrinalini *et al.* 2019).

DSSC exploit the photosynthesis concept which is using the plant's ability of turning sunlight to energy. In DSSC, dye sensitizer (organic or inorganic) was used as light absorption. DSSCs firstly invented in 1988 by Michael Gratzel and Brian O'Regan (O'regan and Grätzel 1991). They are easy to manufacture, semi-transparent and low cost. A typical DSSC consists of (a) transparent conductive oxide (TCO) (b) metal oxide (MO) semiconductor; (c) dye sensitizer (d) electrolyte and (e) catalyst counter electrode (CE). TCO mostly used as a substrate for sensitized MO semiconductor which is known as

photoanode. The MO semiconductor such as Titanium dioxide ( $\text{TiO}_2$ ) provide a suitable porous structure for the sensitizer. The sensitizer can be obtained by the synthesis process or extraction from the natural plants, fruits, and flowers. The electrolyte work as a mediator in DSSC which transport charge carriers between photoanode and cathode (Richhariya *et al.* 2017).

DSSCs have the tendency of working better in a cloudy and dark weather, which makes them a perfect choice for the indoor applications and for the countries that where the silicon based solar cell might face some difficulties to absorb sunlight (Bella *et al.* 2014). These advantages lead to the intensive research to increase the efficiency of the cell which currently reported exhibits the highest efficiency of 14% (O'Regan and Grätzel 2018; Mathew *et al.* 2014).

## **1.2 Problem statement**

Over the last decades, various types of solar cells have been developed. Electrolyte is the one of the indispensable components in DSSCs. Liquid electrolyte gives the best performance of DSSC but prone to leakage and volatile. On the other hand, solid based polymer electrolyte has low ionic conductivity and poor contact with both photoanode and CE which can affect the DSSC performance. The sensitizer is another factor that affects the efficiency of the DSSCs. Synthetic dyes such as N3 and N719 have high efficiency, but they are extremely expensive and toxic.

## **1.3 Research Objectives**

- To study the effect of TBP in gel polymer electrolytes on the performance of dye sensitize solar cells.
- To analyst the role of DMF and DMSO solvents in GPEs, on the performance of DSSCs.

- To determine charges transport properties in DSSC with blueberry, blackberry, raspberry, and saffron dyes.

#### **1.4 Scope and limitations of the study**

This study aims to answer the features and effect of different dyes on the performance of dye sensitized solar cells. The focus of this investigation is to explore the different dyes characteristics as the sensitizer for the DSSCs as well as their efficiency with various gel polymer electrolytes.

#### **1.5 Thesis organization**

The thesis consists of five chapters dealing with different aspects related to the research topic.

- **CHAPTER 1** Includes a brief introduction to the research project.
- **CHAPTER 2** Contains a comprehensive literature survey of DSSCs, followed by overview of the characteristics of blackberry, blueberry, dragon fruit, raspberry and saffron as the potential dyes for the DSSCs.
- **CHAPTER 3** Describes the materials synthesis and characterizations as well as process setups for DSSCs experiments. Furthermore, all experimental design techniques and analysis equipment and processes are explained in detail.
- **CHAPTER 4** Presents the results and data obtained from laboratory experiments. Efficiency evaluation of the new fabricated DSSCs is carried out in terms of absorption, photovoltaic characterization, electrical impedance characteristics (EIS), IMVS and IMPS. Gel polymer electrolytes containing potassium iodide with/without

0.05M of TBP have been applied as charge transport medium in DSSC with dyes of 1/50 concentrations. Furthermore, a comprehensive discussion and explanation of the experimental results have been performed in this section.

- **CHAPTER 5** Summarizes the conclusions according to the study results and findings, followed by a list of recommendations for the further studies.

Universiti Malaya

## CHAPTER 2: LITERATURE REVIEW

### 2.1 Introduction

This chapter discusses the fundamentals and working principle of dye sensitized solar cells (DSSCs). The components of DSSC and their function have also been discussed in this chapter.

### 2.2 Solar cell

Solar energy is one of the alternatives to overcome the energy crisis due to the depletion in fossil fuel. The energy converted from solar is renewable and clean (Ulucak and Khan 2020). Earth receives about  $174 \times 10^3$  terawatts (TW) of solar radiation, whereas our global primary energy consumption is about 15 TW (Sonker and Sabhajeet 2018). Therefore, developing a technology to use only 0.1 % of the sun's energy, could be more than sufficient to meet the energy demand on earth. From the quantum study of solar cell, sunlight consist of the very small and massless particles named photon. These photon with the energy they have, can excite one electron and let it escape from the semiconductor atoms and leaves a "hole" behind to fill with other electrons (Moharam *et al.* 2021). This is the fundamental concept of the working principle of solar cell in general. When the n-type and p-type semiconductors come to contact with each other, they create a p-n junction which has an electric field. The electric field allow electrons to across the junction from the n-type to p-type semiconductor and leaving hole behind in the n-type semiconductor. The holes created on the n-type semiconductor will be filled from the other electrons that flow through the external circuit powering an external load (Moharam *et al.* 2021). Figure 2-1, present the schematic cross section of a p-n junction silicon solar cell.

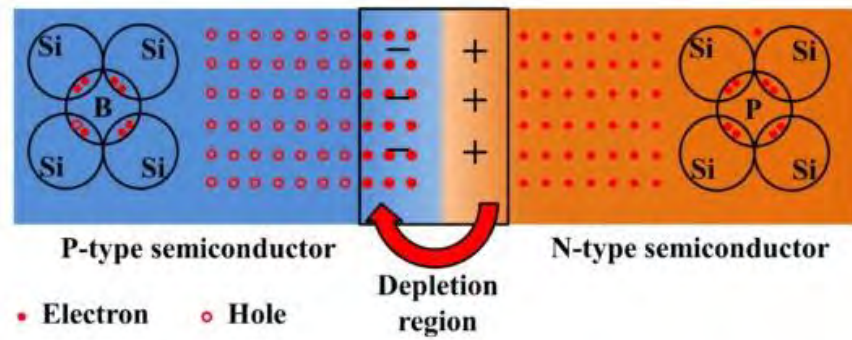


**Figure 2.1.** Schematic figure of p-n junction.

## 2.3 Dye- sensitized solar cells

### 2.3.1 Main component of the DSSC

The structure of a DSSCs is basically a sandwich type. This sandwich is consisting of FTO glass,  $\text{TiO}_2$  layers, dye, electrolyte, Pt, FTO glass (Birel, Nadeem, and Duman 2017).

Figure 2.2 illustrates the structure of a DSSCs, layer by layer.

- 1)  $\text{MO}_1$  and  $\text{MO}_2$  are the metal oxide for first and second layer. The first layer is denser than the second layer.
- 2) Dye is the sensitizer which were adsorbed on the MO surface
- 3) Electrolyte which can be solid, gel, and liquid form.
- 4) Platinum (Pt) which used as catalyst for CE.
- 5) Fluorine doped Tin Oxide glass (FTO) is TCO in which MO and Pt coated on it.

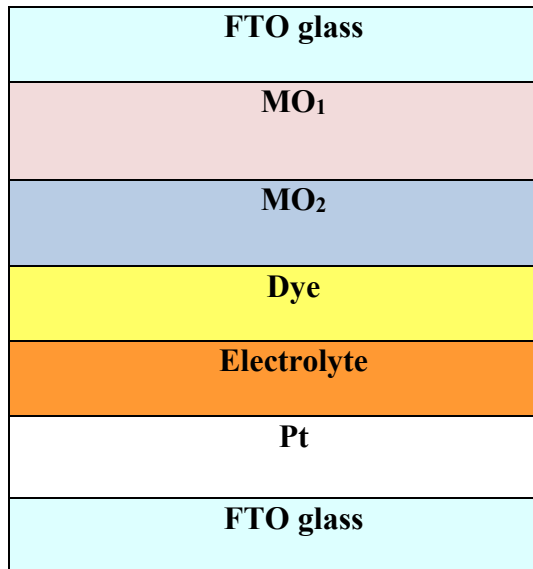


**Figure 2.2.** The structure of a dye sensitized solar cell.

### 2.3.2 Working principle of DSSCs

The mechanism of the DSSC is the resemblance of the natural process of turning sunlight into chemical energy called photosynthesis. The energy of the sunlight is captured in the nanocrystalline TiO<sub>2</sub> photoanode sensitized with dye (K. Sharma, Sharma, and Sharma 2018). The flow of the electrons from photoanode to counter electrode and back to the photoanode is shown in Figure 2.3.

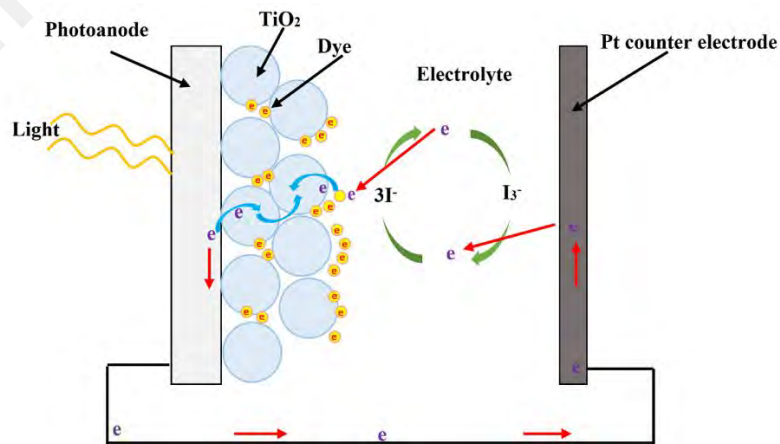


**Figure 2.3.** Schematic diagram of a working DSSCs.

When the energy of the Sun which is photons struck to the surface of the photoanode, it will be absorbed by the dye sensitizer (D) that attached to the MO TiO<sub>2</sub> surface. When enough energy, the dye will get excited (D\*) where electrons from the HOMO of dye molecules will be excited to the LUMO level (equation 2.1). Charges separation occur when the excited electrons be injected into the conduction band (CB) of MO TiO<sub>2</sub> leaving holes in the oxidized dye molecule (equation 2.2). The electrons in the CB of TiO<sub>2</sub> eventually reach to the FTO glass and subsequently moves to the CE through the external circuit (Mahadevi and Sumathi 2020). At the CE, electrons will be transferred into the electrolyte where the triiodide (I<sub>3</sub><sup>-</sup>) ions be reduced to iodide (I<sup>-</sup>) ions after receiving 2 electrons (equation 2.3). The I<sup>-</sup> then move to the photoanode and oxidized back to I<sub>3</sub><sup>-</sup> and regenerate the dye molecules to complete the circuit (equation 2.4 and 2.5).



For the electrons to be collected efficiently at the FTO glass, it must avoid the trapping state the TiO<sub>2</sub>. The trapping and detraining determine the elective lifetime of the electrons ( $\tau_n$ ) and the electron diffusion coefficient ( $D_n$ ) (E. Supriyanto *et al.* 2019) which can be determined from the impedance measurement (Mozaffari *et al.* 2015).

## 2.4 Electrolyte

### 2.4.1 Liquid electrolyte (LE)

In general, The electrolyte manages the transfer of charge between the electrodes (Yu *et al.* 2011). Liquid electrolytes for DSSC consist of a solvent like acetonitrile and ethylene glycol to solvate iodide salt like potassium iodide and lithium iodide. High ionic conductivity, wide electrochemical window and excellent thermal and chemical stabilities are some of the advantages of liquid electrolyte (Miao *et al.* 2021). Table 2.1 shows some of the studies in DSSCs field using liquid electrolytes.

**Table 2.1.** DSSCs with liquid electrolytes.

No.	Dye	Electrolyte	solvent	J <sub>sc</sub> (mA·cm <sup>-2</sup> )	V <sub>oc</sub> (mV)	FF (%)	PCE (%)	References
1	RuC	LiI	Methanol/water	5.82	600	52	1.8	(Pirashanthan <i>et al.</i> 2021)
2	N3	0.17 M Cu(I), 0.04 M Cu(II), 0.6 M TBP, and 0.1 M LiClO <sub>4</sub>	Dry acetonitrile	14.5	690	49	4.99	(Selvaraj <i>et al.</i> 2021)
3	N719	TBAI, 0.6 M; LiI, 0.1 M; I <sub>2</sub> , 0.05 M; GuNCS, 0.1 M; and DNB, 0.1 M, in 3-MPN.	3-MPN	13.96	0.62	0.44	3.8	(P. T. Nguyen and Do Nguyen 2018)
4	Z907	M 1-propyl-3- methylimidazolium iodide (PMII), 0.15 M iodine (I <sub>2</sub> ), 0.1 M guanidinium thiocyanate (GSCN), and 0.5 M 4-tert- butylpyridine (TBP) in MPN	3-MPN	13.69	728.5	70.23	7.00	(Park, Lee, and Ko 2019)
5	N719	0.6 M BMII + 0.03 M I <sub>2</sub> + 0.1 M GNCS + 0.5 M TBP in C <sub>2</sub> H <sub>3</sub> N and C <sub>5</sub> H <sub>9</sub> N (v/v, 85/15)	Acetonitrile/ valeronitrile	17.73	846	72	11.18	(Mohammad K Nazeeruddin <i>et al.</i> 2005)
6	N945	0.60 M BMII + 0.03 M I <sub>2</sub> + 0.1 M GNCS + 0.50 M TBP in C <sub>2</sub> H <sub>3</sub> N and C <sub>5</sub> H <sub>9</sub> N (v/v, 85/15)	Acetonitrile/ valeronitrile	17.96	728	71	9.29	(Md K Nazeeruddin <i>et al.</i> 2007)
7	Z910	0.60 M PMII + 0.1 M I <sub>2</sub> + 0.5 M C <sub>8</sub> H <sub>8</sub> N <sub>2</sub> in C <sub>4</sub> H <sub>7</sub> NO	2- Pyrrolidinone	17.2	777	76.4	10.2	(P. Wang <i>et al.</i> 2004)
8	Z907	0.5 M LiI + 0.05 M I <sub>2</sub> + 0.5 M TBP in C <sub>2</sub> H <sub>3</sub> N	Acetonitrile	14.16	680	67	6.3	(Yen <i>et al.</i> 2011)
9	CYC-B1	0.5 M LiI + 0.05 M I <sub>2</sub> + 0.5 M TBP in C <sub>2</sub> H <sub>3</sub> N	Acetonitrile	23.92	650	55.0	8.54	(Chia-Yuan Chen <i>et al.</i> 2006)
10	CYC-B3	0.60 M BMII + 0.03 M I <sub>2</sub> + 0.1 M GNCS + 0.50 M TBP in C <sub>2</sub> H <sub>3</sub> N and C <sub>5</sub> H <sub>9</sub> N (v/v, 85/15)	Acetonitrile	15.7	669	70.5	7.39	(C-Y Chen <i>et al.</i> 2007)

## 2.4.2 Solid polymer electrolyte (SPE)

Solid polymer electrolytes advantages over liquid electrolyte such as higher energy density, flexibility, no leakage during the process and easy to use in higher temperatures (Asano, Kubo, and Nishikitani 2004; R. Singh *et al.* 2016). Due to their potential use in electrochemical devices like solid-state batteries and separation membranes, SPEs have drawn a lot of attention in recent years. However, due to its high crystallinity, its ionic conductivity is unsuitable for solar cell applications (Kang *et al.* 2005). However it has other disadvantages such as poor physical contact with both electrodes and poor ionic conductivity that made DSSC suffer in performance (Selvanathan *et al.* 2020). Table 2.2 shows some of the studies in DSSCs field using solid polymer electrolytes.

**Table 2.2.** DSSCs with solid polymer electrolytes.

No.	Dye	Electrolytes	J <sub>sc</sub> (mA·cm <sup>-2</sup> )	V <sub>oc</sub> (mV)	FF (%)	PCE (%)	References
1	Ru535	PEODME/MPII/I <sub>2</sub> /SiO <sub>2</sub>	9.5	0.65	-	4.50	(J. H. Kim <i>et al.</i> 2004)
2	Ru535	PEO-KI/I <sub>2</sub>	0.06	0.68	0.26	0.01	(Kang <i>et al.</i> 2005)
3	Ru535	PEO-PPG-KI/I <sub>2</sub>	11.2	0.72	0.48	0.03	(Kang <i>et al.</i> 2005)
4	N719	PU-Li/I <sub>2</sub>	0.06	0.14	0.26	0.003	(Su'Ait <i>et al.</i> 2014)
5	ZnO particle	PEO-KI/I <sub>2</sub>	2.1	0.63	0.67	1.7	(Sonker and Sabhajeet 2018)
6	ZnO needle	PEO-KI/I <sub>2</sub>	20	0.48	0.44	4.2	(Sonker and Sabhajeet 2018)
7	N3	HPA-impregnated PVDF	3.902	0.426	0.25	2.77	(Anandan <i>et al.</i> 2006)
8	N719	PEO-KI/I <sub>2</sub>	0.02	0.54	0.61	0.015	(S. Singh <i>et al.</i> 2021)
9	Raspberry	PEO-KI/I <sub>2</sub>	0.02	0.54	0.60	0.006	(S. Singh <i>et al.</i> 2021)
10	Pomegranate	PEO-KI/I <sub>2</sub>	0.03	0.65	0.80	0.028	(S. Singh <i>et al.</i> 2021)

### 2.4.3 Gel polymer electrolyte (GPE)

Microporous membrane with a liquid electrolyte medium make up a quasi-solid-state (gel-like) electrolyte. These have various benefits for the DSSC, including excellent filling and contact qualities between the electrodes, low vapour pressure, cohesive properties of the solids, great thermal stability, and exceptional ionic conductivity (Manafi *et al.* 2021).

The composition of GPE include high boiling point solvent such as DMSO and DMF, salts like lithium iodide and potassium iodide and polymers like PVA, PAN, PEO, PVDF and etc. Unlike SPE, solvent in GPE remain in the polymer matrix that help in the movement of the polymer chain and therefore improve the ionic conductivity of the polymer based electrolyte. With high ionic conductivity and the advantage of the presence of the polymer (preventing from leakage) have attract more reasearch on the GPE for DSSC (D.-W. Kim *et al.* 2005). Table 2.3 shows some of the studies in DSSCs field using gel polymer electrolytes.

**Table 2.3.** DSSCs with gel polymer electrolytes using synthetic dyes.

No.	Dye	Polymer/ solvent/salt	JSC (mA·cm <sup>-2</sup> )	VOC (mV)	FF (%)	EFF (%)	References
1	N719	PAN / EC, PC/Pr4NI/ KI	13.79	679.1	57.25	5.36	(Dissanayake <i>et al.</i> 2012)
2	N719	PVdF / EC, PC/Pr4NI/ KI	6.148	680.5	69.28	2.90	(A K Arof <i>et al.</i> 2014)
3	-	PAN /DMSO, PC/ LiI, TBAI	11.21	0.66	0.73	5.41	(Chan, Wang, and Chen 2013)
4	N719	PAN/ EC, PC/ Hex4NI/ RbI, BMII	20.0	748.0	50.0	7.5	(T. Bandara <i>et al.</i> 2019)
5	N <sub>3</sub>	PAN/ EC, PC/ BMII, TPAI, LiI	21.0	0.48	53.4	5.4	(A K Arof <i>et al.</i> 2017)
6	N719	PAN /PC, EC/ Tetrabutyl ammonium iodide	15.96	0.751	0.616	7.27	(Ileperuma <i>et al.</i> 2011)
7	MD-153	PVDF/HFP/ acetonitrile/ tributyl phosphate	15.7	0.95	0.69	10.4	(Suzuka <i>et al.</i> 2016)
8	CS28	PhCh/ EC, DMF/TPAI	7.70	0.64	0.58	2.86	(Yusuf <i>et al.</i> 2016)
9	TPAR3	LiI (0.1 g), I2 (0.019 g), propylene carbonate (5 mL), P25 TiO2 (0.0383 g), PEO (0.2648 g), and 4-tert-butylpyridine (0.044 mL) into acetonitrile (5 mL)	17.0	0.70	0.57	6.80	(G. D. Sharma, Suresh, and Mikroyannidis 2010)
10	N719	0.1 M LiI, 0.1 M I2, 0.6 M DMPII, 0.45 M NMBI, MePN, and PEO	0.695	12.21	68.9	5.85	(Shi <i>et al.</i> 2013)

#### 2.4.3.1 4-tert-Butylpyridine (TBP)

4-tert-butyl pyridine (TBP) is highly hydrophobic due to a pyridine group at one end (Liu *et al.* 2017) can increase the hydrophobicity of the layer. TBP is used as an additive in different layers of perovskite solar cells to increase the stability and performance of solar cells (Y.-H. Wu *et al.* 2018; Shi *et al.* 2015; Habisreutinger *et al.* 2017; Tumen-Ulzii *et al.* 2021). Additionally, TBP also was applied as an additive in the gel polymer electrolytes (GPE). TBP has a higher boiling point which could be beneficial for the consistent long-term performance of DSSC (Sun *et al.* 2016). In a study by (T. M. W. J. Bandara *et al.* 2016), they stated that the addition of TBP was largely able to improve the overall performance of the DSSC by improving its open-circuit voltage ( $V_{oc}$ ) value. (J.-Y. Kim *et al.* 2012) have described that there is a shift at the titanium dioxide ( $TiO_2$ ) conduction band, which resulted in an increase of the  $V_{oc}$  value in the DSSC. This is due to the adsorption effect of TBP on the surface of mesoporous  $TiO_2$  at photoanode. The highest power conversion efficiency reported in their work was 7.39%. (X. Zhang *et al.* 2008) also incorporated TBP into the GPE consisting of polymer grafted ZnO nanoparticle. Results shows a drastic improvement in short-circuit current and overall performance of DSSC of 5.0%.

#### 2.4.3.2 Dimethylformamide (DMF)

Dimethylformamide (DMF) is an organic compound with the formula  $(CH_3)_2NC(O)H$ . This colourless liquid is miscible with water and the majority of organic liquids. Figure 2.4 represent the schematic of the chemical structure of DMF.

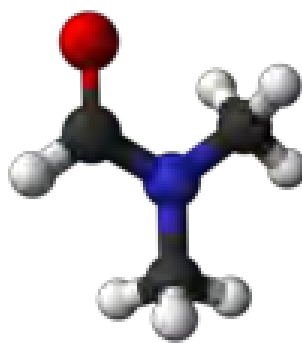


**Figure 2.4.** Schematic of the chemical structure of Dimethylformamide (DMF).

DMF has widely used as a solvent of dyes in DSSCs (Muin, Zakaria, and Zaini 2022; Abdukarimov *et al.* 2022; Selvanathan *et al.* 2020; da Silva, Sánchez, and Freeman 2020). In a recent study by Lakshmi *et al.*, they had applied DMF as a solvent to extract the dye from *Wrightia tinctoria* leaf by grinding the sample with 100 ml of DMF (Lakshmi *et al.* 2022). Novel Co and Zn-Phthalocyanine dyes have been applied in DSSCs by (Ilgün *et al.* 2021). They had stated that the DMF had been selected as the solvents due to its high polarity and the phthalocyanines were very much soluble in this solvent. The polymers such as PhCh, PVA, PVdF, and many others are able to dissolve in the DMF solvent to produce the gel polymer electrolytes (Yusuf *et al.* 2016).

#### 2.4.3.3 Dimethyl sulfoxide (DMSO)

Dimethyl sulfoxide (DMSO) is an organosulfur compound with the formula  $(\text{CH}_3)_2\text{SO}$ . This colourless liquid is an important polar aprotic solvent that dissolves both polar and nonpolar compounds and is miscible in a wide range of organic solvents as well as water. Figure 2.5 represents a schematic of the chemical structure of DMSO.

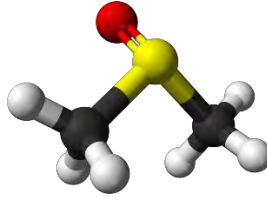


**Figure 2.5.** Schematic of the chemical structure of Dimethyl sulfoxide (DMSO).

Due to several advantages of DMSO over other solvents in solar cell studies, many researchers have applied this solvent (Bist and Chatterjee 2021). (Lobregas and Camacho 2019) investigated the effect of various solvents include water, DMSO, DMF, ethanol, acetone, DCM, toluene, acetonitrile, and ethyl acetate to produce starch-based gel polymer electrolyte. Based on their findings, the good contact filling between the electrodes provided by the gel matrix makes the DMSO better for long-term usage as the gel polymer electrolyte. To produce gel polymer electrolytes, DMSO used as a solvents to dissolve the polymers such as PhCh, PVA and PVdF (Yusuf *et al.* 2016; Goetzberger and Hebling 2000)

## **2.5 Counter electrode (CE)**

CE in DSSC have three functions. 1) as a catalyst, 2) as a positive electrode, and 3) as a mirror (Bera *et al.* 2021; O'regan and Grätzel 1991). It acts as catalyst to improve the completion of the process inside the DSSC, positive electrode to collect the electron from the external circuit and last but not the least as a mirror to reflect the unabsorbed sunlight's beam (Arsyad *et al.* 2019). A good CE that fulfills those three functions must have high electrical conductivity, high catalytic activity, high reflections, chemical, electrochemical and mechanical stability and finally low cost (Sarkar, Bera, and Chakraborty 2020). Platinum, metal transition compound, conductive polymer and carbon are among the materials that can be selected for CE (K. Wu *et al.* 2019).

## **2.6 Photoanode**

### **2.6.1 Fluorine doped Tin Oxide (FTO) Glass Substrate**

As presented in the scheme of Figure 2.3, light must pass through a transparent substrate to reach the active layer formed by the MO layer sensitized by the dye. FTO glass is the most common substrate used in DSSCs due to its electrically stable at high temperature. FTO considers as an advanced ceramic material with vast optical and electronic application. Energy conserving architectural windows, defogging aircraft and automobile windows, heat-reflecting coatings to increase light bulb efficiency, gas sensors, antistatic window coatings, and wear resistant layers on glass are other application of FTO glass (Xu *et al.* 2006; Limmer, Takahashi, and Cao 2003; Hu *et al.* 2003; Antony *et al.* 2004; Patel, Patel, and Vaishnav 2003; Alam and Cameron 2002). There are several method to prepare FTO powder such as vapor–liquid–solid (VLS) (Han *et al.* 2007; Pan and Wang 2001), sol–gel (Han *et al.* 2004), emulsion technique (Han *et al.* 2004), ion exchange, and hydrothermal process (Xu *et al.* 2006; Han *et al.* 2007).

### **2.6.2 Mesoporous Titanium dioxide (TiO<sub>2</sub>) nanoparticles film**

Because of its high stability, low cost, and safety for humans and the environment, titanium dioxide (TiO<sub>2</sub>) is believed to be very near to a perfect semiconductor for photocatalysis .Titanium dioxide TiO<sub>2</sub> is the most famous and used as photocatalysts (Hoffmann *et al.* 1995; Muna Muzahim Abbas 2020) and chemical inertness (Nkele *et al.* 2020; Miyoshi, Nishioka, and Maeda 2018). TiO<sub>2</sub> exists in different forms namely anatase, rutile and brookite (T. Iqbal *et al.* 2020). TiO<sub>2</sub> is a large-band semiconductor, with anatase, rutile, and brookite phases with band gaps of 3.2, 3.02, and 2.96 eV, respectively (Wunderlich *et al.* 2004). Brookite is not much useful in the industry due to the temperature stability issue. Rutile exists after high temperature calcination and their properties like electrical, optical, and thermal had been widely studied (Q. Zhang, Gao,

and Guo 2000). The photocatalytic activity of the rutile phase is often low (Sclafani, Palmisano, and Schiavello 1990). Anatase structure on the other hand has been extensively used as photoanode in DSSC. Due to its better electron mobility, low dielectric constant, and lower density, the anatase structure is chosen over other polymorphs for solar cell applications (Carp, Huisman, and Reller 2004). The role of anatase TiO<sub>2</sub> in the injection process in a photochemical solar cell with a high conversion efficiency has sparked an interest recently in DSSC technology (Tang *et al.* 1994; Gupta and Tripathi 2011). The tolerance temperature of the TiO<sub>2</sub> anatase structure is in between 450 °C to 500 °C. Above 500 °C, the crystal structure of TiO<sub>2</sub> will become rutile (Vorontsov *et al.* 2018; Nkele *et al.* 2020).

### 2.6.3 Dyes

Due to the wide bandgap of TiO<sub>2</sub>, it absorbs high energy photons (~ 390 nm) (T. T. Nguyen *et al.* 2021). To harvest as much as possible of the solar spectrum, dye molecules which chemically bound to the TiO<sub>2</sub> surface acting as antennas. To choose a dye molecule there are few criteria that must be fulfilled to ensure that the sensitization work efficiently (K. Sharma, Sharma, and Sharma 2018).

1. The dye should have a broad absorption spectrum, to capture as much as possible of the solar radiation.
2. The dye should have higher extinction coefficient over the whole absorption spectrum, to absorb most of the light with a minimum of dye.
3. The dye must possess functional groups (-COOH, -H<sub>2</sub>PO<sub>3</sub>, -SO<sub>3</sub>H, etc.) to improve the chemical bonding with the semiconductor surface and work as bridges for electron injection.

4. The LUMO of the dye must slightly higher than the CB of MO semiconductor and the HOMO of the dye must have more positive potential than the redox couple in the electrolyte.
5. The dye should be soluble in some solvent for adsorption on the electrode and should not be desorbed by the electrolyte redox.
6. The photosensitizer should have chemical, thermal and electrochemical stability during exposure to solar radiation and in the electrolyte media.

Figure 2.6 shows the types of dyes which basically can be categorized into two groups namely natural and synthetic. Organic synthetic dyes include indoline and porphyrin (Ji *et al.* 2020). Inorganic synthetic dyes include ruthenium-based such as Z90Z, N719 and N3 (Kanakillam *et al.* 2021; Suhaimi *et al.* 2015). Due to the high efficiency and stability, Ruthenium-based dyes has been used for TiO<sub>2</sub> sensitization since DSSC invention, despite the fact that this component is one of the most expensive in DSSC (O'regan and Grätzel 1991; Shalini *et al.* 2015; Sanda *et al.* 2021; Ding *et al.* 2019; Mbaba, Golding, and Smith 2020). Besides, these dyes exhibit other disadvantages: noble metal scarcity, toxic raw materials, and sophisticated synthesis and purification steps (Shalini *et al.* 2015; Sharmoukh *et al.* 2018). Thus, an alternative organic dye such as natural dyes is suggested with similar characteristics with high absorption coefficients (Jinchu, Sreekala, and Sreelatha 2014).

Synthetic Ruthenium dyes are quite scarce so they will not be available for longer time span (Maurya *et al.* 2019; Ammar *et al.* 2019), however naturally occurring dyes can never get extinct even due to higher usage (K. Sharma, Sharma, and Sharma 2018). Comparing the efficiency of the two, natural dyes sensitizer exhibits lower efficiency because of the degradation (Sangiorgi *et al.* 2021; Zeng *et al.* 2020). Natural dyes show an absorption range from 400 to 700 nm (Semalti and Sharma 2020), whereas synthetic

dye such as N3 has an absorption up to 800 nm of solar spectrum (Kumar, Suresh, and Nagaraju 2004; Mehmood *et al.* 2014).

## 2.7 Natural dyes as photosensitizer

Natural dyes are environmentally safe, fully biodegradable, non-toxic, easy to prepare, cost effective and widely available (Hosseinnezhad *et al.* 2017)(Vishveshvar *et al.* 2018). They can be used to replace the more expensive and toxic synthetic dyes, although efficiency and stability still need improvement for this alternative to be considered. Kumara *et. al* (2017) points several advantages of natural dyes over synthetic ones:

- Simple preparation technique
- Low cost of production
- Complete biodegradation
- Easy access
- High availability
- Purity grade
- Environmental friendliness
- High reduction of noble metals usage

The natural dyes categorized in 5 group of anthocyanin (Richhariya *et al.* 2017), betalain (Wendel *et al.* 2017), flavonoid (Zdyb and Krawczyk 2019), carotenoid (A. Supriyanto, Nurosyid, and Ahliha 2018), and chlorophyll (Abdul Kariem Arof and Ping 2017). The first category is anthocyanin such as reddish and barley, the second category is betalain such as beetroot and amaranth leave, third category is flavonoid such as cherries and peltophorum, fourth category is carotenoid such as green algae and orange peel and the fifth category is chlorophyll such as turmeric.

Anthocyanin dye molecule consist of carbonyl and hydroxyl responsible for the colour pigment in visible red-to-blue spectrum (Lin *et al.* 2007). Teoli *et al* (2016), investigated natural dyes extracted from cherry, blackberry, blueberry, raspberry, and strawberry fruits for DSSCs. They obtained the highest efficiency of 1.13 % from the dye extracted from blueberry fruit. Hamadani *et al*, (2014) have studied several natural dyes as sensitizer include *reseda luteola*, *berberis integerrima*, *panica granatum pleniflora*, *consolida orientalis*, *reseda gredensis*, *clemetis orientalis*, *adonis flammea*, *salvia sclarea* and *consolida orientalis*. They observed that *consolida ajacis* is the best sensitizer compared to other dyes due to the fact that Delphinidin is the main pigment of *C. ajacis* and have good interaction between the hydroxyl groups of the Delphinidin and the TiO<sub>2</sub> surface (Hamadani *et al.* 2014). A. Lim *et al*, (2015) has reported the possibility of using dye extracted from skin of *canarium odontophyllum*, in DSSC. Three main groups of flavonoid pigments were detected from UV-vis absorption spectra. The highest conversion efficiency of 1.43% was obtained for cyaniding derivatives (Lim *et al.* 2015). Natural dyes extracted from purple cabbage, coffee, blueberry and turmeric DSSC have been reported by Syafinar *et al*, (2015). They reported that the combination of purple cabbage and blueberries as cocktail dye have the best DSSC performance. Dagher *et al*, (2014) reported the performance of DSSCs using natural dyes extracted from black cherry and hibiscus. The power conversion efficiencies of 0.45% and 0.54 % was obtained for hibiscus and black cherry respectively.

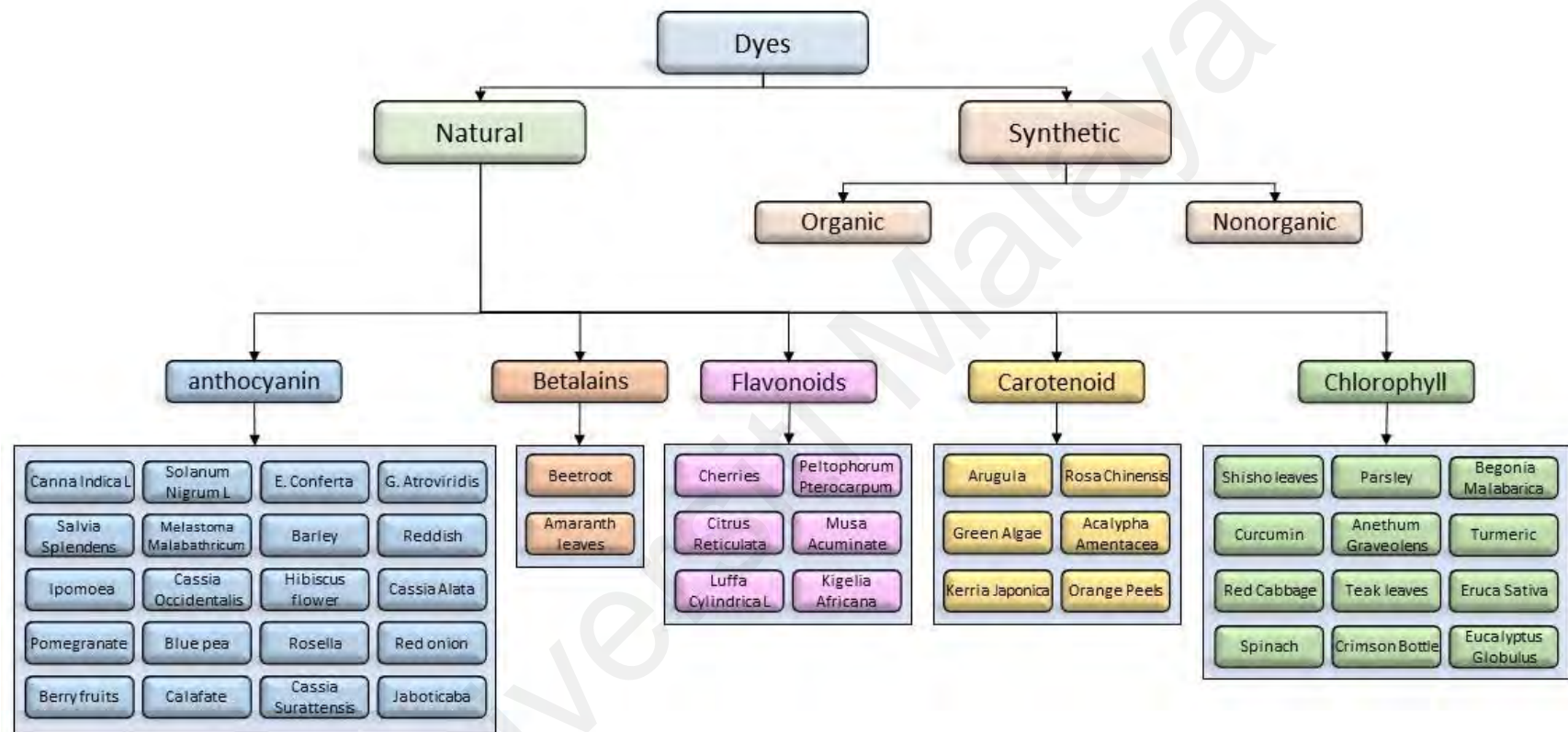


Figure 2.6. Organogram of natural pigments extracted from different fruits, flowers, seeds, leaves, and vegetables.

**Table 2.4.** Photovoltaic performance of DSSC utilizing various natural dyes as photosensitizer (M. Z. Iqbal, Ali, and Khan 2019).

NO.	Dye	J <sub>sc</sub> (mA/cm <sup>2</sup> )	V <sub>oc</sub> (V)	P <sub>max</sub> (mW/cm <sup>2</sup> )	FF	Efficiency (%)	Reference
1	Pomegranate juice	0.20	0.40	0.45	1.50	–	(Sirimanne <i>et al.</i> 2006)
2	Calafate extract	6.2	0.47	1.1	0.36	–	(Polo and Iha 2006)
3	Jaboticaba extract	9.0	0.57	1.7	0.42	–	(Polo and Iha 2006)
4	Shisonin and chlorophyll	4.80	0.53	–	0.51	1.31	(Kumara <i>et al.</i> 2006)
5	Shisonin	3.56	0.55	–	0.51	1.01	(Kumara <i>et al.</i> 2006)
6	Chlorophyll	3.52	0.43	–	0.39	0.59	(Kumara <i>et al.</i> 2006)
7	Crocin	2.84	0.43	–	0.46	0.56	(Yamazaki <i>et al.</i> 2007)
8	Crocin	0.45	0.58	–	0.60	0.16	(Yamazaki <i>et al.</i> 2007)
9	Rosella	1.63	0.40	–	0.57	0.37	(Wongcharee <i>et al.</i> , 2007)
10	Blue pea	0.37	0.37	–	0.33	0.05	(Wongcharee <i>et al.</i> , 2007)
11	Rosella & Blue pea mixture	0.82	0.38	–	0.47	0.15	(Wongcharee <i>et al.</i> , 2007)
12	Red cabbage in water extract	0.66	0.37	0.14	0.54	0.17	(Dumbravă <i>et al.</i> 2008)
13	Red cabbage in EtOH extract	0.58	0.36	0.11	0.52	0.14	(Dumbravă <i>et al.</i> 2008)
14	Red cabbage in MeOH extract	0.23	0.39	0.47	0.54	0.06	(Dumbravă <i>et al.</i> 2008)
15	Red onion in water extract	0.60	0.40	0.10	0.42	0.13	(Dumbravă <i>et al.</i> 2008)
16	Red onion in EtOH extract	0.53	0.39	0.95	0.45	0.12	(Dumbravă <i>et al.</i> 2008)
17	Red onion in MeOH extract	0.52	0.44	0.11	0.48	0.14	(Dumbravă <i>et al.</i> 2008)
18	<i>C. indica</i> L.	0.82	0.54	0.26	0.59	0.29	(Luo <i>et al.</i> 2009)
19	<i>S. splendens</i>	0.70	0.56	0.24	0.61	0.26	(Luo <i>et al.</i> 2009)
20	Cowberry	0.4	0.56	0.12	0.54	0.13	(Luo <i>et al.</i> 2009)
21	<i>S. nigrum</i> L.	1.01	0.54	0.28	0.51	0.31	(Luo <i>et al.</i> 2009)
22	Red cabbage and Curcumin (70:1)	0.81	0.53	0.30	0.69	0.60	(Furukawa <i>et al.</i> 2009)
23	Mulberry	6.10	0.49	1.60	0.52	–	(Patrocínio <i>et al.</i> 2009)
24	Blueberry	1.00	0.59	0.40	0.61	–	(Patrocínio <i>et al.</i> 2009)
25	Jaboticaba's skin	3.9	0.45	1.00	0.56	–	(Patrocínio <i>et al.</i> 2009)
26	Spinach	0.47	0.55	–	0.51	0.13	(Chang <i>et al.</i> 2010)
27	Ipomoea	0.91	0.54	–	0.56	0.28	(Chang <i>et al.</i> 2010)
28	Delonix regia liquid	1.33	0.30	–	0.39	0.317	(Senthil <i>et al.</i> 2011)
29	Delonix regia polymer	0.84	0.30	–	0.48	0.245	(Senthil <i>et al.</i> 2011)
30	Eugenia jambolana liquid	1.49	0.35	–	0.48	0.505	(Senthil <i>et al.</i> 2011)
31	Eugenia jambolana polymer	1.58	0.30	–	0.46	0.444	(Senthil <i>et al.</i> 2011)
32	<i>Ixora coccinea</i> on ZnO nanorode	2.65	0.21	–	0.29	0.33	(Thambidurai <i>et al.</i> 2011)
33	Mulberry on ZnO nanorode	2.90	0.23	–	0.30	0.41	(Thambidurai <i>et al.</i> 2011)
34	Beetroot on ZnO nanorode	2.30	0.20	–	0.30	0.28	(Thambidurai <i>et al.</i> 2011)
35	<i>K. japonica</i>	0.5597	0.5839	–	0.68	0.22	(Hemalatha <i>et al.</i> 2012)
36	<i>K. japonica</i> with sugar	0.7509	0.5526	–	0.70	0.29	(Hemalatha <i>et al.</i> 2012)
37	<i>R. chinensis</i>	0.8017	0.5433	–	0.66	0.29	(Hemalatha <i>et al.</i> 2012)
38	<i>R. chinensis</i> with sugar	0.7025	0.5373	–	0.69	0.27	(Hemalatha <i>et al.</i> 2012)
39	Bahraini Henna	0.368	0.426	–	0.24	0.128	(Jasim 2012)
40	Yemeni Henna	0.407	0.306	–	0.28	0.117	(Jasim 2012)
41	Cherries	0.466	0.305	–	0.38	0.181	(Jasim 2012)
42	Pomegranate juice	1.70	0.395	–	0.48	1.07	(Jasim 2012)
43	Raspberries	0.566	0.360	–	0.45	0.309	(Jasim 2012)
44	<i>Eruca sativa</i>	2.90	0.62	–	0.40	0.72	(Abdel-Latif <i>et al.</i> 2013)
45	<i>Eruca sativa</i> with LiI electrolyte	4.6	0.64	–	0.54	1.6	(Abdel-Latif <i>et al.</i> 2013)
46	Dried Spinach with TiO <sub>2</sub>	1.11	0.583	0.301	0.46	0.29	(Taya <i>et al.</i> 2013)
47	Teak	0.29	0.460	0.105	0.79	–	(Kushwaha, Srivastava, and Bahadur 2013)
48	Hibiscus (Red)	0.765	0.515	–	0.47	0.19	(Mulati <i>et al.</i> , 2012)
49	<i>Dianthus barbatus</i>	0.53	0.58	0.14	0.48	0.15	(Taya <i>et al.</i> 2015)
50	<i>L. cylindrica</i> L.	0.44	0.52	0.13	0.60	0.13	(Maurya <i>et al.</i> , 2016)
51	Pomegranate	12.20	0.39	–	0.41	2.00	(Ghann <i>et al.</i> 2017)
52	Henna extract with TiO <sub>2</sub> nanoparticles	1.63	0.40	–	–	1.08	(Sathyajothi, Jayavel, and Dhanemozhi 2017)
53	Beetroot extract with TiO <sub>2</sub> nanoparticles	1.7	0.46	1.3	–	1.3	(Sathyajothi, Jayavel, and Dhanemozhi 2017)
54	<i>P. amaryllifolius</i> extract	0.4	0.55	0.1	0.61	0.1	(Al-Alwani <i>et al.</i> 2017)
55	<i>C. tora</i>	0.06	0.29	–	0.72	0.013	(Maurya <i>et al.</i> 2018)
56	<i>C. surattensis</i>	0.13	0.47	–	0.74	0.046	(Maurya <i>et al.</i> 2018)
57	<i>C. alata</i>	0.16	0.80	–	0.95	0.122	(Maurya <i>et al.</i> 2018)
58	<i>C. occidentalis</i>	0.20	0.83	–	0.90	0.150	(Maurya <i>et al.</i> 2018)

**Table 2.4, continued.**

59	A. amentacea+P. pterocarpum in Water	14.19	0.809	–	0.64	7.38	(Sanjay <i>et al.</i> 2018)
60	A. amantacea+P. pterocarpum in Ethnl.	14.95	0.834	–	0.65	8.22	(Sanjay <i>et al.</i> 2018)
61	E. conferta	4.63	0.37	–	0.56	1.00	(Jaafar, Ain, and Ahmad 2018)
62	G. atroviridis	2.55	0.32	–	0.63	0.51	(Jaafar, Ain, and Ahmad 2018)
63	Red beans	–	0.84	–	0.56	0.40	(P. K. Singh, Bhattacharya, and Khan 2018)
64	Orange peel	–	0.76	–	0.49	0.25	(P. K. Singh, Bhattacharya, and Khan 2018)
65	Barley grass	–	0.69	–	0.60	0.18	(P. K. Singh, Bhattacharya, and Khan 2018)
66	Gallocatechin (1.5 pH)	1.87	0.50	–	0.47	0.44	(Prima <i>et al.</i> 2017)
67	Hesperidin (1.5 pH)	3.23	0.48	–	0.45	0.71	(Prima <i>et al.</i> 2017)
68	Dry Turmeric in Acetone	0.40	0.53	–	0.51	0.10	(Ruhane <i>et al.</i> 2017)
69	Dry Turmeric in Ethanol	0.81	0.50	–	0.29	0.12	(Ruhane <i>et al.</i> 2017)
70	Dry Turmeric in Methanol	0.65	0.57	–	0.44	0.16	(Ruhane <i>et al.</i> 2017)

### 2.7.1 Dye preparation

There are many reported protocols for both steps in the available literature. Some are simple, others require special equipment and more time-consuming techniques. In general, the preparation of natural dyes requires 2 basic steps:

1. Plant processing to obtain an extract, which may involve the dissolution in a solvent (usually water and/or alcohol).
2. Extract filtration and purification. Frequently, paper filtering and centrifugation but may include others like chromatography and lyophilization.

Extraction is a very important step in isolating and identifying plant pigments and no single or standard method of extraction is available (Amogne, Ayele, and Tsigie 2020). Fruits, vegetables, flowers, and leaves may be ground, dried, or lyophilized, and some fresh plants may be soaked to extract phenolic compounds (Xie *et al.* 2017) (Sinopoli, Calogero, and Bartolotta 2019).

Mehmood *et al.* 2020, used a drying step at ambient temperature to transform Curcumin extract in a glass like residue for dissolution in methanol. Leyer *et al.* 2018

dried, ground and sieved maqui berry and blackberry fruits for later dissolution in water. This technique can eliminate water from the plant easier. Silva *et al.* (2017) did not use drying step during plant processing but included chromatography for purification of carotenoid and anthocyanin extracted from mondo-grass berries and blackberries (DeSilva *et al.* 2017). They also kept the extract and pulp in the refrigerator for 24h for saturation.

Gusti *et al.* (Gusti *et al.* 2021) purified the filtrated dye from *Melastoma malabathricum* fruit with a rotary evaporator to obtain thick extracts. Several solvents can be used during dye extraction from plants, the most commons are water, ethanol, methanol, and organic acids. Iqbal *et al.* (2020) states that the chosen solvent will impact on the dye adsorption and the cell performance. Kumara *et al.* (2017) also highlights the importance of solvents including acidity, polarity and temperature during the extraction of dye. The polarity of the solvent need to match the compound for efficient extraction (P. K. Singh *et al.* 2018). Hossain *et al.* (2017) applied five distinct types of solvents for the extraction turmeric and reported that the DSSC performance was obtained for 2h adsorption time of dye on TiO<sub>2</sub> nano-porous surface with ethanol extracted dye from dry turmeric (Hossain *et al.* 2017).

For the extract purification step, a wide range of techniques have been investigated, ranging from solid phase (SPE) and liquid–liquid (LLE) extractions to the use of sophisticated chromatographic techniques such as counter current chromatography (Schwarz *et al.* 2003; Wybraniec *et al.* 2009), medium-pressure liquid chromatography (MPLC) and High Performance Liquid Chromatography (HPLC) (Wybraniec *et al.* 2009). HPLC with UV–Vis or photodiode array (PDA) detectors is the most common method used to separate anthocyanin (Sinopoli, Calogero, and Bartolotta 2019). High-performance liquid chromatography, also known as high-pressure liquid chromatography,

is an analytical chemistry technique for separating, identifying, and quantifying individual components in a mixture.

### 2.7.2 Blackberry

The blackberry is a fruit from the Rosaceae family that existed in many species. The worldwide production of the blackberry is estimated 154,578 tons every year. Blackberry is an edible fruit that consumed in different forms such as, quick frozen packs, bulk frozen, seedless or seeded puree, freeze-dried, and dried fruit which used in this study (Strik 2007). Many countries produce blackberry as the daily based use fruits like, America, Australia, and Europe. Blackberry has high amount of anthocyanins as well as other phenolic components which subsidize into its high antioxidant volume (Cho *et al.* 2004). Blackberry has medicinal usage to treat infections of the mouth and eyes due to the presence of high antioxidant activity in 16<sup>th</sup> century (Dai, Patel, and Mumper 2007). Figure 2.7 shows the fresh blackberry fruit that had been used in this study.



**Figure 2.7.** Fresh blackberry fruit.

The phenolic component of blackberry is anthocyanin that responsible for the red to black color of the fruit (Leyrer *et al.* 2018). Dyes with  $-\text{COOH}$  or  $-\text{OH}$  functional groups that attach to  $\text{TiO}_2$  nanoparticles via metal complexation cause electron transfer from the dye molecules to the  $\text{TiO}_2$  conduction band (Patrocínio *et al.* 2009; Ramamoorthy *et al.* 2016).

Anthocyanin classified as the flavonoid and can be found in berries and red grapes (Cho *et al.* 2004). The chemical structure of the blackberry anthocyanin showed in the Figure 2-8.

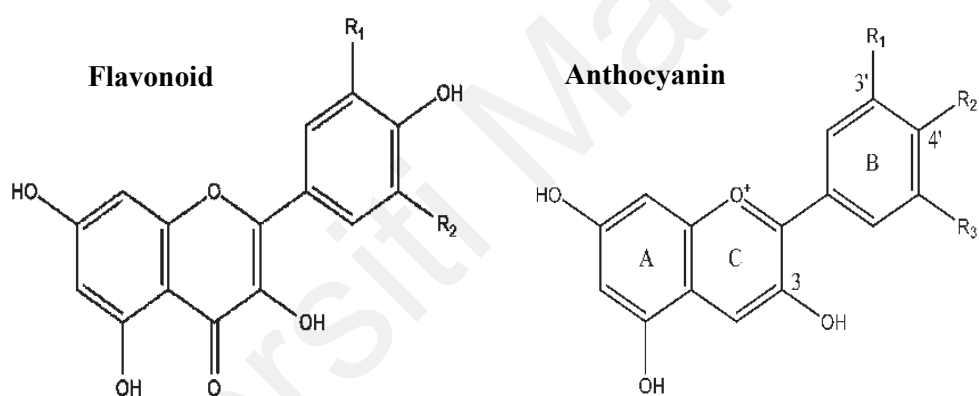


**Figure 2.8.** Chemical structure of Blackberry Flavonoid and Anthocyanin (Kaume, Howard, and Devareddy 2012).

Blackberry anthocyanins include cyanidin 3-glucoside, cyanidin 3-galactoside, cyanidin 3-xyloside, cyanidin 3-dioxalyl-glucoside, cyanidin 3-rutinoside, cyanidin 3-sophoroside, cyanidin 3-glucosylrutinoside, cyanidin 3-arabinoside, malvidin 3-arabinoside, pelargonidin 3-glucoside, cyanidin 3-(3-malonyl)glucoside, and cyanidin 3-(6-malonyl)glucoside.40,41 Cyanidin 3-dioxaloylglucoside, and zwitterionic anthocyanin components which are is exceptional to blackberries (Kaume, Howard, and Devareddy 2012).

### 2.7.3 Blueberry

Blueberry is one of the world's famous fruits from Ericaceae family. Blueberry contain phenolic components such as anthocyanin and flavonoids with bioactivity like antioxidant (Koca and Karadeniz 2009). Blueberries can be consumed in fresh, frozen dried or dried types. Based on the study, total flavonoid and anthocyanin of blueberry had been measured to  $96.0 \pm 0.96$  mg/100 and  $360.0 \pm 0.76$  mg/100 respectively (Diaconeasa *et al.* 2015).

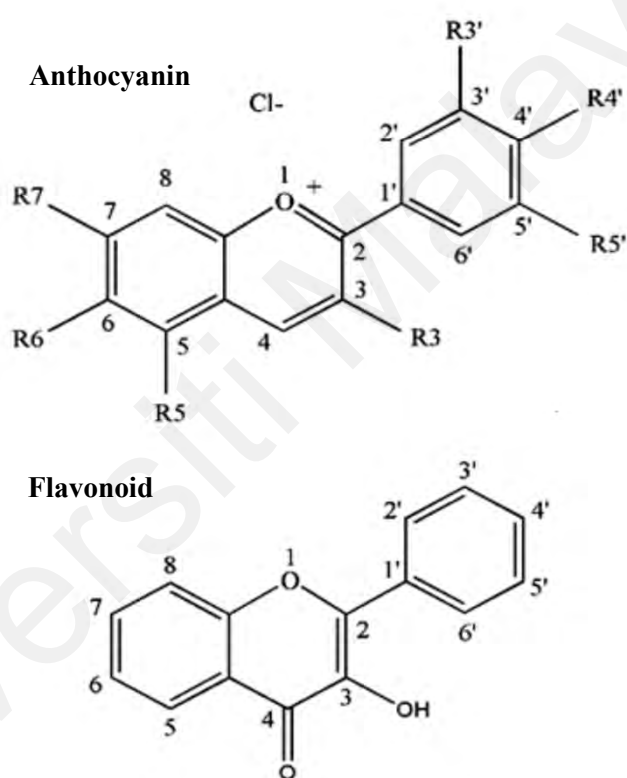


**Figure 2.9.** Chemical Structure of Blueberry Anthocyanin and Flavonoid (Miles and Schilder 2013).

Figure 2.9 indicates the chemical structure of flavonoid and anthocyanin of blueberry. The image of fresh blueberry before drying procedure shown in Figure 2-10.



**Figure 2.10.** Fresh Blueberry fruit.

#### **2.7.4 Dragon fruit**

Dragon fruit is form the Cactoideae of the tribe Cacteae family (Freitas and Mitcham 2013). Dragon fruit or pitaya has gained popularity in many countries over the world because of the bright red (figure 2.11) skin with overlapping green fins all over the fruits (Ruzainah *et al.* 2009). There are three varieties of the dragon fruits which are, red-skinned fruit with red pulp called red pitaya, red-skinned fruits with white pulp called red pitaya too and yellow skinned fruit with white pulp called yellow pitaya (Choo and Yong 2011).



**Figure 2.11.** Fresh dragon fruit.

Due to the antioxidative activity of the dragon fruit, it drawn more attention for its growth (Rebecca, Boyce, and Chandran 2010; Esquivel, Stintzing, and Carle 2007; Nurliyana *et al.* 2010). Betanin, phylloactin, hylocerenin, and betacyanin with 5-O-glycosides or 6-O-glycosides have been discovered in many species of the Cactaceae family (Herbach *et al.* 2006). These types of compounds are responsible for many pharmacological activities such as antitumor, antioxidant, and anti-inflammatory actions (Herbach, Stintzing, and Carle 2005). Figure 2.12, indicate the chemical structure of Betanin of dragon fruit.

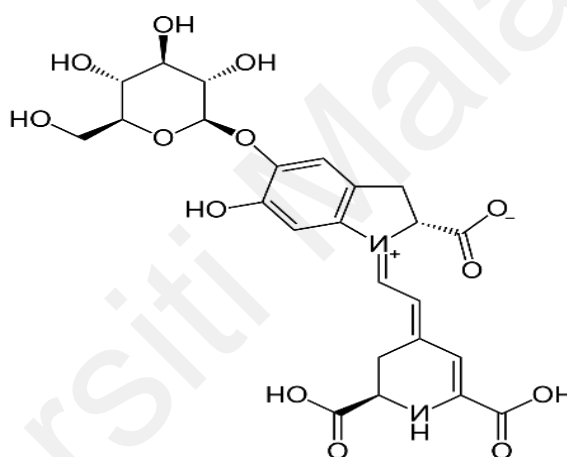


**Figure 2.12.** Chemical structure of Betanin.

### 2.7.5 Raspberry

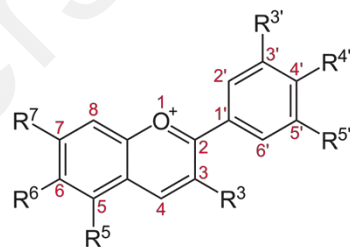
Raspberries are from rose family. There are various types of raspberries such as black, purple, golden and red raspberries or *Rubus Idaeus*. Raspberry mostly cultivate in the temperate areas so as Europe and North Asia (Middleton, Kandaswami, and Theoharides 2000). Figure 2.13 shows the fresh Raspberry fruit that used in this study.



**Figure 2.13.** Fresh Raspberry fruit.

In addition to containing vitamin C, raspberries have high antioxidant levels which include two components of anthocyanins and ellagitannins. Figure 2.14 Shows the chemical structure of anthocyanin and chemical structure of Raspberry ellagitannin (Beekwilder *et al.* 2005).

**Anthocyanin**



**Ellagitannin**

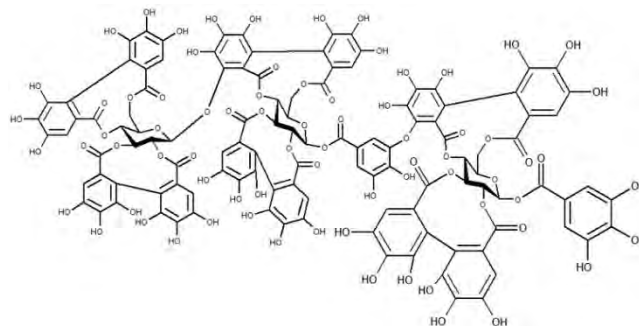


**Figure 2.14.** Chemical structure of Anthocyanin and Ellagitannin of Raspberry.

### 2.7.6 Saffron

Saffron is a spice from the flower of *Crocus sativus* known as red gold that is collected and dried to be used as food coloring, fragrance, and medicine. The cultivation and use of saffron are more than 3500 years that extended to cultures and countries. Saffron has a bitter taste, hay-like fragrance (Cardone *et al.* 2020). Saffron cultivates are in Iran, Greece, Asia, India, Italy, Morocco, Spain, Switzerland, and Turkey. However, Iran and Spain are known as the main saffron producers (Tashakkori *et al.* 2021). As shown in Figure 2.15, the saffron flower contained stigma, petal, stem and corm which stigmas are the important part that known as saffron (Hassan-Beygi *et al.* 2010).

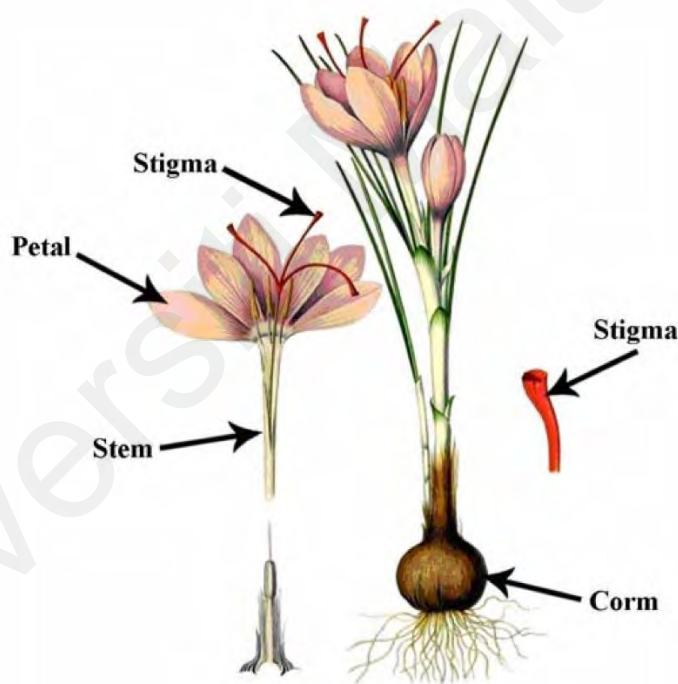


**Figure 2.15.** Saffron flower's structure.

Saffron has three components that each represent a feature of saffron. Safranal, Crocin and picrocrocin. Safranal with scientific name of 2,6,6-trimethyl-1,3-cyclohexadiene-1-carboxaldehyde is responsible for the aroma of saffron (Kanakis *et al.* 2004). Picrocrocin with scientific name of 4-( $\beta$ -D-glucopyranosyloxy)-2,6,6-trimethyl-1-cyclohexene-1-carboxaldehyde is responsible for the bitter taste of saffron (Sánchez *et al.* 2008). And

Crocin with the scientific name of Bis [(2*S*,3*R*,4*S*,5*S*,6*R*)-3,4,5-trihydroxy-6-({[(2*R*,3*R*,4*S*,5*S*,6*R*)-3,4,5-trihydroxy-6-(hydroxymethyl) tetrahydro-2*H*-pyran-2-yl]oxy}methyl) tetrahydro-2*H*-pyran-2-yl] (2*E*,4*E*,6*E*,8*E*,10*E*,12*E*,14*E*)-2,6,11,15-tetramethyl-2,4,6,8,10,12,14-hexadecaheptaenedioate is responsible for the color of saffron (Scalzo, Todaro, and Rapisarda 2012). These three components are found in the flowers *crocus sativus* (Zareena *et al.* 2001). Carotenoid is crocetin, which has a carboxylic group on its molecule and Crocetin is a natural carotenoid dicarboxylic acid that is found in the crocus flower and *Gardenia jasminoides* (Hug *et al.* 2014). The structure of safranal, crocin, picrocrocin, and crocetin are shown in Figure 2.16. Figure 2.17 shows the saffron stigma that used in this study.

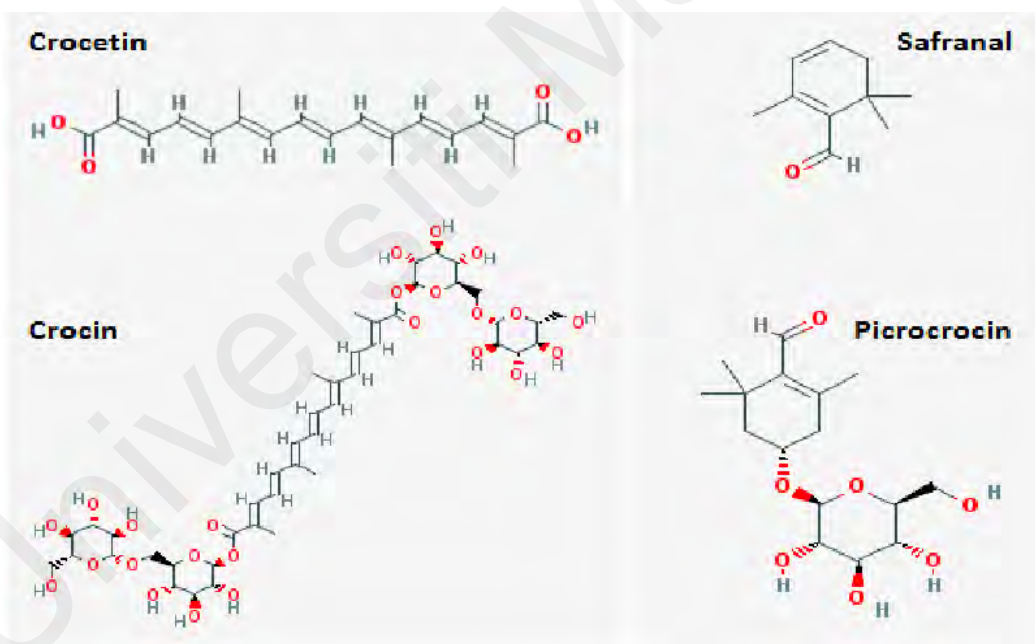


**Figure 2.16.** The structure of Crocetin, Safranal. Crocin and Picrocrocin of saffron (Mashmoul *et al.* 2013).



**Figure 2.17.** Fresh saffron stigma.

### 2.7.7 Anthocyanin

Anthocyanin is a pigment that uses broad band gap semiconductor sensitization. Several hues, including those in the purple-red spectrum, show how anthocyanin provides plants' flowers, fruit, and leaves their colors. As shown in Figure 2-18 (a), the carbonyl and hydroxyl groups will be bound to the surface of  $\text{TiO}_2$  and stimulate the transfer of electrons from the sensitizer to the conduction band of the surface of  $\text{TiO}_2$  (Figure 2-18 (b)). Due to charge transfer transitions from HOMO (Highest occupied molecular orbital) to LUMO, anthocyanins exhibit a broad absorption band in the visible area (Lowest unoccupied molecular orbital) (Alhamed, Issa, and Doubal 2012; Syafinar *et al.* 2015).

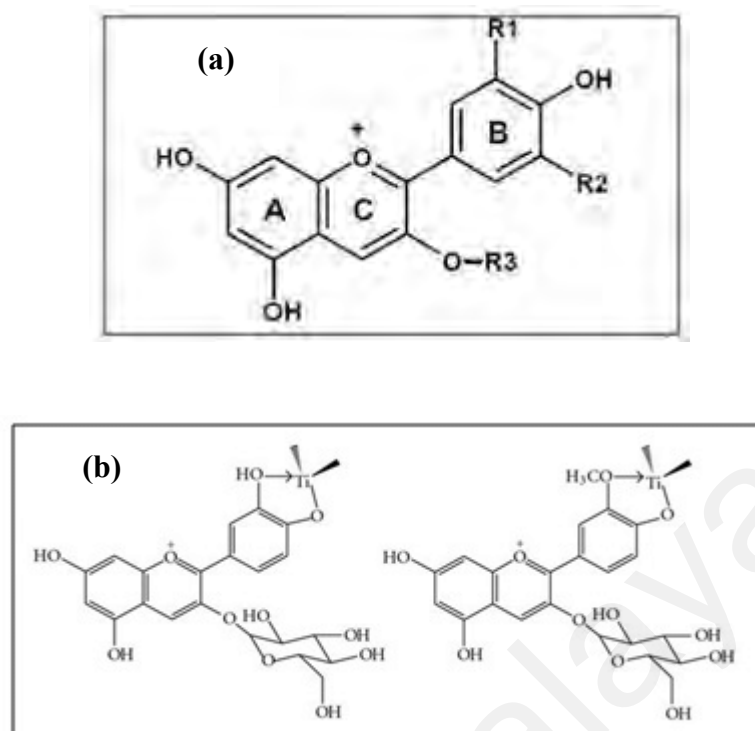


**Figure 2.18.** Structure of anthocyanin pigments and the binding between anthocyanin molecule and TiO<sub>2</sub> particle (Alhamed, Issa, and Doubal 2012).

### 2.7.8 Carotenoid

Figure 2-19 represent several carotenoids with various functional groups were chosen, including 7'-apo7'-(4-carboxyphenyl)- $\beta$ -carotene (1), 8'-apo- $\beta$ -caroten-8'-oic acid (2), 8'-apo- $\beta$ -caroten-8'-aldoxime (3), 8'-apo- $\beta$ -caroten-8'-al (4), and canthaxanthin (5). Carboxylate groups can substitute OH groups at the TiO<sub>2</sub> surface and chemically connect to surface Ti atoms, according to infrared measurements 6a,7,23. Therefore, it was anticipated that carotenoids with terminal -CO<sub>2</sub>H groups would have a high interaction with the semiconductor surface (Konovalova, Kispert, and Konovalov 1999; Li *et al.* 2018).

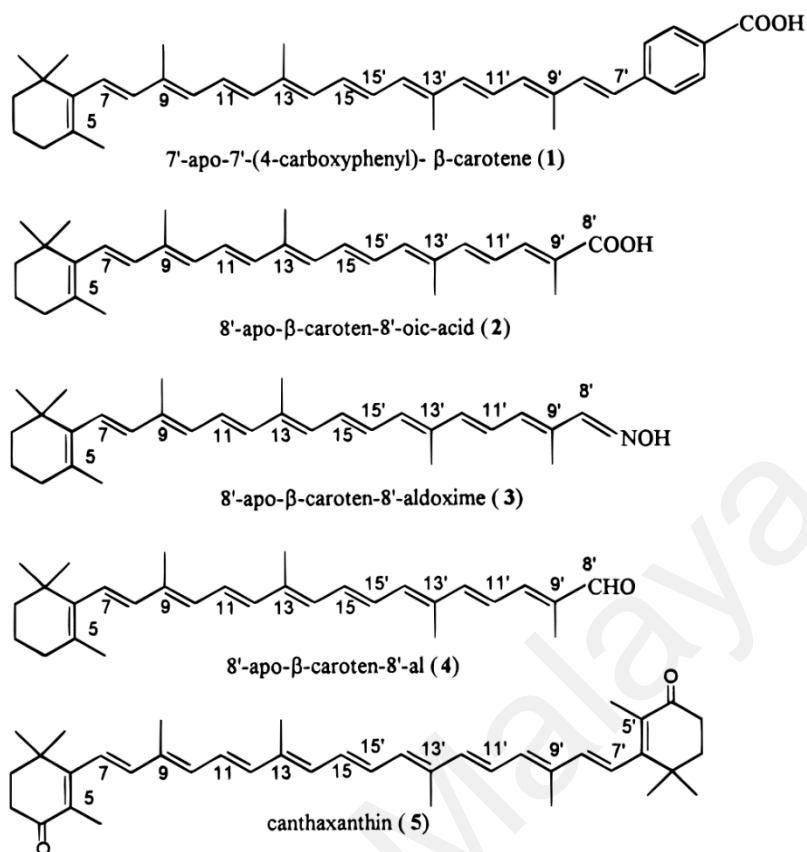


**Figure 2.19.** Several carotenoids with different functional group (Konovalova, Kispert, and Konovalov 1999).

## 2.8 Summary of the chapter

In this section the fundamentals of solar cells as well as its various types, and the DSSCs have been introduced as an advanced structure of a solar cell demonstrated. In continue, various sections of the DSSCs have been reviewed. Various types of the applied dyes and electrolytes have also been reviewed.

- Introduction
- Solar cell
- Dye sensitized solar cells
- Main component of the DSSC

- Working principle of DSSC
- Electrolytes
- Liquid electrolytes
- Solid electrolytes
- Gel electrolytes
- Counter electrolyte
- Photoanode
- Substrate (FTO glass)
- Mesoporous TiO<sub>2</sub> nanoparticles film
- Dyes
- Natural dyes as photosensitizer
- Dye preparation
- Plant processing
- Extract purification
- Blackberry
- Blueberry
- Dragon fruit
- Raspberry
- Saffron
- Anthocyanin
- Carotenoid

## CHAPTER 3: RESEARCH METHODOLOGY

### 3.1 Introduction

In this section, firstly, the applied materials for this research have been introduced. Furthermore, the explanation of different methods that were applied for preparation of the elements of experiment such as dyes, gel polymer electrolytes, preparation of TiO<sub>2</sub> layers and photo electrodes, preparation of Pt counter electrode, fabrication, and characterization of DSSCs are presented. In continue, the procedure and conditions for each applied analysis method have been precisely described. The applied analysis methods include X-ray diffraction (XRD), Fourier-transform infrared spectroscopy (FTIR), J-V characteristics, Electrical impedance spectroscopy (EIS), intensity-modulated photocurrent spectroscopy (IMPS), and intensity-modulated photovoltage spectra (IMVS). Finally, the DSSCs assembly and its conditions have been detailed in this section. Figure 3.1 represent the methodology flowchart of this investigation.

### 3.2 Materials

All materials that have been used for preparation of the samples and analyses include Iodine (I<sub>2</sub>), potassium iodide (KI), ethanol, poly vinyl alcohol (PVA), 4. tert-Butyl pyridine (TBP), dimethyl formamide (DMF) and dimethyl sulfoxide (DMSO) were purchased from sigma Aldrich. Saffron was purchased form a saffron farm in Torbat Jam city, Khorasan Razavi province, Iran. All fresh fruits include Blackberry, Blueberry, Dragon, and raspberry were purchased from a local market (Village grocer) in Malaysia and were used as received.

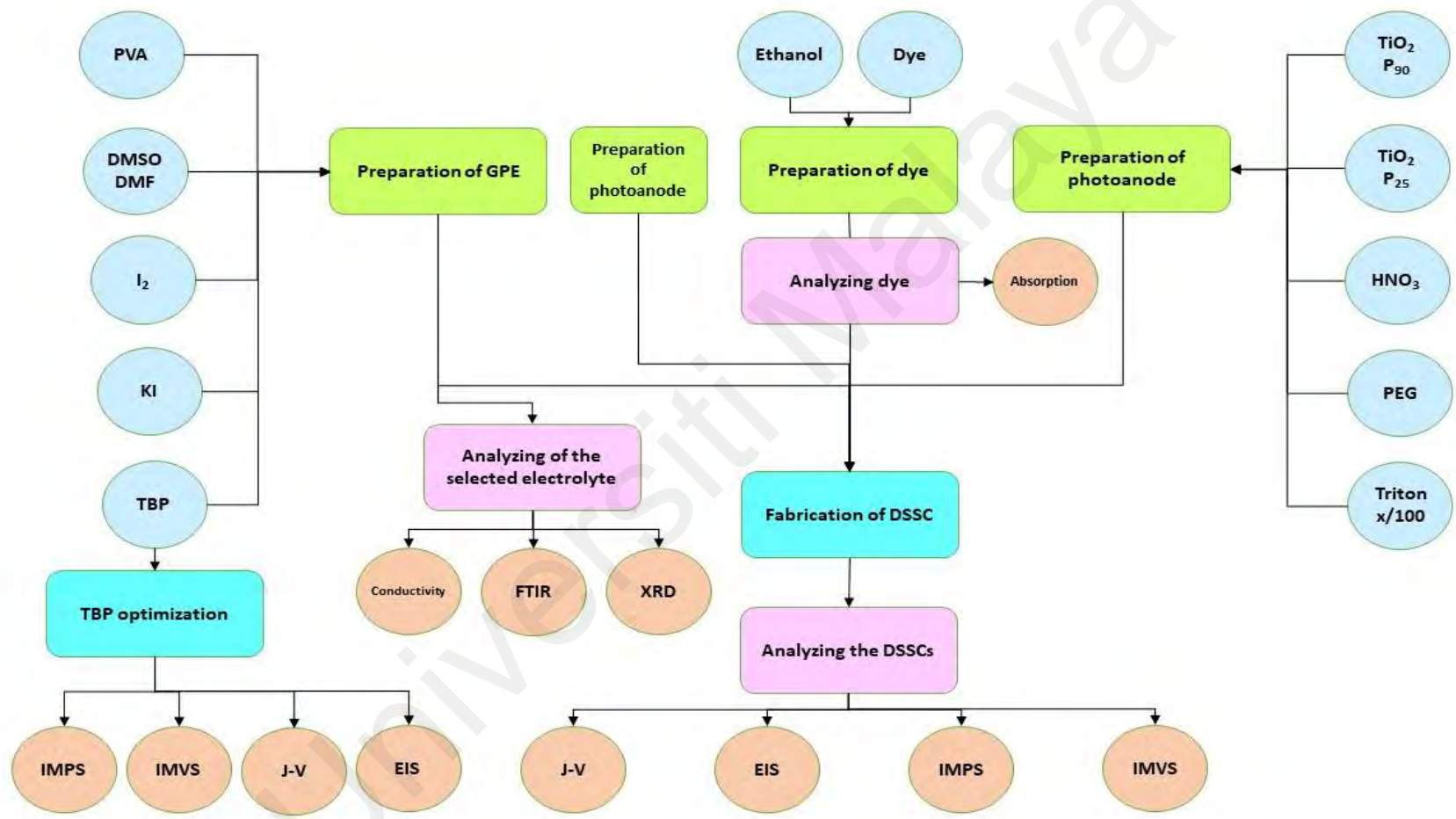


Figure 3.1. Methodology flowchart of this research.

### 3.3 Preparation of the dyes

#### 3.3.1 Drying process

During this process, the fruits and flowers were washed with distilled water and dried in two steps. First, they were placed on a hot plate during the daytime, at 40 °C, and second, in a climate chamber, at 40 °C, at night until they were fully dried. The weight of each sample, before and after drying as well as the required time for the drying process were recorded. Table 3.1 represents the weight of the samples and their corresponding times for the drying process. The saffron sample was purchased in the dry form and no drying process was required for this sample.

**Table 3.1.** Time and weight of the fruits before and after drying.

Name	Drying time (h)	Weight before (g)	Weight after (g)
Raspberry	18	101.23	10.63
Blackberry	24	102.89	10.02
Blueberry	144	100.09	16.84
Dragon fruit	100	182.25	9.12
Saffron	-	-	-

#### 3.3.2 Dye extraction

After drying process, in order to extract the dye from the samples, the fruits and saffron stigma were grounded in a mixer to a powder form. Powder forms would speed up the extraction process. Then, they were mixed with ethanol with the ratio of 1:50 (1 gram of the dried fruits: 50 ml of ethanol). The mixture was then stirred on a magnet stirrer at room temperature for 24 hours. Next, the mixtures were centrifuged to get a clear and homogeneous solution.

### 3.4 Preparation of gel polymer electrolytes

The applied PVA-based gel polymer electrolyte was prepared based on the previous work (Shamsuddin *et al.* 2017). First, 0.611g of potassium iodide was mixed with 2g of DMF/DMSO and the mixture has been stirred for 1h at the room temperature. Then, 0.1g of PVA polymer was added to the mixture and stirred at 120 °C for about 4h until the mixture became homogenous and viscous. During the cooling procedure, 0.042g of I<sub>2</sub> and 0.05M TBP were added and stirred for about 30 mins. GPEs having 0.05M of TBP have also been prepared to obtain a better performance in DSSC (Ji *et al.* 2020). All the electrolytes were kept in a desiccator over night before being used.

**Table 3.2.** The composition of GPEs.

Electrolyte	DMF (g)	DMSO (g)	I <sub>2</sub> (g)	PVA (g)	KI (g)	TBP (M)
A	2	-	0.0042	0.1	0.611	-
B	2	-	0.0042	0.1	0.611	0.05
C	-	2	0.0042	0.1	0.611	-
D	-	2	0.0042	0.1	0.6111	0.05

### 3.5 Preparation of photoanode

#### 3.5.1 Cleaning process of FTO glasses

FTO glasses were cut in 1cm × 2cm pieces and they being soaked in a soap and water solution for 20 minutes. All the glasses then washed individually with a tissue to remove any dirty and rinsed and soaked in distilled water again with 2 drops of nitric acid for 10 minutes. At last, the FTO glasses were soaked in isopropanol alcohol and boiled until the bobbles appeared. After cooling down, they were removed from the alcohol and let it dry.

### 3.5.2 Preparation of conductive layers of TiO<sub>2</sub> (photoanode)

TiO<sub>2</sub> photoanode consists of two layers of titanium dioxide with different particle size. The first layer of photoanode was prepared by grinding 0.5g P90 TiO<sub>2</sub> with mortar and pestle. Then, 2mL of nitric acid were added to the TiO<sub>2</sub> powder and grounded to form a paste. The paste was coated on the FTO glasses using spin coat with 3000 rpm. Next, the glasses were sintered at 450 °C for 30 minutes. For the second layer, 0.5g TiO<sub>2</sub> (P25) were grounded with mortar and pestle, then 2mL of nitric acid were added to the powder. 0.25g of PEG and two drops of triton x-100 as surfactant were added. After mixing all the material, the paste was grounded to get a homogenous mixture with soft and smooth texture. Finally, the prepared paste was coated on to FTO glass with one layer of TiO<sub>2</sub> using doctor blade method. The coated FTO glasses were sintered for 30 minutes at 450 °C (Wongcharee *et al.*, 2007). Electron recombination at the FTO/TiO<sub>2</sub> interface can be prevented by applying a compact layer to the FTO substrate before the mesoporous oxide coating. This so-called blocking layer prevents the electrolyte from making physical contact with the FTO surface, reducing the likelihood of triiodine reduction by photoinjected electrons (Patrocínio, Paterno, and Iha 2010). The TiO<sub>2</sub> second layer provide better surface to adsorbed dyes due to the porosity of the second layer (Rho *et al.* 2015).

### 3.5.3 Sensitizing of the photoanode

The prepared photoanodes was heated to 100 °C for 10 mins. After 10 mins when the photoanodes reach the room temperature they were soaked in dye solution for 24h.

### 3.6 Preparation of Pt counter electrode (Cathode)

To prepare the Pt counter electrode, the plastisol solution was brushed on the conductive side of the FTO glasses at 120 °C on a hot plate. The coating was continued

until all the surface of the glass covered by a thin layer of plastisol. The provided electrode was sintered at 450 °C for 30 minutes.

### **3.7 DSSCs fabrication**

The photoanodes were removed from the dye and washed with absolute ethanol to remove any sprinkles of dyes on the electrodes and then dried with hair dryer to avoid any stain on the glass. Next a thin layer of gel polymer electrolytes coated on the surface of TiO<sub>2</sub> and dye. Then the Pt counter electrode placed faced down on the GPE layer and the glasses clipped on both sides to avoid the glasses from slipping. Figure 3.2 shows the fabricated DSSC.



**Figure 3.2.** Image of the assembled DSSCs.

### **3.8 Characterization**

#### **3.8.1 Characterization of gel polymer electrolyte**

The ionic conductivity, X-ray diffraction (XRD) and Fourier transform infrared spectroscopy (FTIR) experiments have been performed.

### 3.8.1.1 Ionic Conductivity

Impedance spectroscopy of GPE were performed using HIOKI 3532-50 LCR Hi-Tester in the frequency range of 50Hz to 5MHz. To find the conductivity, GPEs were filled into the coin cell which was sandwiched in between two stainless steels. The bulk resistance,  $R_b$  was obtained from the impedance plot and the ionic conductivity can be calculated from equation (3.1).

$$\sigma = \frac{t}{R_b A} \quad (3.1)$$

Here A is the area which is  $3.14 \text{ cm}^2$  and t is the thickness of 0.16 cm (Shamsuddin *et al.* 2017).

### 3.8.1.2 X-Ray Diffractometer (XRD)

The XRD was performed by Olumpus BTX-II Benchtop x-ray diffraction, from intensity of 0 to 400 and  $2\theta$  angles of  $5^\circ$  to  $55^\circ$  with 30 kV accompanied by 0.35 mA using Cu  $K\alpha$  radiation at  $0.05^\circ$  step size (Shamsuddin *et al.* 2017; Buraidah *et al.* 2016).

### 3.8.1.3 FTIR

FTIR spectra were performed in the range of wavenumber from 4000 to  $650 \text{ cm}^{-1}$  during 64 scans, with  $2 \text{ cm}^{-1}$  resolutions (Paragon 1000, PerkinElmer, USA). The FTIR spectra were normalized, and major vibration bands were associated with chemical groups.

## 3.8.2 Characterization of DSSCs

The characterization of DSSCs were performed using solar simulator and metrohm autolab (Metrohm Autolab B.V. PGSTAT 128N Netherlands) connected to the computer with software Nova 1.11. Figure 3.3 shows the solar simulator and Metrohm lab.



**Figure 3.3.** Solar simulator with reference cell positioned for testing.

### 3.8.3 Photovoltaic characteristics

The photovoltaic characteristics of the cells were measured under solar simulator with intensity of  $100 \text{ mW cm}^{-2}$  (AM 1.5). An external bias was applied to the cells and the generated photocurrent was measured. Short circuit current density,  $J_{sc}$  and open circuit voltage,  $V_{oc}$  were obtained from the  $J$ - $V$  curve characteristic. Figure 3.4 shows an example of  $J$ - $V$  curve characteristic of a DSSC under illumination.  $J_{sc}$  is dependent on several factors such as the light intensity, light absorption, injection efficiency and regeneration of the oxidized dye.  $J_{sc}$  is obtained when voltage is equal to zero. The  $V_{oc}$  is measured when the current through the cell is equal to zero (open circuit).

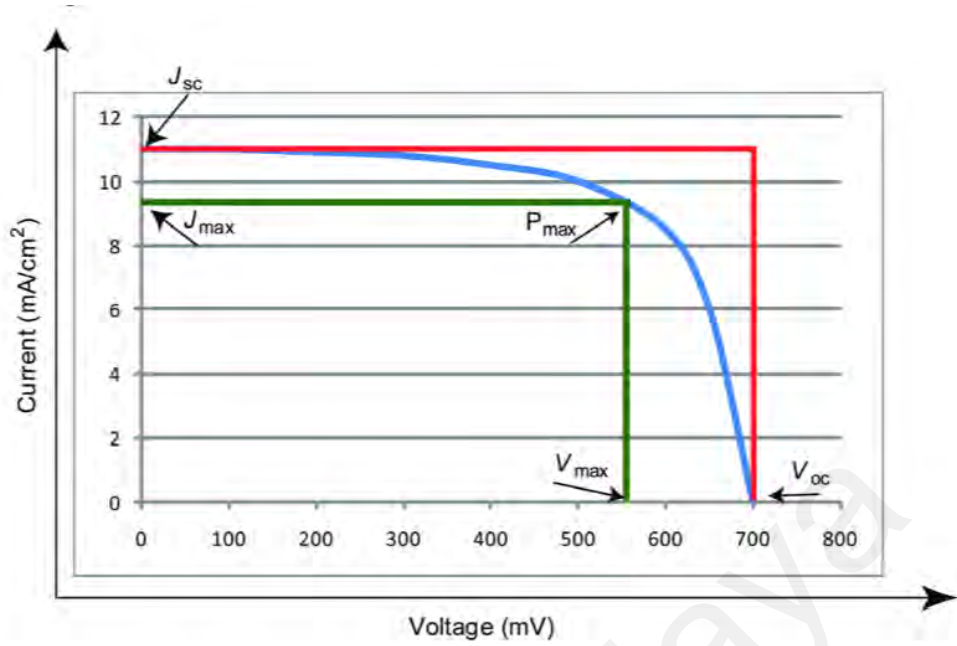


**Figure 3.4.** Illustration of  $J$ - $V$  characteristics of a solar cell. Blue line: measured current-voltage curve. Red line: area of  $V_{OC} * J_{SC}$ . Green line: area of  $V_{max} * J_{max}$ .

The fill factor,  $FF$  measures the ideality of the device and is defined as the ratio of the maximum power output per unit area to the product of  $V_{oc}$  and  $J_{sc}$  (area within the green square divided by the area of the red square in Figure 3.4). Several factors can influence the  $FF$ , such as a high inner resistance (e.g., a bad counter electrode), which will give a low fill factor and a decreased overall efficiency. The  $FF$  can be calculated by using equation (3.2).

$$FF = \frac{V_{max} J_{max}}{V_{oc} J_{sc}} \quad (3.2)$$

The overall solar energy to electricity conversion efficiency,  $\eta$  of a solar cell is defined as the ratio of the maximum output of the cell divided by the power of the incident light. It can be determined by  $J_{sc}$ ,  $V_{oc}$ ,  $FF$ , and the intensity of the incident light ( $P_{in}$ ) as shown in equation (3.3) (Ning, Fu, and Tian 2010; Sokolský and Cirák 2010).

$$\eta = \frac{V_{oc} J_s FF}{P_{in}} \times 100\% \quad (3.3)$$

### 3.8.4 Electrochemical impedance spectroscopy (EIS)

The electrochemical impedance spectroscopy was carried out using metrohm autolab to evaluate the resistivity of charge transfer between electrodes and electrolytes in DSSCs. The impedance of DSSCs were performed in the frequency range of 1 -1000 Hz.

### 3.8.5 IMPS/IMVS

Intensity-modulated photovoltage spectroscopy (IMVS) and intensity-modulated photocurrent spectroscopy (IMPS) can get significant data about DSSCs. IMPS and IMVS yield time constants which are related to the electron transport and electron recombination, respectively. IMPS and IMVS are related to the EIS. In EIS, a constant potential or current signal is applied to a cell which is superimposed by an AC signal. The frequency is modulated. The measured sinusoidal signal has the same frequency as the applied signal, but it is phase-shifted.

Both IMPS and IMVS operate in a similar way. Instead of modulating the amplitude of a current or potential signal, the intensity of a light beam focused on a DSSC is modulated. Figure 3.5 illustrates both techniques.

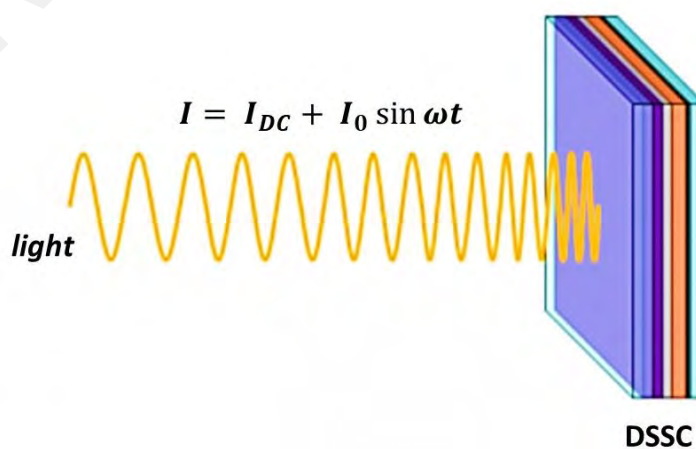


**Figure 3.5.** Sketch of the light signal focused on a DSSC during IMPS and IMVS.

During IMPS and IMVS experiments, light with a base intensity  $I_{DC}$  is focused on a DSSC. Upon the constant base intensity, a sinusoidal waveform with amplitude  $I_0$  is superimposed. The frequency  $f$  of the sine wave is changed during an experiment. The angular frequency  $\omega$  can be expressed as  $\omega = 2\pi f$ . The photocurrent (IMPS) or photovoltage (IMVS) respectively of a DSSC is measured. Similar to EIS, but in this case, the resultant signal has the same frequency as the applied signal, but its phase is shifted. By changing the frequency of the light signal, time-dependent information about various processes such as diffusion coefficients or reaction rates can be obtained. EIS and IMPS/IMVS can be further differentiated by looking at the I-V curve of a DSSC. Figure 3.6 shows stylized sketches of I-V curves with increasing light intensity. The regions covered by EIS, IMPS, and IMVS are highlighted.

The power generated by a DSSC rises with increasing light intensity. As a result, the photocurrent increases leading to a higher short-circuit current  $I_{SC}$  at 0V. In addition, the open-circuit potential  $E_{OC}$  shifts towards higher potentials. Typically, experiments with DSSCs are performed under constant illumination. When measuring EIS spectra, only one point of a single I-V curve can be analyzed. In contrast, the light intensity is modulated during IMPS and IMVS. This way, the cell's response within a series of I-V curves can be measured. The regions for IMPS and IMVS are highlighted in green and red in Figure 3.6. During IMPS, the potential of a DSSC is potentiostatically controlled and set to 0V (short-circuit conditions). The generated photocurrent is measured. The green line-segment in Figure 3.6 indicates the range measured during IMPS.

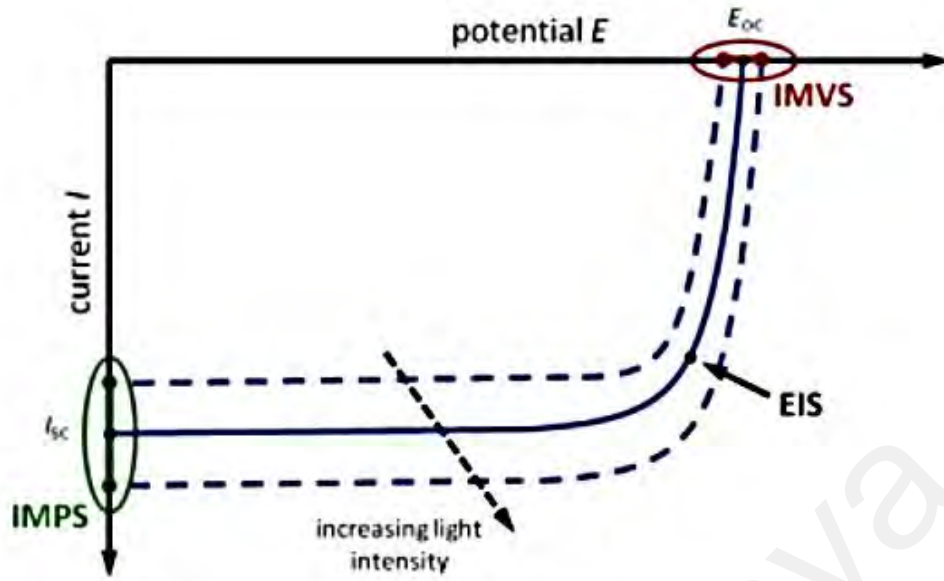


**Figure 3.6.** I-V curves of a DSC showing the regions covered by EIS, IMPS, and IMVS.

(a) **The electron transport lifetime ( $\tau_{tr}$ )**

At short-circuit conditions, the band gap between non-conductive valence band and conduction band of the semiconductor is maximum. As a result, nearly no electrons are injected into the conduction band. Most reactions occur on the back layer of the anode and electrons are migrating from the location where they are generated to the electrode's back layer. The corresponding electron transport time constant  $\tau_{tr}$  can be evaluated by IMPS. The technique exhibits a specific frequency  $f_{IMPS}$  which is inversely proportional to  $\tau_{tr}$  according to Equation 3.4.

$$\tau_{tr} = \frac{1}{2\pi \cdot f_{IMPS}} \quad (3.4)$$

(b) **Electron recombination lifetime ( $\tau_{rec}$ )**

IMVS experiments are performed under open-circuit conditions. As the name implies, the cell is open and the open-circuit potential of a DSSC is measured. The red line-segment in Figure 3.6 indicates the measured range during an IMVS experiment. The

open-circuit potential is the maximum potential of a DSSC before power is dissipated instead of being generated. The band gap between valence band and conduction band is small at this potential. Hence reactions on the back layer of the anode are less likely. Most generated photoelectrons are injected into the semiconductor's conduction band. In addition, the DSSC reaches steady-state at the open-circuit potential. This means that the rate of electron injection into the conduction band is equal to the electron recombination rate. IMVS can be used to evaluate the rate of electron recombination or the electron lifetime. The technique yields a frequency  $f_{IMVS}$  which is inversely proportional to the electron recombination time constant  $\tau_{rec}$ , as in Equation (3.5).

$$\tau_{rec} = \frac{1}{2\pi \cdot f_{IMVS}} \quad (3.5)$$

### 3.9 Safety aspects

Throughout the experiments, care is taken to prevent the health, fire, reactivity, and contact hazards associated with all the chemicals and hazards related with all the equipment and instrument used in the research project. Besides, normal laboratory safety precaution procedures including the use of appropriate personal protective equipment and use of standard operating procedures and waste disposal system is followed to eliminate and minimize the risk.

### 3.10 Summary of the chapter

All materials used in this work including sample preparation have been described in this chapter. Impedance of GPEs was obtained from HIOKI whereas the impedance of DSSCs was performed by using metrohm equipment. FTIR and XRD were conducted to analyse the structural properties of GPEs. The DSSCs performance were analyzed from the J-V characteristic, EIS and IMPS/IMVS data.

## CHAPTER 4: RESULTS AND DISCUSSION

### Introduction

This chapter discusses the conductivity of the GPEs and DSSCs performance. The DSSCs were characterized by J-V curve, EIS, IMPS and IMVS. The conductivity of the GPEs were characterized via impedance spectroscopy, and their structural properties were studied via FTIR and XRD

### 4.1 Ionic conductivity of the selected gel polymer electrolytes

The Nyquist plot of 4 electrolytes (A, B, C and D) at room temperature (RT) is shown in Figure 4.1. From the figure, it can be observed that the impedance of all GPEs exhibits tilted spike. This indicates that the plot can be represented as a series connection of resistor and constant phase element (CPE). CPE is also known as leaky capacitor. The impedance of CPE can be described as:

$$Z_{CPE} = 1/Q(j\omega)^n \quad (4.1)$$

where Q is a constant related to the CPE and  $1/Q$  is the capacitance of the CPE. The distance from the tilted spike to origin at the real axis indicates the bulk resistance of the electrolyte. As can be seen from the figure, the largest bulk resistance was observed for GPE C. Therefore, GPE C has the lowest RT conductivity. The composition of GPE C is similar to the like of GPE D having DMSO as a solvent except that TBP is incorporated in the GPE D. Therefore, it seems that the addition of TBP slightly affect the conductivity value of the electrolyte. However, the bulk resistance of GPE A and B are quite similar. Therefore, the changes in conductivity cannot be seen when the TBP is added into the electrolyte containing DMF as a solvent (GPE B).

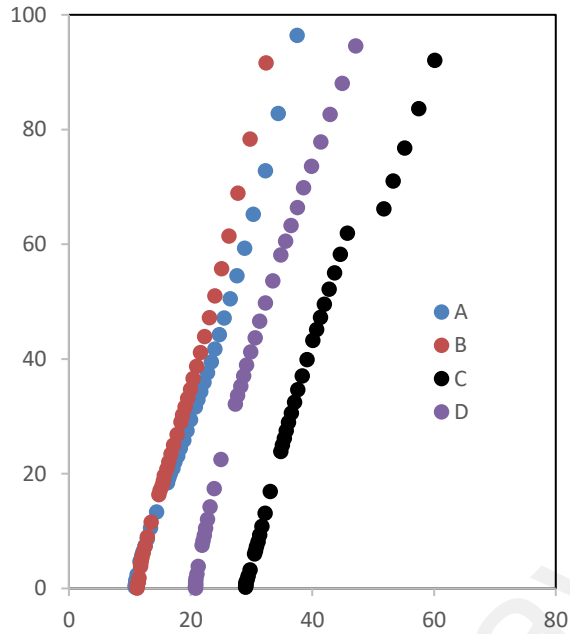


**Figure 4.1.** Bulk resistance from the Cole-Cole plot of real and imaginary  $R_s$ .

The Nyquist plot presented in Figure 4.1 is a selected sample from the repeated measurement for all 4 electrolytes. Figure 4.2 shows the variation of average conductivity with temperature. The average values of conductivity for all GPEs are tabulated in Table 4.1. After calculating standard deviation, it seems TBP does not improve the conductivity of GPE. From the average values of the conductivity, it can be observed that the addition of TBP does not change significantly. The GPE consist of DMF solvent (A and B) exhibits the better ionic conductivity as compared to the GPE with DMSO solvent. These might be due to the DMF is less viscous than the DMSO (Yang *et al.* 2008). The  $R^2$  values of the graph in Figure 4.2 are close to 1 for all GPEs. This indicates that, the temperature dependance ionic conductivity of all electrolytes obeys Arrhenius relationship which can be described as:

$$\sigma = \sigma_0 \exp \frac{-E_A}{k_b T} \quad (4.2)$$

where  $E_A$  is the activation energy,  $\sigma_0$  is a constant,  $k_b$  is a Boltzmann constant and  $T$  is the temperature.

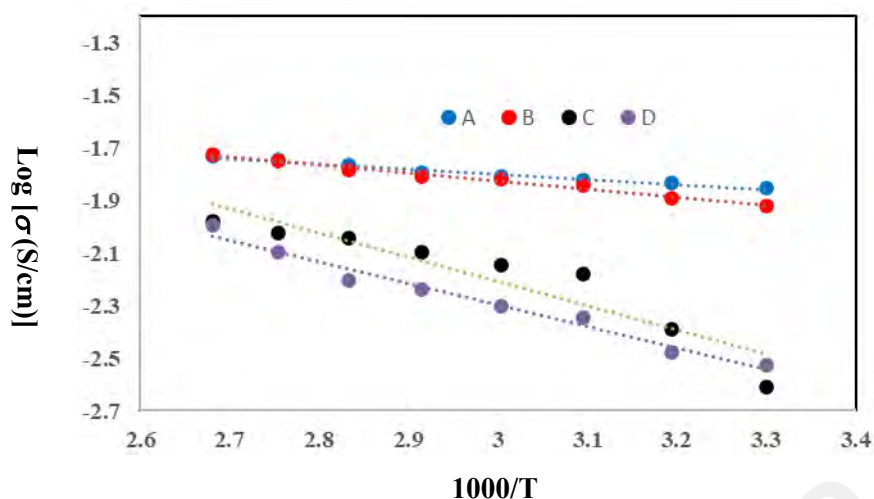


**Figure 4.2.** Log conductivity of the gel polymer electrolytes.

**Table 4.1.** Conductivity of gel polymer electrolytes in different temperatures.

Temperature (K)	Conductivity, $\sigma$ (mS cm <sup>-1</sup> )			
	A	B	C	D
303	14.05 ± 3.50	11.99 ± 6.84	2.45 ± 1.51	2.98 ± 1.35
313	14.75 ± 3.63	12.88 ± 8.54	4.06 ± 2.05	3.33 ± 1.43
323	14.99 ± 3.57	14.32 ± 3.52	6.61 ± 3.70	4.49 ± 1.02
333	15.61 ± 3.78	15.27 ± 3.50	7.17 ± 3.82	4.96 ± 1.01
343	16.02 ± 3.90	15.57 ± 3.57	8.04 ± 4.26	5.79 ± 1.80
353	17.19 ± 4.15	16.49 ± 3.35	9.02 ± 4.63	6.26 ± 1.86
363	17.93 ± 4.05	17.71 ± 3.42	9.45 ± 4.90	7.96 ± 2.94
373	18.61 ± 4.55	18.90 ± 4.25	10.52 ± 5.20	10.17 ± 3.23
$E_A$ (eV)	0.04	0.06	0.18	0.16

The values of  $E_A$  for all GPEs are tabulated in Table 4.1. It can be observed that the  $E_A$  values are almost identical for GPEs with and without TBP (A/B and C/D). As expected, the GPEs having DMF solvent (A and B) exhibits the lowest  $E_A$  since they have the higher ionic conductivity as compared to the GPEs having DMSO solvent (C and D).  $E_A$  is the energy required for ions to move from one site to another sites. When the temperature increases the polymer matrix is expanding and produces more free spaces. In addition, the rise in temperature will cause the re-dissociation of ions pair and ions aggregates. The conductivity represents the ions mobility and the polymer expansion around the polymer

chain. It means that, with the increasing temperature, the free ions increases and the polymer segment will move faster and results in conductivity increases (Saikia, Han, and Chen-Yang 2008). The increase in ionic conductivity in the electrolyte due to the presence of the co-additives does not appear to be contributing directly to the rise in photocurrent in the DSSC (Dissanayake *et al.* 2021). And due to the presence of hydrogen bonds in protic solvents such as (water, formamide, N-methylformamide), the DC value is excessively high (Shcherbakov *et al.* 2021).

#### **4.2 Fourier-transform infrared spectroscopy (FTIR) of the selected electrolytes**

FTIR spectra of all GPEs are shown in Figure 4.3. In the GPE A and B, the peaks which is attributed to the DMF are observed at  $1387\text{ cm}^{-1}$ ,  $1652\text{ cm}^{-1}$ ,  $2867\text{ cm}^{-1}$ ,  $866\text{ cm}^{-1}$ ,  $2929\text{ cm}^{-1}$ ,  $1502\text{ cm}^{-1}$  and  $1440\text{ cm}^{-1}$  correspond to N-C-H bending, C=O stretching, C-H stretching, C-N symmetric stretching,  $\text{CH}_3$  symmetric stretching, C-N stretching mode and  $\text{CH}_3$  asymmetric deformation respectively (Jacob and Arof 2000). Addition of TBP to the host polymer and solvent (DMF) has not affected on the polymer structures, as no significant change in the intensity of the constituent peaks has been observed. However, a broad band stretching around  $3200\text{-}3600\text{ cm}^{-1}$ , belonging to the -O-H bonding, suggests that many intramolecular and intermolecular hydrogen bonds are formed by the interaction of GPE A and TBP (Saidi *et al.* 2021; Perrin *et al.* 2014).

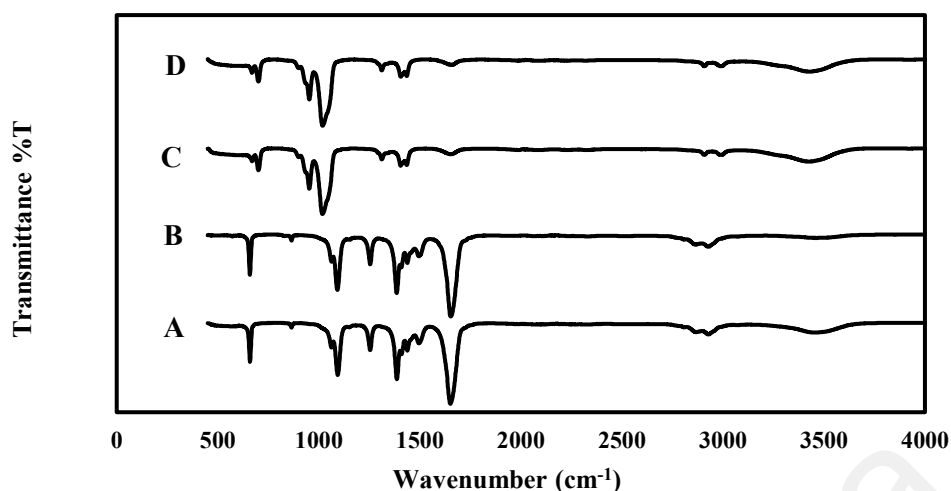


**Figure 4.3.** FTIR spectra recorded between 0 and 4000  $\text{cm}^{-1}$  for gel polymers electrolytes (A, and C) and samples containing TBP additive (B, and D).

In GPE C and D, the peaks which is attributed to the DMSO solvent are observed at  $673 \text{ cm}^{-1}$ ,  $953.15 \text{ cm}^{-1}$ ,  $702 \text{ cm}^{-1}$ ,  $1020$  to  $1030 \text{ cm}^{-1}$ ,  $1311 \text{ cm}^{-1}$ ,  $1406 \text{ cm}^{-1}$ ,  $1437 \text{ cm}^{-1}$ ,  $1659 \text{ cm}^{-1}$ ,  $2909 \text{ cm}^{-1}$  and,  $2995 \text{ cm}^{-1}$  correspond to Symmetric C–S stretch, Asymmetric C–S stretch, S=O stretch and C–S stretch, CH–OH bending and  $\text{CH}_3$  inplane deformation, NH deformation, vibration, and asymmetric  $\delta(\text{CH}_3)$ ,  $\text{CH}_2$  bending, C=O stretch, combination of  $\nu(\text{CH})$  and  $\nu(\text{CS})$  and C=C stretching, symmetric C–H stretching, and, C–H stretching respectively (Awadhia and Agrawal 2007). The effect of TBP also cannot be observed in the FTIR spectrum (Noor *et al.* 2014; Saikia, Han, and Chen-Yang 2008).

### 4.3 Characterization of the electrolyte: X-ray diffraction (XRD) studies

Figure 4.4 shows the XRD pattern for all 4 GPEs. It can be observed that the GPEs studied are amorphous. There are no crystalline peaks of KI salts were observed from the figure. This indicate that all KI salts were fully dissolved in the PVA based GPEs.

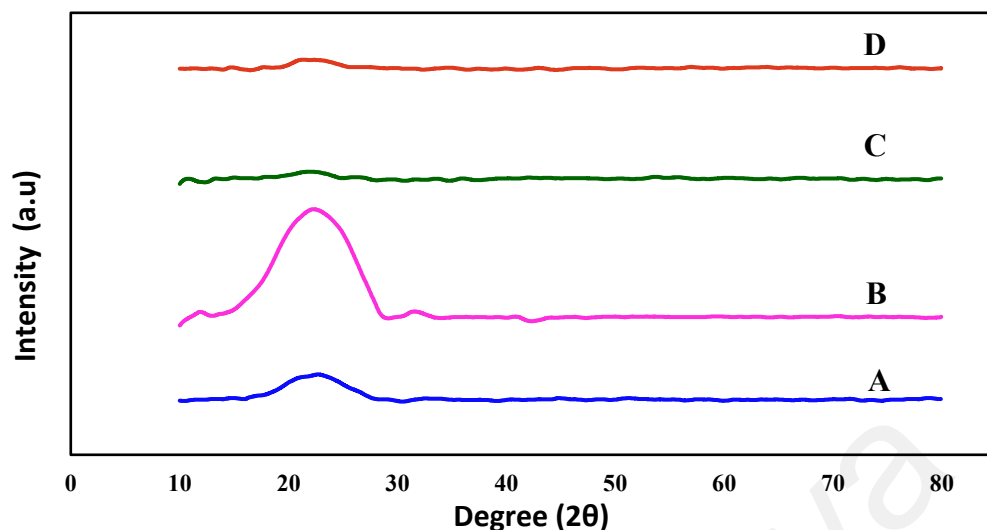


**Figure 4.4.** The XRD pattern of the gel polymer electrolyte A, B, C and D.

Broad peaks were observed at  $2\theta = 22.59^\circ$  and  $20.64^\circ$  for the GPEs having DMF (A and B) and DMSO (C and D) solvents respectively. The peaks were attributed to the amorphous nature of the GPEs. From Figure 4.4, it also can be seen that the amorphous peak intensity of the GPE A had elevated slightly after the addition of TBP (electrolyte B). Similar increment in intensity was observed for the GPEs with DMSO solvent. The increase of the peak intensity may be due to the existence of a bulky cation in the electrolyte (Syairah *et al.* 2019). The bulky cations were come from the interaction between the lone pair of nitrogen atom in TBP with  $K^+$  of the KI salt.

#### 4.4 DSSCs performance analyses of Blackberry

##### 4.4.1 Photovoltaic (*J-V*) characteristics

The *J-V* curve of DSSC using sensitizer extracted from dry blackberry with four gel polymer electrolytes A, B, C and D are shown in Figure 4.5.

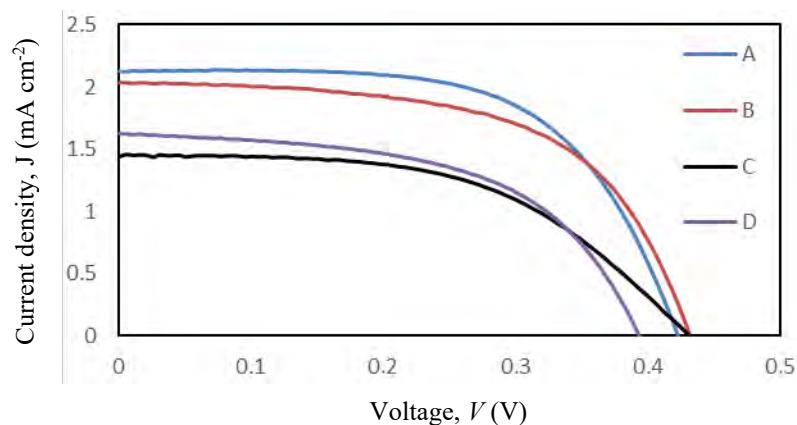


**Figure 4.5.** Blackberry J-V Curves of photovoltaic cells with different GPEs.

The average values of short circuit current density ( $J_{sc}$ ), open circuit voltage ( $V_{oc}$ ), fill factor (FF), and efficiency  $\eta$  are shown in Table 4.2.

**Table 4.2.** Photovoltaic parameters of Blackberry with different GPEs.

Dye	GPE	$J_{sc}$ (mA cm <sup>-2</sup> )	$V_{oc}$ (V)	FF	$\eta$ %
Blackberry	A	2.16 ± 0.23	0.42 ± 0.01	0.55 ± 0.04	0.50 ± 0.02
	B	2.18 ± 0.19	0.44 ± 0.01	0.57 ± 0.01	0.54 ± 0.04
	C	1.40 ± 0.11	0.44 ± 0.01	0.60 ± 0.02	0.37 ± 0.01
	D	1.65 ± 0.17	0.43 ± 0.01	0.58 ± 0.02	0.41 ± 0.05

From Table 4.2, it can be observed that the  $J_{sc}$  and efficiency of DSSCs having gel polymer electrolyte containing DMF solvent (A and B) are higher than the electrolyte containing DMSO solvent (C and D). The higher  $J_{sc}$  and efficiency may be due to the higher conductivity value of electrolyte A and B as compared to the electrolyte C and D. Electrolyte conductivity affect the performance of DSSC. As discussed in previous chapter, the function of the electrolyte is to carry charges from counter electrode to photoanode. A complete circuit will be achieved when electrons in counter electrode reached photoanode and regenerate oxidized dye molecules. It is known that the mobility of charge carries affect the conductivity of the electrolyte. Therefore, the higher conductivity, the faster the circuit to be completed thus led to higher  $J_{sc}$  and efficiency

(Mohammed 2020). It also can be observed that the incorporation of TBP into the electrolyte improving the  $J_{sc}$  and efficiency of DSSC. For the DSSC having electrolytes A, the  $J_{sc}$  increased to  $2.18 \text{ mAcm}^{-2}$  after the addition of TBP (DSSC with electrolyte B). The efficiency is also increased to 0.54%. For the DSSC having electrolytes C and D which represented the electrolytes with solvent DMSO, the values of  $J_{sc}$  increased from  $1.40 \text{ (mA cm}^{-2}\text{)}$  to  $1.65 \text{ (mAcm}^{-2}\text{)}$  and the efficiency increased from 0.37 % to 0.41 %. TBP in the electrolyte help to suppress electron recombination and improve the charge transportation. When excited electron in dye molecules be injected into the CB of MO  $\text{TiO}_2$ , they can recombine back to triiodide ions in the electrolyte. Therefore, by having TBP in the electrolyte, the recombination process or also known as dark current in DSSC can be suppressed by the adsorption of TBP on the empty surface (no dyes) of the  $\text{TiO}_2$ . This led to higher  $J_{sc}$  and efficiency of DSSC using gel polymer electrolyte incorporated with TBP.

#### 4.4.2 Electrical impedance spectroscopy (EIS)

Figure 4.6 shows the impedance plot of DSSCs based blackberry dye. From the impedance plot, the series and charge transfer resistance of DSSC can be analyzed. The series resistance can be determined by measuring the distance from the origin to the first semicircle at the real axis. The semicircle represents the charge transfer resistance at the electrode/electrolyte interface and diffusion of ions in the electrolyte (C. Wang *et al.* 2019).

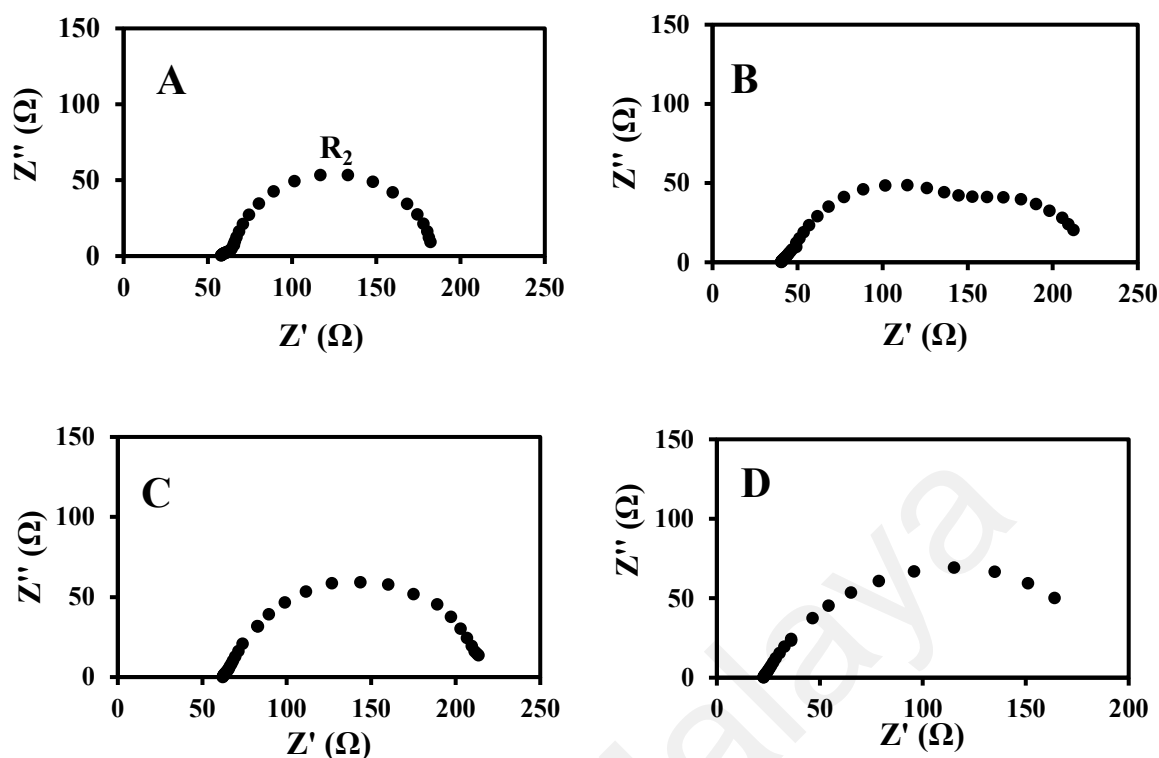


**Figure 4.6.** The Nyquist plots of EIS for the blackberry fabricated photovoltaic cells with different GPEs.

Two semicircles in which small at the high frequency region can be observed for DSSC having gel polymer electrolyte A, C and D. The small semicircle at the high frequencies represents the charge transfer resistance at the counter electrode/electrolyte interface ( $R_{CE}$ ). The second semicircle at the medium frequencies represents the charge transfer at the photoanode/electrolyte interface ( $R_P$ ). On the other hand, three semicircles were observed for DSSC having gel polymer electrolyte B. The third semicircle at the low frequencies is represent as the ion's diffusion in the electrolyte. However, third semicircle does not clearly been seen in other DSSCs. Therefore, the main focus in this work was the charge transfer resistance at the photoanode/electrolyte interface. From Figure 4.6, it can be observed that the values of  $R_{CE}$  are quite similar for all DSSCs. The  $R_P$  values of all DSSCs are listed in Table 4.3. It can be observed that the  $R_P$  of DSSCs having gel polymer electrolyte A and B is smaller than the DSSCs having gel polymer electrolyte C and D. This indicates that the charge transfer from the electrolyte containing DMF solvent

to the photoanode of DSSC is faster than the DMSO. This is agreed with the conductivity of the gel polymer,  $J_{sc}$  and efficiency obtained in the previous section.

**Table 4.3.**  $R_p$  value of DSSCs using blackberry dyes.

Dye	GPE	$R_p$
Blackberry	A	121
	B	103
	C	149
	D	128

#### 4.4.3 IMPS and IMVS study of photovoltaic cells

Figure 4.7 shows the IMPS graphs of the DSSCs based blackberry dye.

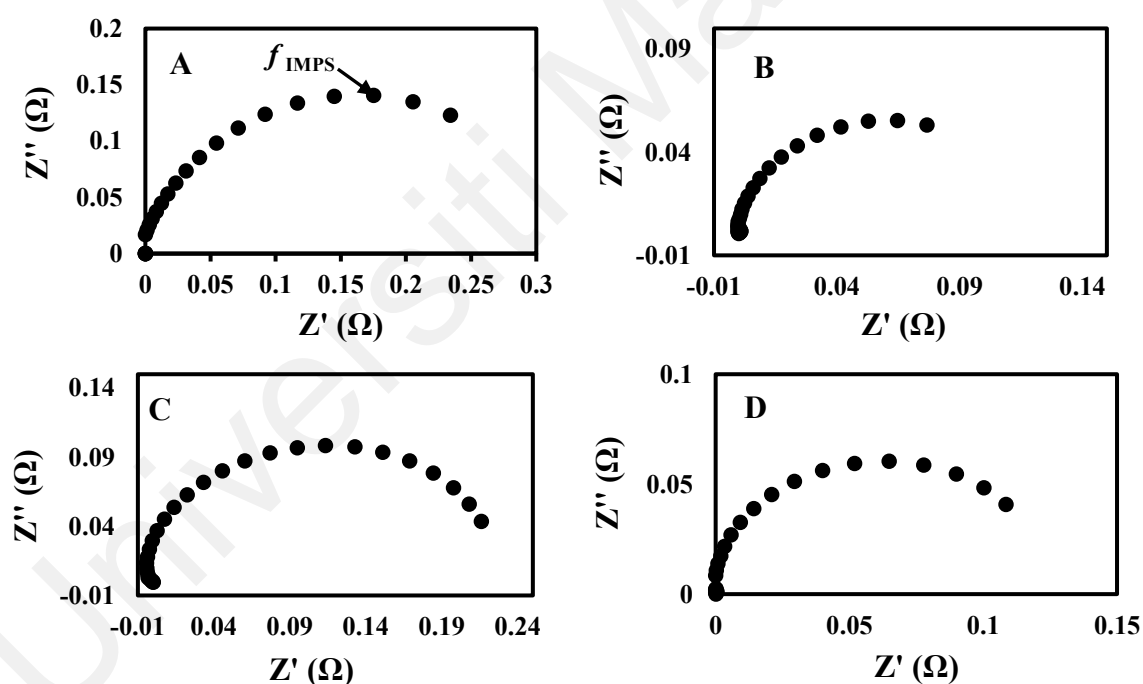


**Figure 4.7.** IMPS plot for the DDSCs based blackberry dye with different GPEs.

The maximum value at intermediate frequency is the IMPS characteristic frequency,  $f_{IMPS}$ . This value was used to calculate electron transport,  $\tau_{tr}$  through the pores of the photoanode to the FTO glass by using the equation (3.4). Figure 4.8 shows the IMVS graphs of the DSSCs based blackberry dye. Same as the  $f_{IMPS}$ , the IMVS characteristic

frequency,  $f_{IMVS}$  was determined at the maximum value of intermediate frequencies. This value was used to calculate the electron recombination time,  $\tau_{rec}$  by using the equation (3.5).

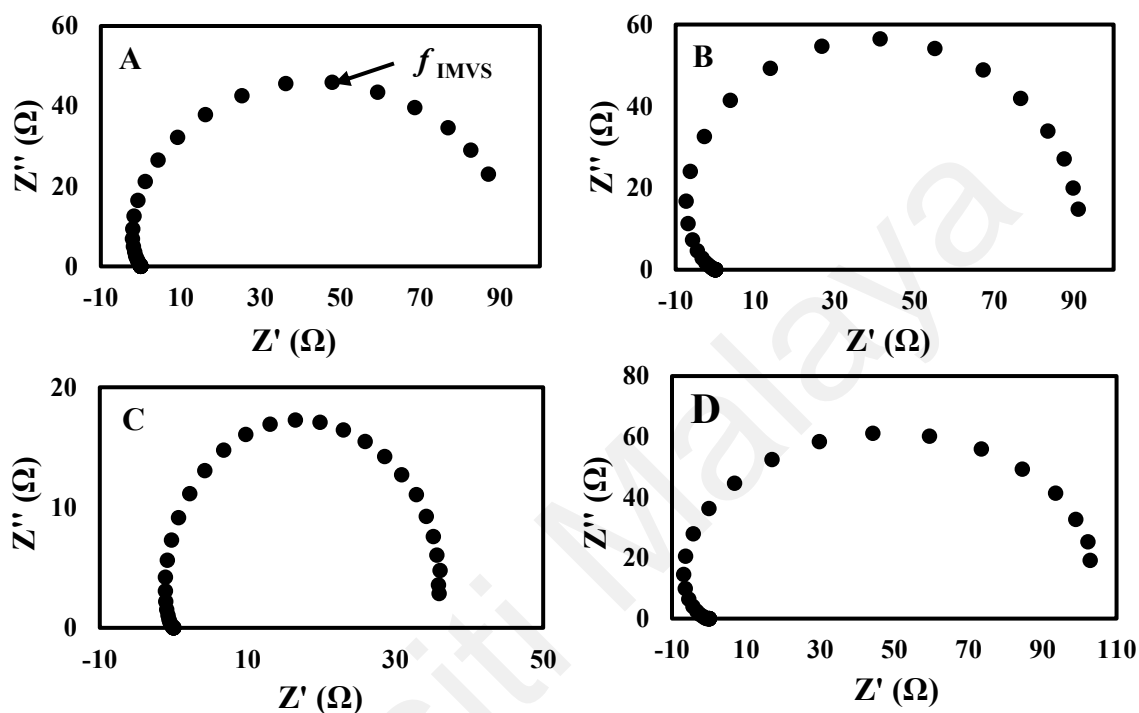


**Figure 4.8.** IMVS plot for the DDSCs based blackberry dye with different GPEs.

The  $f_{IMPS}$ ,  $f_{IMVS}$ ,  $t_{tr}$ , and  $t_{rec}$  are listed in Table 4.4. Overall, it can be seen that the  $t_{tr}$  for both DSSC having GPE A and B is faster than the DSSC having GPE D. This explains the better performance of both DSSC. Although the  $t_{rec}$  for DSSC with GPE A and B is faster than GPE C and D, the ionic conductivity of GPE A and B is higher and therefore better efficiency. The value of the electron transfer of sample C is less than the sample A which may be due to the dielectric properties of the solvents.

**Table 4.4.** The parameters obtained from IMPS and IMVS experiments for the DSSCs using blackberry dye with different GPEs.

GPE	$f_{IMPS}$ (Hz)	$f_{IMVS}$ (Hz)	$t_{tr}$ (s)	$t_{rec}$ (s)
A	1.18	0.57	0.13	0.28
B	0.99	0.60	0.16	0.26
C	3.32	1.38	0.05	0.12
D	2.82	1.26	0.06	0.13

## 4.5 DSSCs performance analyses of Blueberry

### 4.5.1 Photovoltaic ( $J$ - $V$ ) characteristics

The  $J$ - $V$  curve of DSSC using sensitizer extracted from blueberry with GPE A, B, C and D are shown in Figure 4.9.

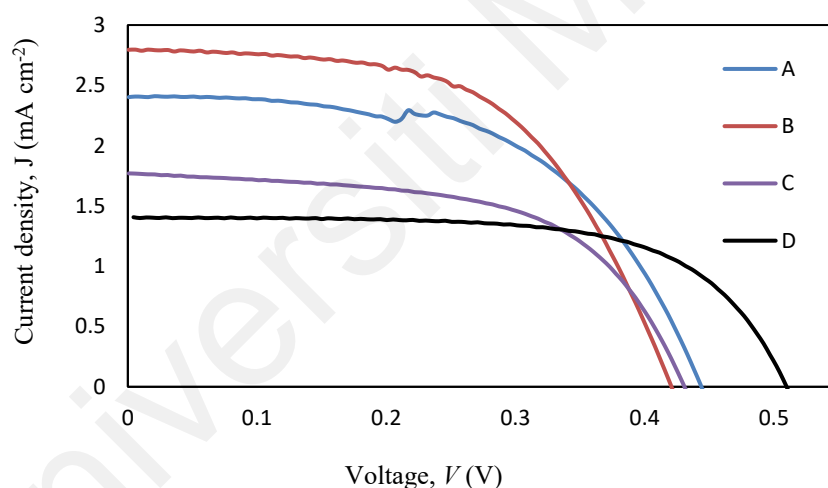


**Figure 4.9.** Blueberry  $J$ - $V$  curves of photovoltaic cells with different GPEs.

The average values of short circuit current density ( $J_{sc}$ ), open circuit voltage ( $V_{oc}$ ), fill factor (FF), and efficiency  $\eta$  are shown in Table 4.5.

**Table 4.5.** Photovoltaic parameters of Blueberry with different GPEs.

Dye	GPE	$J_{sc}$ (mA cm <sup>-2</sup> )	$V_{oc}$ (V)	FF	$\eta$ %
Blueberry	A	2.40 ± 0.17	0.44 ± 0.008	0.57 ± 0.01	0.60 ± 0.03
	B	2.79 ± 0.27	0.42 ± 0.02	0.57 ± 0.02	0.66 ± 0.06
	C	1.41 ± 0.20	0.43 ± 0.01	0.58 ± 0.04	0.44 ± 0.07
	D	1.77 ± 0.24	0.51 ± 0.02	0.65 ± 0.04	0.46 ± 0.08

From Table 4.5, the  $J_{sc}$  values increased with the additional of TBP in the electrolyte. For the DSSC having GPEs with DMF solvent, the  $J_{sc}$  increased from 2.40 mA cm<sup>-2</sup> (GPE A without TBP) to 2.79 mA cm<sup>-2</sup> (GPE B with TBP) resulted in the increasing of the efficiency from 0.60 % to 0.66 %. Similar trend has been observed for the DSSC having GPEs with DMSO solvent where the  $J_{sc}$  increased from 1.41 mA cm<sup>-2</sup> (GPE A without TBP) to 1.77 mA cm<sup>-2</sup> (GPE B with TBP) and the efficiency increased from 0.44 % to 0.46 %. As mentioned before the addition of TBP into the GPE can minimize the possible charges recombination in the DSSC and thus improve the cell performance. Overall, the DSSCs having GPEs with DMF solvent are better as compared to the DSSCs having GPEs with DMSO solvent. This is due to the higher conductivity of GPE with DMF solvent than the GPE with DMSO solvent.

#### 4.5.2 Electrical impedance spectroscopy (EIS)

Figure 4.10 shows the impedance plot of DSSCs based blueberry dye. The EIS was performed to measure the impedance in which involving the mobility charges transfer characteristic. Since DSSC consist of three main components namely photoanode, electrolyte and counter electrode, the impedance of these three components can be analyzed via EIS.

The  $R_p$  values of all DSSCs are listed in Table 4.6. Based on Table 4-6, it can be observed that DSSCs having GPEs with DMSO solvent exhibits larger  $R_p$  than the GPEs

with DMF solvent. The larger resistivity implies lesser charges were transferred between photoanode and electrolytes causing the low current density and efficiency of the DSSC. Therefore, the higher  $J_{sc}$  and efficiency of DSSC based blueberry dye having GPEs with DMF solvent may be due to the faster charges transfer at the photoanode/electrolyte interface. The decrease in  $R_p$  values when TBP was added into GPE indicating that the DSSCs perform better with GPEs incorporated with TBP.

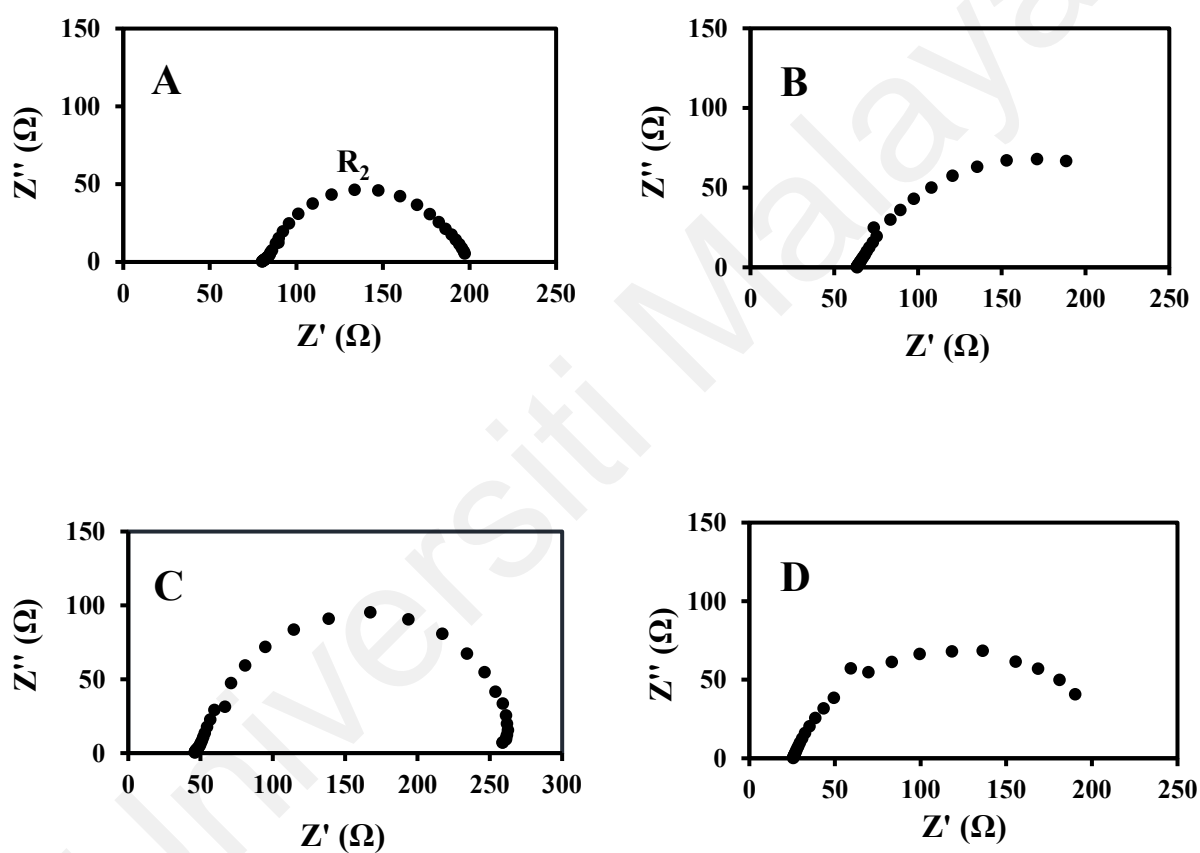


**Figure 4.10.** The Nyquist plots of EIS for the blueberry fabricated photovoltaic cells with different GPEs.

**Table 4.6.**  $R_p$  value of DSSCs using blueberry dye.

Dye	GPE	$R_p$
Blueberry	A	115
	B	113
	C	192
	D	121

### 4.5.3 IMPS and IMVS study of photovoltaic cells

The IMPS and IMVS graphs of the DSSCs based blueberry dye are shown in Figure 4.11 and 4.12 respectively. The  $f_{IMPS}$ ,  $f_{IMVS}$ ,  $t_{tr}$ , and  $t_{rec}$  obtained from Figure 4.11 and 4.12 are listed in Table 4.7.

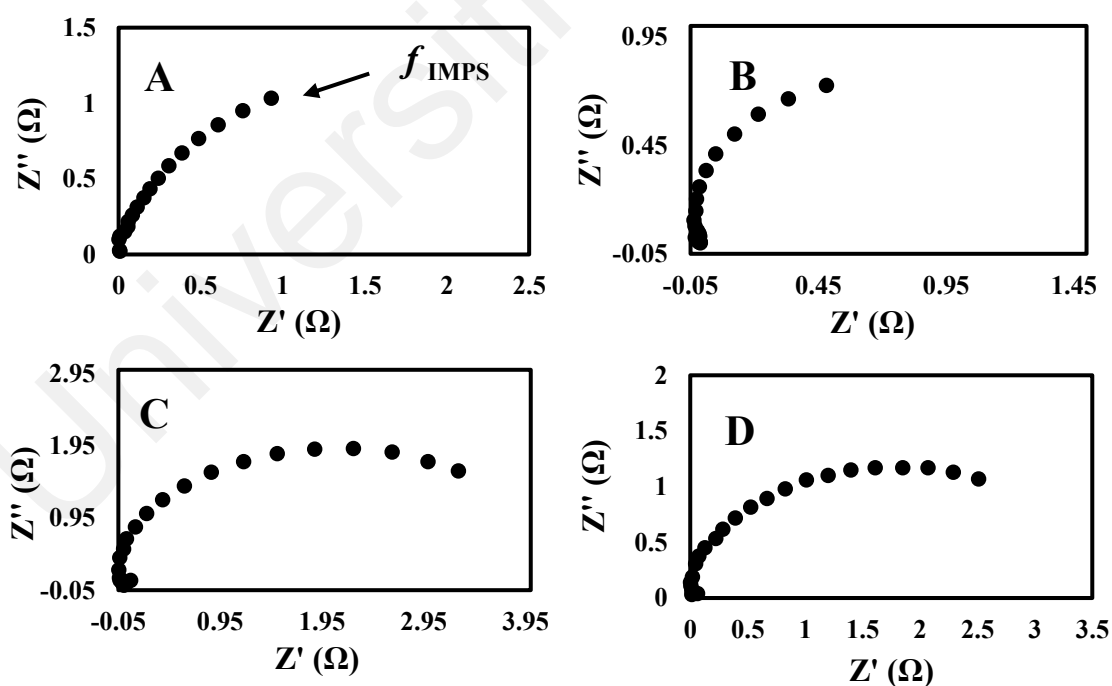


**Figure 4.11.** IMPS Nyquist type plot for the blueberry fabricated photovoltaic cells with different GPEs.

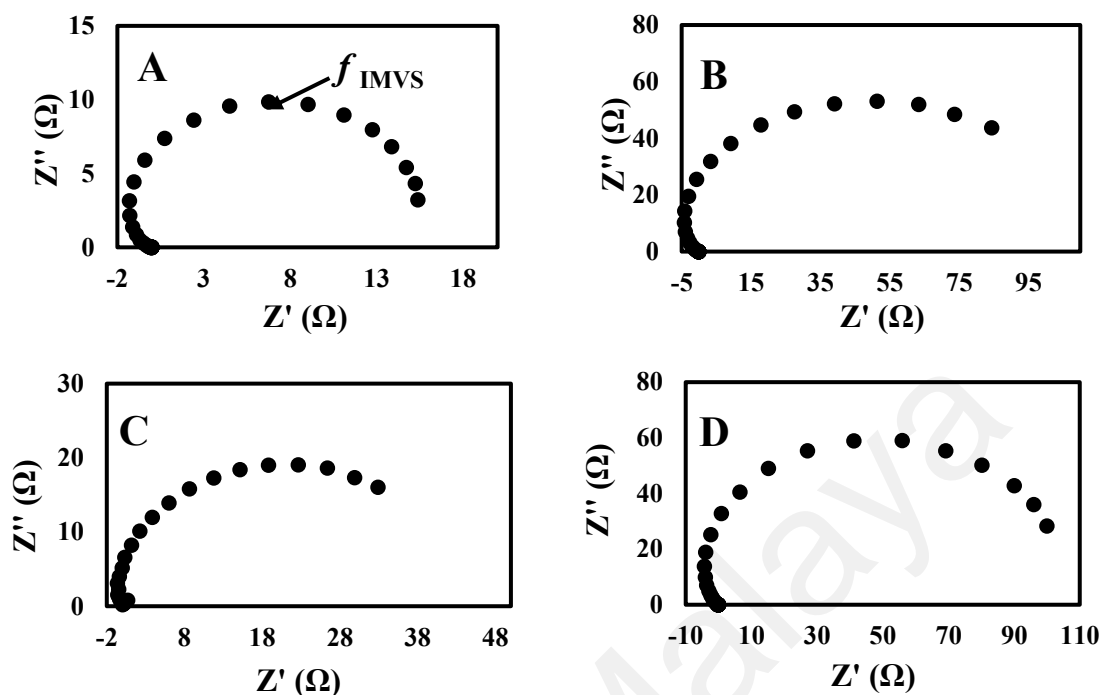


**Figure 4.12.** IMVS Nyquist type plot for the blueberry fabricated photovoltaic cells with different GPEs.

From Table 4.7, It can be seen that the  $t_{tr}$  of DSSCs having GPE with TBP is smaller than the GPE without TBP indicates that the charges transportation in the photoanode of DSSCs having GPE with TBP is faster than the GPE without TBP. On the other hand, the  $t_{rec}$  is bigger for DSSC having GPE with TBP indicating the charge recombination is slower than the DSSC having GPE without TBP. Therefore, the better performance of DSSCs having GPE with TBP can be explained based on these two parameters (charges transportation and recombination).

**Table 4.7.** The parameters obtained from IMPS and IMVS experiments for the DSSCs using blueberry dye with different GPEs.

GPE	$f_{IMPS}$ (Hz)	$f_{IMVS}$ (Hz)	$t_{tr}$ (s)	$t_{rec}$ (s)
A	1.00	0.50	0.16	0.32
B	1.26	0.25	0.13	0.64
C	1.99	1.00	0.08	0.16
D	2.51	0.32	0.06	0.57

## 4.6 DSSCs performance analyses of Raspberry

### 4.6.1 Photovoltaic ( $J$ - $V$ ) characteristics

The  $J$ - $V$  curve of DSSC using sensitizer extracted from raspberry with GPE A, B, C and D are shown in Figure 4.13.

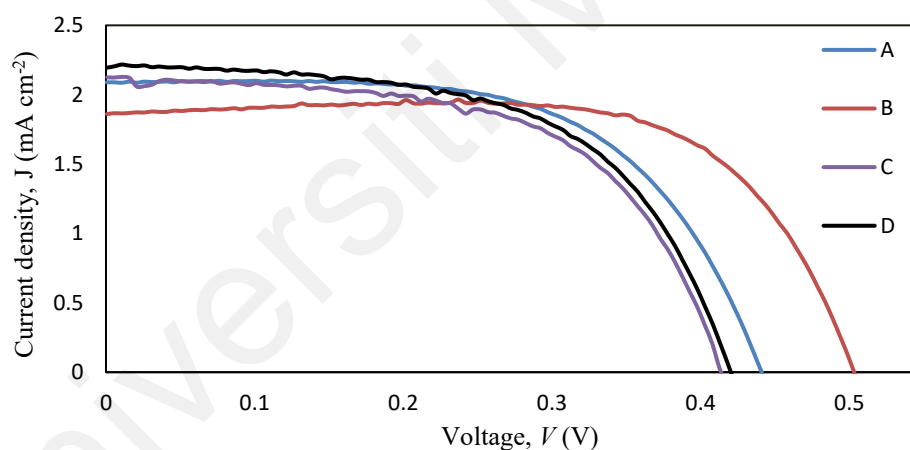


**Figure 4.13.** Raspberry  $J$ - $V$  curves of photovoltaic cells with different GPEs.

The average values of short circuit current density ( $J_{sc}$ ), open circuit voltage ( $V_{oc}$ ), fill factor (FF), and efficiency  $\eta$  are shown in Table 4.8. The efficiency of the DSSC with raspberry dye having GPE A, B, C and D show a similar trend as the DSSCs using blackberry and blueberry dyes with the same GPEs. Therefore, it is shows that the conductivity of the GPEs is the main factor to the improvement of the DSSC performance. In addition, GPEs with incorporation of TBP also improved the overall efficiency. From

Table 4.8, it can be seen that the efficiency increased from 0.57% to 0.66 % for the DSSC having GPE A and GPE B respectively.

**Table 4.8.** Photovoltaic parameters of raspberry with different GPEs.

Dye	GPE	$J_{sc}$	$V_{oc}$	$FF$	$Eff$
Raspberry	A	$2.09 \pm 0.22$	$0.44 \pm 0.01$	$0.62 \pm 0.04$	$0.57 \pm 0.01$
	B	$2.86 \pm 0.24$	$0.50 \pm 0.01$	$0.71 \pm 0.04$	$0.66 \pm 0.05$
	C	$2.13 \pm 0.24$	$0.41 \pm 0.01$	$0.59 \pm 0.01$	$0.51 \pm 0.04$
	D	$2.20 \pm 0.24$	$0.42 \pm 0.01$	$0.59 \pm 0.01$	$0.54 \pm 0.04$

#### 4.6.2 Electrical impedance spectroscopy (EIS)

Figure 4.14 shows the impedance plot of DSSCs based raspberry dye and their  $R_p$  values are listed in Table 4.6. Based on Table 4.8 and 4.9 it can be observed that the highest efficiency of DSSC (having GPE B) does not exhibit the lowest  $R_p$  value of  $127 \Omega$  which belongs to the DSSC having GPE D. In Table 4.8 it can be observed that the DSSC with GPE A is slightly better than the DSSC with GPE C and D. However, if based on the standard deviation shown in the table, the efficiency of DSSC having GPE D and A are quite similar even though the conductivity of GPE A is greater than the GPE D. This may be due to the larger  $R_p$  of DSSC with GPE A which is  $247 \Omega$  affecting the overall efficiency of the DSSC.

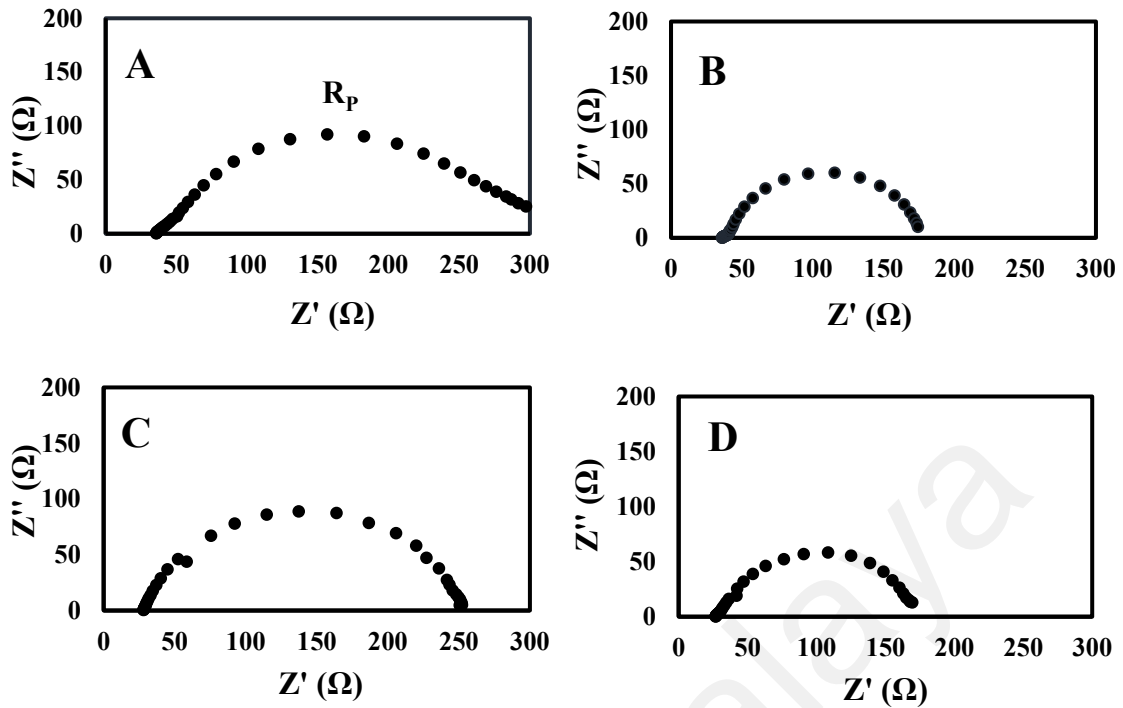


**Figure 4.14.** The Nyquist plots of EIS for the raspberry fabricated photovoltaic cells with different GPEs.

**Table 4.9.**  $R_p$  value of DSSCs using raspberry dye with different GPEs.

Dye	GPE	$R_p$
Raspberry	A	247
	B	134
	C	194
	D	127

#### 4.6.3 IMPS and IMVS study of photovoltaic cells

The IMPS and IMVS graphs of the DSSCs based raspberry dye are shown in Figure 4.15 and 4.16 respectively. The  $f_{IMPS}$ ,  $f_{IMVS}$ ,  $t_{tr}$ , and  $t_{rec}$  obtained from Figure 4.15 and 4.16 are listed in Table 4.10. From the Figure 4.15, a slight decrease in the semicircle radius of the plot B (DSSC having GPE B) can be observed compared to plot A (DSSC having GPE A). It seems that the IMPS plot of DSSC having GPE with TBP exhibits smaller radius of the semicircle where the DSSC having GPE C and D are also shows a similar behaviour.

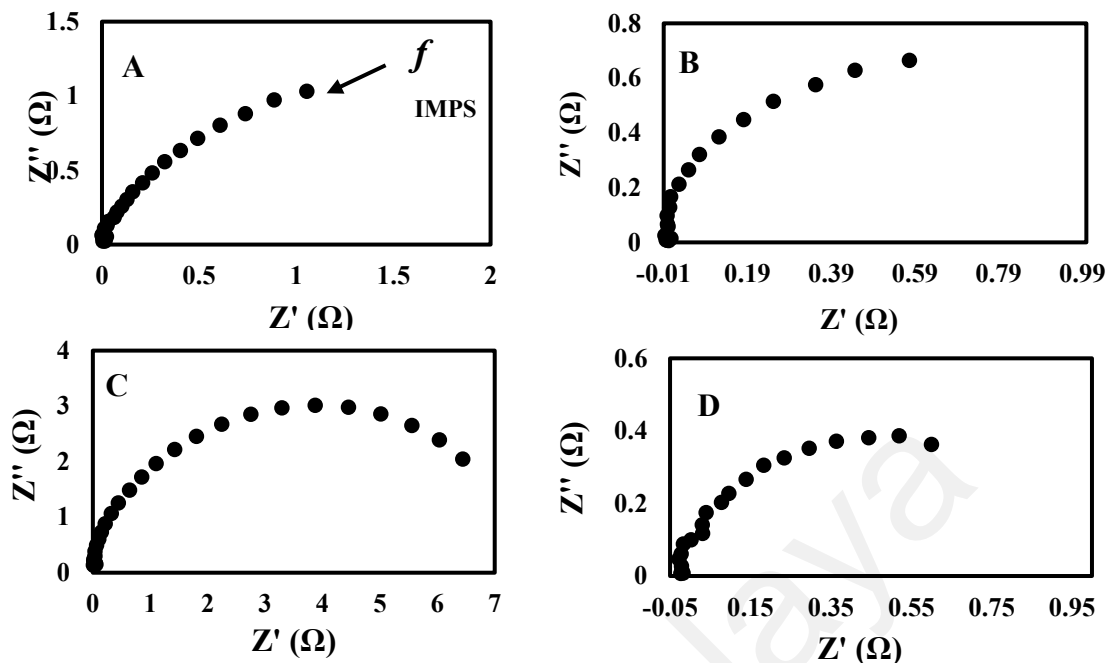


**Figure 4.15.** IMPS Nyquist type plot for the raspberry fabricated photovoltaic cells with different GPEs.

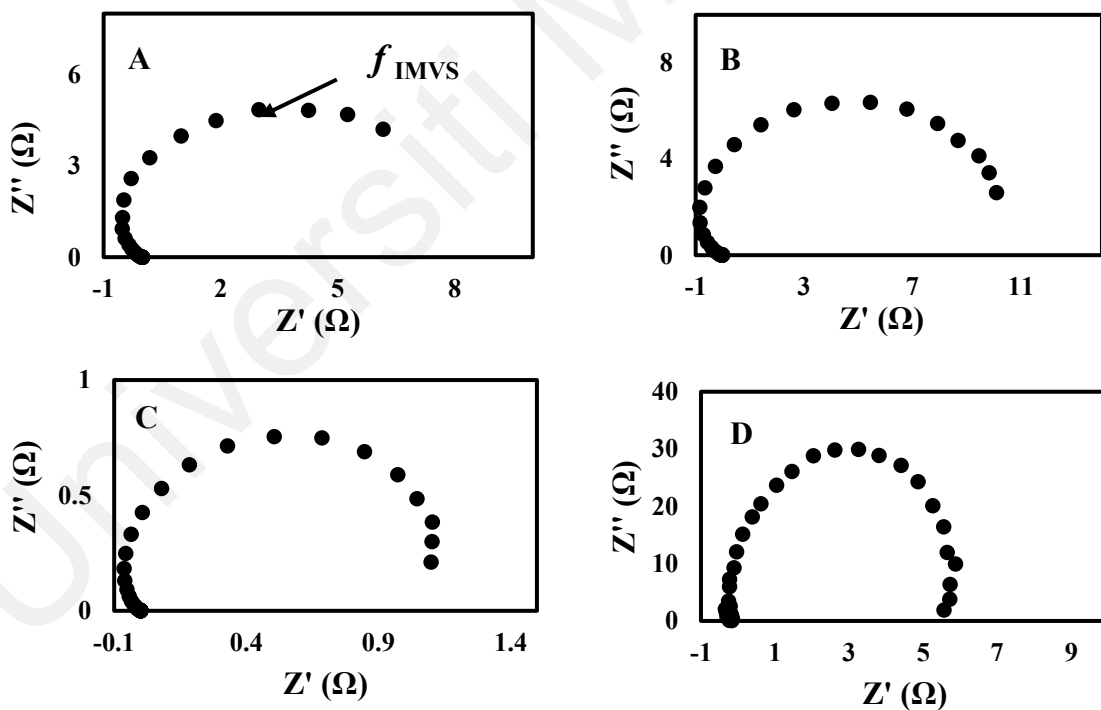


**Figure 4.16.** IMVS Nyquist type plot for the blueberry fabricated photovoltaic cells with different GPEs.

From Table 4.10, it can be seen that the charges transport in the photoanode of DSSC having GPE with TBP is faster whereas the charge recombination is slower compared to

the DSSC having GPE without TBP. This is agreed with the efficiency of DSSCs presented in Table 4.8.

**Table 4.10.** The parameters obtained from IMPS and IMVS experiments for the DSSCs using raspberry dye with different GPEs.

GPE	$f_{IMPS}$ (Hz)	$f_{IMVS}$ (Hz)	$t_{tr}$ (s)	$t_{rec}$ (s)
A	1.23	0.20	0.13	0.80
B	0.70	0.62	0.23	0.26
C	2.10	0.67	0.08	0.24
D	1.48	0.83	0.11	0.20

## 4.7 DSSCs performance analyses of Saffron

### 4.7.1 Photovoltaic ( $J$ - $V$ ) characteristics

The  $J$ - $V$  curve of DSSC using sensitizer extracted from saffron with GPE A, B, C and D are shown in Figure 4.17. The average values of the short circuit current density ( $J_{sc}$ ), open circuit voltage ( $V_{oc}$ ), fill factor (FF), and efficiency  $\eta$  are shown in Table 4.11. It can be observed that the performance of DSSCs using saffron dye does not follow the conductivity of the GPEs. As discussed in previous section, the conductivity of GPE A is higher than the GPE C. However, this was not reflected to the DSSC performance where they both have similar efficiency. The DSSC having GPE D exhibits the highest efficiency of 0.62%. This may be due to the faster of charge transfer at the photoanode/electrolyte interface which will be explained in the next section.

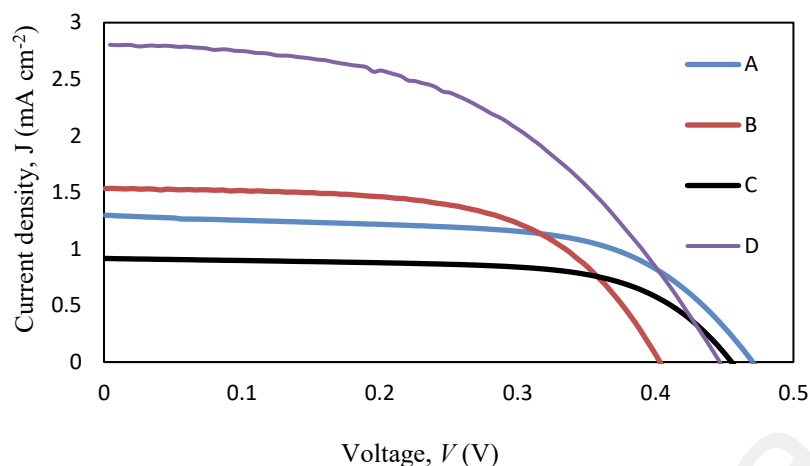


**Figure 4.17.** Saffron J-V curves of photovoltaic cells with different GPEs.

**Table 4.11.** Photovoltaic parameters of raspberry with different GPEs.

Dye	GPE	$J_{sc}$	$V_{oc}$	$FF$	$Eff$
Saffron	A	$0.92 \pm 0.15$	$0.46 \pm 0.007$	$0.62 \pm 0.01$	$0.26 \pm 0.04$
	B	$1.37 \pm 0.08$	$0.41 \pm 0.01$	$0.61 \pm 0.01$	$0.35 \pm 0.009$
	C	$0.91 \pm 0.08$	$0.45 \pm 0.01$	$0.65 \pm 0.008$	$0.27 \pm 0.02$
	D	$2.80 \pm 0.300$	$0.44 \pm 0.01$	$0.50 \pm 0.05$	$0.62 \pm 0.06$

#### 4.7.2 Electrical impedance spectroscopy (EIS)

Figure 4.18 shows the impedance plot of DSSCs based saffron dye and their  $R_p$  values are listed in Table 4.12. As can be seen, the smallest  $R_p$  shows the better performance of DSSC. Based on the DSSC performance, it seems that the saffron dye is more compatible with the DMSO solvent. Unlike blackberry, blueberry and raspberry where the major pigments are anthocyanins, saffron contain carotenoid pigment. The higher efficiency of DSSC based saffron dye probably due to the different in structure of carotenoid pigment which has been discussed in chapter two. Pigments and solvents affect the ability of adsorption dye on MO TiO<sub>2</sub> surface and eventually the efficiency of the charge transfer at the photoanode.

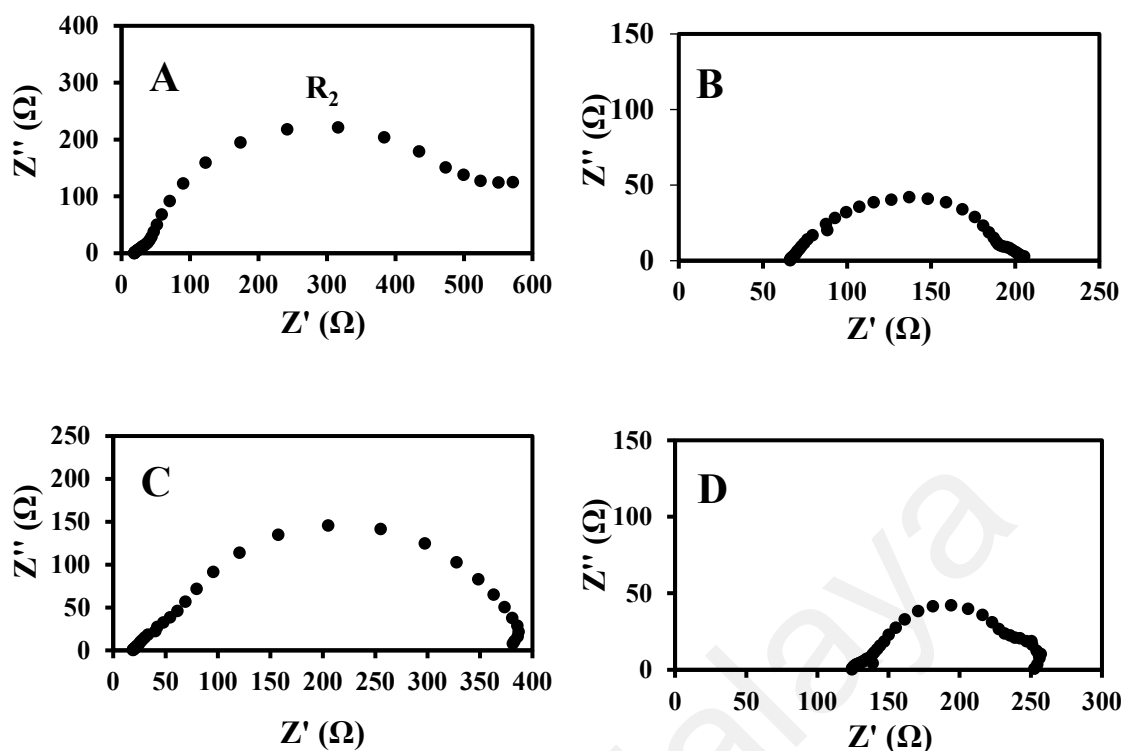


**Figure 4.18.** The Nyquist plots of EIS for the saffron fabricated photovoltaic cells with different GPEs.

**Table 4.12.** EIS parameters of fabricated DSSCs for saffron dye with different GPEs.

Dye	GPE	$R_p$
Saffron	A	533
	B	117
	C	341
	D	118

### 4.7.3 IMPS and IMVS study of photovoltaic cells

The IMPS and IMVS graphs of the DSSCs based saffron dye are shown in Figure 4.19 and 4.20 respectively. The  $f_{IMPS}$ ,  $f_{IMVS}$ ,  $t_{tr}$ , and  $t_{rec}$  obtained from Figure 4.19 and 4.20 are listed in Table 4.13. It can be observed that the charge transport in the photoanode of DSSCs having GPE with DMSO solvent is faster than the GPE with DMF solvent. This is agreed with the DSSCs performance where the efficiency is higher for DSSC having GPE with DMSO solvent than the DMF solvent. Therefore it can be deduced that the

saffron dye is probably more compatible with the DMSO than the DMF. In addition, the charge recombination time is also slower in the DSSC having GPE with TBP indicates that TBP successfully suppresses the dark current thus leading to better DSSC performance.

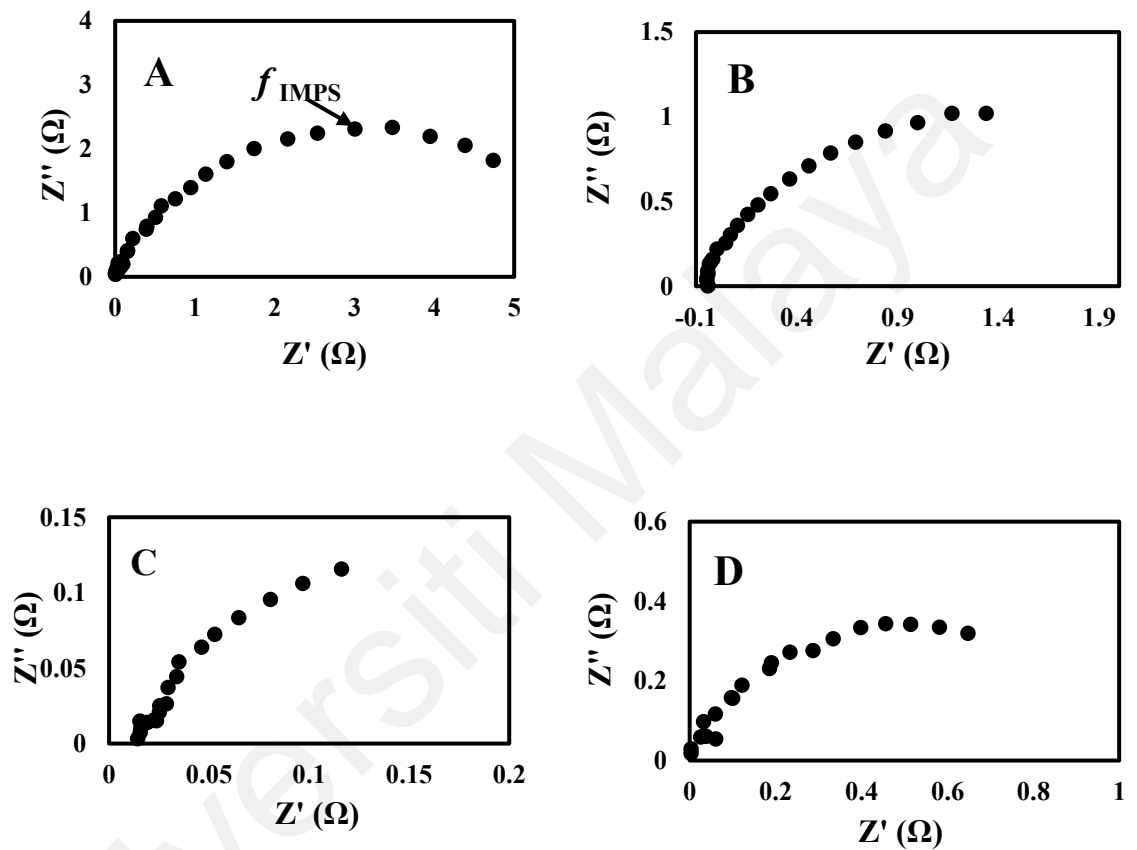


**Figure 4.19.** IMPS Nyquist type plot for the saffron fabricated photovoltaic cells with different GPEs.

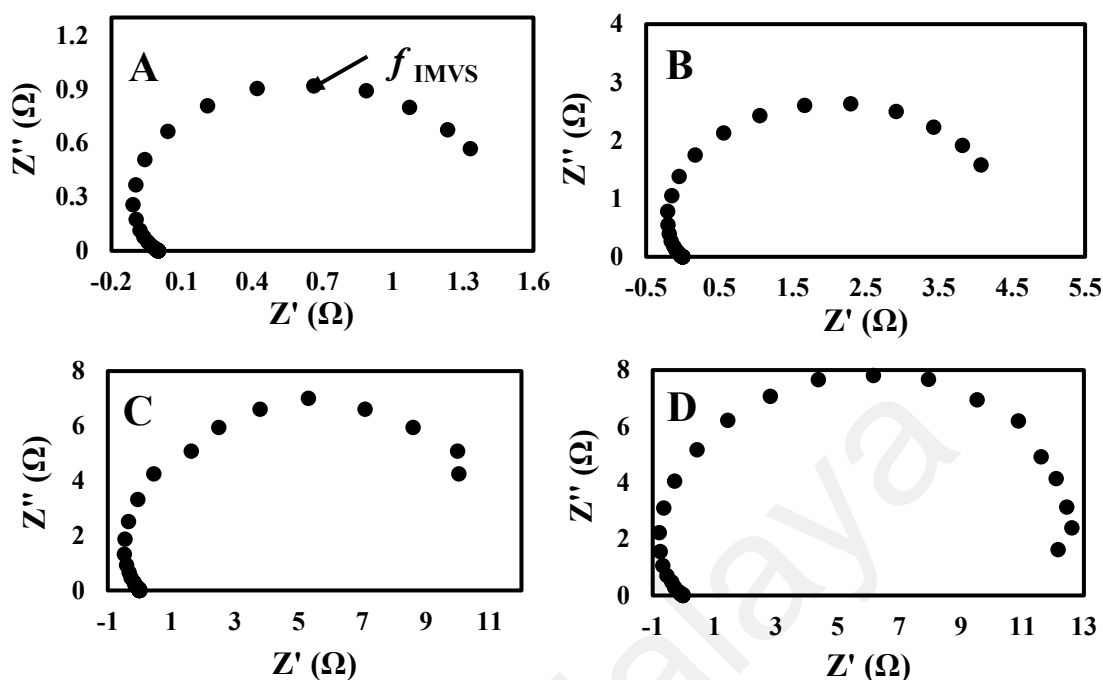


**Figure 4.20.** IMVS Nyquist type plot for the saffron fabricated photovoltaic cells with different GPEs.

**Table 4.13.** The parameters obtained from IMPS and IMVS experiments for the DSSCs using saffron dye with different GPEs.

<i>Electrolytes</i>	$f_{IMPS}$ (Hz)	$f_{IMVS}$ (Hz)	$t_{tr}$ (s)	$t_{rec}$ (s)
<b>A</b>	1.83	0.40	0.09	0.40
<b>B</b>	1.15	0.60	0.14	0.27
<b>C</b>	0.37	0.21	0.43	0.76
<b>D</b>	0.91	0.32	0.17	0.50

#### 4.8 Summary of chapter

The highest conductivity of GPE was obtained for the GPE with DMF solvent. The conductivity of the GPE reflect the performance of DSSC where the DSSCs having GPE A and B exhibits higher efficiency compared to the DSSCs having GPE C and D. Although GPE A and GPE B have the same ionic conductivity, the DSSC having GPE A is still lower than the DSSC having GPE B. This is because TBP in GPE B help to reduce charges recombination in DSSC thus leads to higher efficiency. This trend can be

observed for DSSC based anthocyanin dyes which is blackberry ( $\eta = 54\%$ ), blueberry ( $\eta = 66\%$ ) and raspberry ( $\eta = 66\%$ ) dye sensitizers. In DSSC using saffron as sensitizer, the highest efficiency was observed for the DSSC having GPE with DMSO solvent which is GPE D ( $\eta = 62\%$ ). This may be due to the compatibility of carotenoid of saffron with the DMSO solvent. Impedance and IMPS/IMVS characteristics have also been presented in this chapter. Charges transfer resistance, charges transportation time and charges recombination time has also been calculated.

Universiti Malaya

## CHAPTER 5: CONCLUSION

GPE with DMF solvent exhibits better in conductivity compared to the GPE with DMSO solvent. The conductivity-temperature relationship of all GPEs followed Arrhenius rule. Addition of TBP into both GPE does not significantly change the value of the conductivity. TBP in GPE plays a special role for the improvement of DSSC. The additional of TBP caused an increment of 8% in the efficiency of DSSC based blackberry dye having GPE with DMF solvent. 11% increment in the efficiency was observed for DSSC based blackberry dye having GPE with DMSO solvent. In DSSC using blueberry as sensitizer, an increment of 10% in efficiency was observed for DSSC having GPE with DMF solvent (A and B) and 4.54% efficiency increment for DSSC having GPE with DMSO solvent (C and D). Similar observation can be said for the DSSC using raspberry dye as sensitizer. 37% and 33% efficiency increment of DSSC are obtained when the TBP was added into GPE A and GPE D respectively. For DSSC using saffron dye as sensitizer, the highest efficiency was observed for DSSC having GPE with DMSO solvent. The higher efficiency of DSSC having GPE with TBP can also be explained based on the charge transfer resistance calculated from impedance data. All DSSCs having GPE with TBP exhibit smaller charge transfer resistance,  $R_p$  compared to the without TBP. This indicates that faster charge transfer occurred at the photoanode/electrolyte interface thus led to improve in the DSSC efficiency. From all the data's that have been collected, the DSSCs with anthocyanin components exhibit almost similar efficiency than that saffron which from the carotenoid group but using different electrolyte system. Due to the presence of OH and COOH groups in both anthocyanin and saffron where they can chemically be adsorbed on the  $TiO_2$  surface, the excited electrons from HOMO to LUMO in dyes can easily be injected into the conduction band

of TiO<sub>2</sub>. However, DSSC using natural dyes generally still exhibits lower efficiency in comparison to the ruthenium dyes.

For the future work, some thought, and insight have been developed in this study. Based on the findings of the present work there are some knowledge that can be explored for better understanding and improved the performance of DSSC based natural sensitizers.

1. Study the shifting of the conduction band of the semiconductors with various types of additives to the GPE such as N-methylbenzimidazole (NMBI) and guanidinium thiocyanate (GuNCS).
2. Modeling and simulate the  $J-V$  characteristics of DSSCs to understand better in the charges transport properties of DSSC.
3. Study the effect of more different types of solvents in GPEs system to obtain the best performance of DSSC.

## REFERENCES

- Abdel-Latif, M. S., El-Agez, T. M., Taya S. A., Batniji, A. Y., & El-Ghamri. H. S. (2013). "Plant seeds-based dye-sensitized solar cells." *Materials Sciences and Applications*, 4 (9), 516-520.
- Abdukarimov, A., Noor, I. S. M., Mamatkarimov, O., & Arof, A. K. M. (2022). Influence of charge carrier density, mobility and diffusivity on conductivity–temperature dependence in polyethylene oxide–based gel polymer electrolytes. *High Performance Polymers*, 34(2), 232-241.
- Al-Alwani, M. A., Mohamad, A. B., Kadhum, A. A. H., Ludin, N. A., Safie, N. E., Razali, M. Z., & Sopian, K. (2017). Natural dye extracted from *Pandanus amaryllifolius* leaves as sensitizer in fabrication of dye-sensitized solar cells. *International Journal of Electrochemical Science*, 12(1), 747-761.
- Alam, M. J., & Cameron, D. C. (2002). Investigation of annealing effects on sol–gel deposited indium tin oxide thin films in different atmospheres. *Thin Solid Films*, 420, 76-82.
- Alhamed, M., Issa, A. S., & Doubal, A. W. (2012). Studying of natural dyes properties as photo-sensitizer for dye sensitized solar cells (DSSC). *Journal of Electron Devices*, 16(11), 1370-1383.
- Ammar, A. M., Mohamed, H. S., Yousef, M. M., Abdel-Hafez, G. M., Hassanien, A. S., & Khalil, A. S. (2019). Dye-sensitized solar cells (DSSCs) based on extracted natural dyes. *Journal of Nanomaterials*, 2019.
- Amogne, N. Y., Ayele, D. W., & Tsigie, Y. A. (2020). Recent advances in anthocyanin dyes extracted from plants for dye sensitized solar cell. *Materials for Renewable and Sustainable Energy*, 9(4), 1-16.
- Anandan, S., Pitchumani, S., Muthuraaman, B., & Maruthamuthu, P. (2006). Heteropolyacid-impregnated PVDF as a solid polymer electrolyte for dye-sensitized solar cells. *Solar Energy Materials and Solar Cells*, 90(12), 1715-1720.
- Antony, A., Nisha, M., Manoj, R., & Jayaraj, M. K. (2004). Influence of target to substrate spacing on the properties of ITO thin films. *Applied Surface Science*, 225(1-4), 294-301.
- Arof, A. K., Aziz, M. F., Noor, M. M., Careem, M. A., Bandara, L. R. A. K., Thotawatthage, C. A., & Dissanayake, M. A. K. L. (2014). Efficiency enhancement by mixed cation effect in dye-sensitized solar cells with a PVdF based gel polymer electrolyte. *International Journal of Hydrogen Energy*, 39(6), 2929-2935.
- Arof, A. K., Noor, I. M., Buraidah, M. H., Bandara, T. M. W. J., Careem, M. A., Albinsson, I., & Mellander, B. E. (2017). Polyacrylonitrile gel polymer electrolyte-based dye sensitized solar cells for a prototype solar panel. *Electrochimica Acta*, 251, 223-234.
- Arof, A. K., & Ping, T. L. (2017). Chlorophyll as photosensitizer in dye-sensitized solar cells. *Chlorophyll*, 7, 105-121.

- Arsyad, W. S., Wardianto, A., Variani, V. I., Ilmawati, W. S., Agus, L., & Hidayat, R. (2019, August). *A Preliminary result on the rGO functionalization as counter-electrode in dye-sensitized solar cells (DSSC)*. In *Journal of Physics: Conference Series* (Vol. 1245, No. 1, p. 012067). IOP Publishing.
- Asano, Tsuyoshi, Takaya Kubo, and Yoshinori Nishikitani. 2004. "Electrochemical properties of dye-sensitized solar cells fabricated with PVDF-type polymeric solid electrolytes." *Journal of Photochemistry and Photobiology A: Chemistry* 164 (1–3): 111–15.
- Awadhia, A., & Agrawal, S. L. (2007). Structural, thermal and electrical characterizations of PVA: DMSO: NH<sub>4</sub>SCN gel electrolytes. *Solid State Ionics*, 178(13-14), 951-958.
- Bandara, T. M., Fernando, H. D. N. S., Furlani, M., Albinsson, I., Dissanayake, M. A. K. L., & Mellander, B. E. (2016). Performance enhancers for gel polymer electrolytes based on LiI and RbI for quasi-solid-state dye sensitized solar cells. *RSC Advances*, 6(105), 103683-103691.
- Bandara, T. M. W. J., DeSilva, L. A., Ratnasekera, J. L., Hettiarachchi, K. H., Wijerathna, A. P., Thakurdesai, M., & Mellander, B. E. (2019). High efficiency dye-sensitized solar cell based on a novel gel polymer electrolyte containing RbI and tetrahexylammonium iodide (Hex<sub>4</sub>NI) salts and multi-layered photoelectrodes of TiO<sub>2</sub> nanoparticles. *Renewable and Sustainable Energy Reviews*, 103, 282-290.
- Beekwilder, J., Jonker, H., Meesters, P., Hall, R. D., van der Meer, I. M., & Ric de Vos, C. H. (2005). Antioxidants in raspberry: on-line analysis links antioxidant activity to a diversity of individual metabolites. *Journal of Agricultural and Food Chemistry*, 53(9), 3313-3320.
- Bella, F., Chiappone, A., Nair, J. R., Meligrana, G., & Gerbaldi, C. (2014). Effect of different green cellulosic matrices on the performance of polymeric dye-sensitized solar cells. *Chemical Engineering Transactions*, 41, 211-216.
- Bera, S., Sengupta, D., Roy, S., & Mukherjee, K. (2021). Research into dye-sensitized solar cells: a review highlighting progress in India. *Journal of Physics: Energy*, 3(3), Article#032013.
- Birel, Ö., Nadeem, S., & Duman, H. (2017). Porphyrin-based dye-sensitized solar cells (DSSCs): a review. *Journal of Fluorescence*, 27(3), 1075-1085.
- Bist, A., & Chatterjee, S. (2021). Review on efficiency enhancement using natural extract mediated dye-sensitized solar cell for sustainable photovoltaics. *Energy Technology*, 9(8), Article#2001058.
- Buraidah, M. H., Teo, L. P., Yong, C. A., Shah, S., & Arof, A. K. (2016). Performance of polymer electrolyte based on chitosan blended with poly (ethylene oxide) for plasmonic dye-sensitized solar cell. *Optical Materials*, 57, 202-211.
- Cardone, L., Castronuovo, D., Perniola, M., Cicco, N., & Candido, V. (2020). Saffron (*Crocus sativus* L.), the king of spices: An overview. *Scientia Horticulturae*, 272, Article#109560.

- Carp, O., Huisman, C. L., & Reller, A. (2004). Photoinduced reactivity of titanium dioxide. *Progress in Solid State Chemistry*, 32(1-2), 33-177.
- Chan, Y. F., Wang, C. C., & Chen, C. Y. (2013). Quasi-solid DSSC based on a gel-state electrolyte of PAN with 2-D graphene incorporated. *Journal of Materials Chemistry A*, 1(18), 5479-5486.
- Chang, H., Wu, H. M., Chen, T. L., Huang, K. D., Jwo, C. S., & Lo, Y. J. (2010). Dye-sensitized solar cell using natural dyes extracted from spinach and ipomoea. *Journal of Alloys and Compounds*, 495(2), 606-610.
- Chen, C. Y., Wu, S. J., Li, J. Y., Wu, C. G., Chen, J. G., & Ho, K. C. (2007). A new route to enhance the light-harvesting capability of ruthenium complexes for dye-sensitized solar cells. *Advanced Materials*, 19(22), 3888-3891.
- Chen, C. Y., Wu, S. J., Wu, C. G., Chen, J. G., & Ho, K. C. (2006). A Ruthenium complex with superhigh light-harvesting capacity for dye-sensitized solar cells. *Angewandte Chemie*, 118(35), 5954-5957.
- Cho, M. J., Howard, L. R., Prior, R. L., & Clark, J. R. (2004). Flavonoid glycosides and antioxidant capacity of various blackberry, blueberry and red grape genotypes determined by high-performance liquid chromatography/mass spectrometry. *Journal of the Science of Food and Agriculture*, 84(13), 1771-1782.
- Choo, W. S., & Yong, W. K. (2011). Antioxidant properties of two species of *Hylocereus* fruits. *Advances in Applied Science Research*, 2(3), 418-425.
- Dai, J., Patel, J. D., & Mumper, R. J. (2007). Characterization of blackberry extract and its antiproliferative and anti-inflammatory properties. *Journal of Medicinal Food*, 10(2), 258-265.
- DeSilva, L. A., Pitigala, P. K. D. D. P., Gaquere-Parker, A., Landry, R., Hasbun, J. E., Martin, V., & Perera, A. G. U. (2017). Broad absorption natural dye (Mondo-Grass berry) for dye sensitized solar cell. *Journal of Materials Science: Materials in Electronics*, 28(11), 7724-7729.
- Dewan, J., & Yadav, M. K. (2021). *Characteristics of thin film organic photovoltaic solar cells*. In AIP Conference Proceedings, 2352, 020040. AIP Publishing LLC.
- Diaconeasa, Z., Leopold, L., Rugină, D., Ayvaz, H., & Socaciu, C. (2015). Antiproliferative and antioxidant properties of anthocyanin rich extracts from blueberry and blackcurrant juice. *International Journal of Molecular Sciences*, 16(2), 2352-2365.
- Ding, W., Wei, C., Wang, S., Zou, L., Gong, Y., Liu, Y., & Zang, L. (2019). Preparation and properties of a high-performance EOEOEA-based gel-polymer-electrolyte lithium battery. *Polymers*, 11(8), Article#1296.
- Dissanayake, M. A. K. L., Thotawatthage, C. A., Senadeera, G. K. R., Bandara, T. M. W. J., Jayasundera, W. J. M. J. S. R., & Mellander, B. E. (2012). Efficiency enhancement by mixed cation effect in dye-sensitized solar cells with PAN based gel polymer electrolyte. *Journal of Photochemistry and Photobiology A: Chemistry*, 246, 29-35.

- Dissanayake, M. A. K. L., Umair, K., Senadeera, G. K. R., & Kumari, J. M. K. W. (2021). Effect of electrolyte conductivity, co-additives and mixed cation iodide salts on efficiency enhancement in dye sensitized solar cells with acetonitrile-free electrolyte. *Journal of Photochemistry and Photobiology A: Chemistry*, 415, Article#113308.
- Dumbravă, A., Georgescu, A., Damache, G., Badea, C., Enache, I., Oprea, C., & Gîrțu, M. A. (2008). Dye-sensitized solar cells based on nanocrystalline TiO<sub>2</sub> and natural pigments. *The Journal of Optoelectronics and Advanced Materials*, 10(11), 2996-3002.
- Esquivel, P., Stintzing, F. C., & Carle, R. (2007). Phenolic compound profiles and their corresponding antioxidant capacity of purple pitaya (*Hylocereus* sp.) genotypes. *Zeitschrift für Naturforschung C*, 62(9-10), 636-644.
- Freitas, S. T. D., & Mitcham, E. J. (2013). Quality of pitaya fruit (*Hylocereus undatus*) as influenced by storage temperature and packaging. *Scientia Agricola*, 70, 257-262.
- Furukawa, S., Iino, H., Iwamoto, T., Kukita, K., & Yamauchi, S. (2009). Characteristics of dye-sensitized solar cells using natural dye. *Thin Solid Films*, 518(2), 526-529.
- Ghann, W., Kang, H., Sheikh, T., Yadav, S., Chavez-Gil, T., Nesbitt, F., & Uddin, J. (2017). Fabrication, optimization and characterization of natural dye sensitized solar cell. *Scientific Reports*, 7(1), 1-12.
- Goetzberger, A., & Hebling, C. (2000). Photovoltaic materials, past, present, future. *Solar Energy Materials and Solar Cells*, 62(1-2), 1-19.
- Gupta, S. M., & Tripathi, M. (2011). A review of TiO<sub>2</sub> nanoparticles. *Chinese Science Bulletin*, 56(16), 1639-1657.
- Gusti, D. R., Mastutik, D., Lestari, I., & Rofiah, Y. W. (2021). The effect of graphite concentration in TiO<sub>2</sub> semiconductors on efficiency of dye sensitized solar cells (DSSC) using dye melastoma malabathricum L fruit extract. *Eksakta: Berkala Ilmiah Bidang MIPA* (E-ISSN: 2549-7464), 22(1), 10-17.
- Habisreutinger, S. N., Noel, N. K., Snaith, H. J., & Nicholas, R. J. (2017). Investigating the Role of 4-Tert Butylpyridine in Perovskite Solar Cells. *Advanced Energy Materials*, 7(1), 1601079.
- Hamadani, M., Safaei-Ghomi, J., Hosseinpour, M., Masoomi, R., & Jabbari, V. (2014). Uses of new natural dye photosensitizers in fabrication of high potential dye-sensitized solar cells (DSSCs). *Materials Science in Semiconductor Processing*, 27, 733-739.
- Han, C. H., Han, S. D., Gwak, J., & Khatkar, S. P. (2007). Synthesis of indium tin oxide (ITO) and fluorine-doped tin oxide (FTO) nano-powder by sol-gel combustion hybrid method. *Materials Letters*, 61(8-9), 1701-1703.
- Han, C. H., Jousseume, B., Rasclé, M. C., Toupance, T., Cachet, H., & Vivier, V. (2004). Nanocrystalline F-doped tin dioxide materials: texture, morphology and

photosensitization with a perylene-substituted organotin. *Journal of Fluorine Chemistry*, 125(8), 1247-1254.

Hassan-Beygi, S. R., Ghanbarian, D., Kianmehr, M. H., & Farahmand, M. (2010). Some physical properties of saffron crocus corm. *Cercetări Agronomice în Moldova*, 141(1), 17-29.

Hemalatha, K. V., Karthick, S. N., Raj, C. J., Hong, N. Y., Kim, S. K., & Kim, H. J. (2012). Performance of Kerria japonica and Rosa chinensis flower dyes as sensitizers for dye-sensitized solar cells. *Spectrochimica Acta Part A: Molecular and Biomolecular Spectroscopy*, 96, 305-309.

Herbach, K. M., Stintzing, F. C., & Carle, R. (2005). Identification of heat-induced degradation products from purified betanin, phyllocactin and hylocerenin by high-performance liquid chromatography/electrospray ionization mass spectrometry. *Rapid Communications in Mass Spectrometry: An International Journal Devoted to the Rapid Dissemination of Up-to-the-Minute Research in Mass Spectrometry*, 19(18), 2603-2616.

Herbach, K. M., Stintzing, F. C., Elss, S., Preston, C., Schreier, P., & Carle, R. (2006). Isotope ratio mass spectrometrical analysis of betanin and isobetanin isolates for authenticity evaluation of purple pitaya-based products. *Food Chemistry*, 99(1), 204-209.

Hoffmann, M. R., Martin, S. T., Choi, W., & Bahnemann, D. W. (1995). Environmental applications of semiconductor photocatalysis. *Chemical Reviews*, 95(1), 69-96.

Hossain, M. K., Pervez, M. F., Mia, M. N. H., Mortuza, A. A., Rahaman, M. S., Karim, M. R., & Khan, M. A. (2017). Effect of dye extracting solvents and sensitization time on photovoltaic performance of natural dye sensitized solar cells. *Results in Physics*, 7, 1516-1523.

Hosseinnezhad, M., Gharanjig, K., Moradian, S., & Saeb, M. R. (2017). In quest of power conversion efficiency in nature-inspired dye-sensitized solar cells: Individual, co-sensitized or tandem configuration?. *Energy*, 134, 864-870.

Hu, J., Zhu, F., Zhang, J., & Gong, H. (2003). A room temperature indium tin oxide/quartz crystal microbalance gas sensor for nitric oxide. *Sensors and Actuators B: Chemical*, 93(1-3), 175-180.

Hug, H., Bader, M., Mair, P., & Glatzel, T. (2014). Biophotovoltaics: natural pigments in dye-sensitized solar cells. *Applied Energy*, 115, 216-225.

Ileperuma, O. A., Kumara, G. A., Yang, H. S., & Murakami, K. (2011). Quasi-solid electrolyte based on polyacrylonitrile for dye-sensitized solar cells. *Journal of Photochemistry and Photobiology A: Chemistry*, 217(2-3), 308-312.

Ilgün, C., Sevim, A. M., Çakar, S., Özacar, M., & Gül, A. (2021). Novel Co and Zn-Phthalocyanine dyes with octa-carboxylic acid substituents for DSSCs. *Solar Energy*, 218, 169-179.

Iqbal, M. Z., Ali, S. R., & Khan, S. (2019). Progress in dye sensitized solar cell by incorporating natural photosensitizers. *Solar Energy*, 181, 490-509.

- Iqbal, T., Ara, G., Khalid, N. R., & Ijaz, M. (2020). Simple synthesis of Ag-doped CdS nanostructure material with excellent properties. *Applied Nanoscience*, *10*(1), 23-28.
- Jaafar, H., Ain, M. F., & Ahmad, Z. A. (2018). Performance of *E. conferta* and *G. atroviridis* fruit extracts as sensitizers in dye-sensitized solar cells (DSSCs). *Ionics*, *24*(3), 891-899.
- Jacob, M. M. E., & Arof, A. K. (2000). FTIR studies of DMF plasticized polyvinylidene fluoride-based polymer electrolytes. *Electrochimica Acta*, *45*(10), 1701-1706.
- Jasim, K. E. (2012). Natural dye-sensitized solar cell based on nanocrystalline TiO<sub>2</sub>. *Sains Malaysiana*, *41*(8), 1011-1016.
- Ji, J. M., Zhou, H., Eom, Y. K., Kim, C. H., & Kim, H. K. (2020). 14.2% efficiency dye-sensitized solar cells by co-sensitizing novel thieno [3, 2-b] indole-based organic dyes with a promising porphyrin sensitizer. *Advanced Energy Materials*, *10*(15), 2000124.
- Jinchu, I., Sreekala, C. O., & Sreelatha, K. S. (2014). *Dye sensitized solar cell using natural dyes as chromophores-review*. In *Materials science forum* (Vol. 771, pp. 39-51). Trans Tech Publications Ltd.
- Kanakis, C. D., Daferera, D. J., Tarantilis, P. A., & Polissiou, M. G. (2004). Qualitative determination of volatile compounds and quantitative evaluation of safranal and 4-hydroxy-2, 6, 6-trimethyl-1-cyclohexene-1-carboxaldehyde (HTCC) in Greek saffron. *Journal of Agricultural and Food Chemistry*, *52*(14), 4515-4521.
- Kanackillam, S. S., Krishnan, B., Guzman, S. S., Martinez, J. A. A., Avellaneda, D. A., & Shaji, S. (2021). Defects rich nanostructured black zinc oxide formed by nanosecond pulsed laser irradiation in liquid. *Applied Surface Science*, *567*, Article#150858.
- Kang, M. S., Kim, J. H., Kim, Y. J., Won, J., Park, N. G., & Kang, Y. S. (2005). Dye-sensitized solar cells based on composite solid polymer electrolytes. *Chemical Communications*, (7), 889-891.
- Kaume, L., Howard, L. R., & Devareddy, L. (2012). The blackberry fruit: a review on its composition and chemistry, metabolism and bioavailability, and health benefits. *Journal of Agricultural and Food Chemistry*, *60*(23), 5716-5727.
- Kim, D. W., Jeong, Y. B., Kim, S. H., Lee, D. Y., & Song, J. S. (2005). Photovoltaic performance of dye-sensitized solar cell assembled with gel polymer electrolyte. *Journal of Power Sources*, *149*, 112-116.
- Kim, J. Y., Kim, J. Y., Lee, D. K., Kim, B., Kim, H., & Ko, M. J. (2012). Importance of 4-tert-butylpyridine in electrolyte for dye-sensitized solar cells employing SnO<sub>2</sub> electrode. *The Journal of Physical Chemistry C*, *116*(43), 22759-22766.
- Kim, J. H., Kim, D. H., So, J. H., & Koo, H. J. (2021). Toward eco-friendly dye-sensitized solar cells (DSSCs): Natural dyes and aqueous electrolytes. *Energies*, *15*(1), Article#219.

- Kim, J. H., Kang, M. S., Kim, Y. J., Won, J., Park, N. G., & Kang, Y. S. (2004). Dye-sensitized nanocrystalline solar cells based on composite polymer electrolytes containing fumed silica nanoparticles. *Chemical Communications*, (14), 1662-1663.
- Koca, I., & Karadeniz, B. (2009). Antioxidant properties of blackberry and blueberry fruits grown in the Black Sea Region of Turkey. *Scientia Horticulturae*, 121(4), 447-450.
- Konovalova, T. A., Kispert, L. D., & Konovalov, V. V. (1999). Surface modification of TiO<sub>2</sub> nanoparticles with carotenoids. EPR study. *The Journal of Physical Chemistry B*, 103(22), 4672-4677.
- Kumar, R. A., Suresh, M. S., & Nagaraju, J. (2004). GaAs/Ge solar cell AC parameters under illumination. *Solar Energy*, 76(4), 417-421.
- Kumara, G. R. A., Kaneko, S., Okuya, M., Onwona-Agyeman, B., Konno, A., & Tennakone, K. (2006). Shiso leaf pigments for dye-sensitized solid-state solar cell. *Solar Energy Materials and Solar Cells*, 90(9), 1220-1226.
- Kushwaha, R., Srivastava, P., & Bahadur, L. (2013). Natural pigments from plants used as sensitizers for TiO<sub>2</sub> based dye-sensitized solar cells. *Journal of Energy*, 2013.
- Lakshmi, U. M., Raj, A., Salam, J. A., Jayakrishnan, R., Priji, S., Gangaprasad, A., ... & Biju, V. (2022). DSSC using *Wrightia tinctoria* (Roxb.) R Br.: A trail. *Materials Today: Proceedings*, 49, 1631-1636.
- Leyrer, J., Rubilar, M., Morales, E., Pavez, B., Leal, E., & Hunter, R. (2018). Factor optimization in the manufacturing process of dye-sensitized solar cells based on naturally extracted dye from a Maqui and blackberry mixture (*Aristotelia chilensis* and *Rubus glaucus*). *Journal of Electronic Materials*, 47(10), 6136-6143.
- Lim, A., Kumara, N. T. R. N., Tan, A. L., Mirza, A. H., Chandrakanthi, R. L. N., Petra, M. I., ... & Ekanayake, P. (2015). Potential natural sensitizers extracted from the skin of *Canarium odontophyllum* fruits for dye-sensitized solar cells. *Spectrochimica Acta Part A: Molecular and Biomolecular Spectroscopy*, 138, 596-602.
- Limmer, S. J., Takahashi, K., & Cao, G. (2003, November). Electrochromic and transparent conducting oxide nanorods. In *Nanomaterials and Their Optical Applications*, 5224, 25-32. SPIE.
- Lin, T. W., Lin, J. R., Tsai, S. Y., Lee, J. N., & Ting, C. C. (2007). *Absorption spectra analysis of natural dyes for applications in dye-sensitized nano solar cells*. In The 31st National Conference on Theoretical and Applied Mechanics (Vol. 96, No. 12, pp. 21-22).
- Liu, C., Ding, W., Zhou, X., Gao, J., Cheng, C., Zhao, X., & Xu, B. (2017). Efficient and stable perovskite solar cells prepared in ambient air based on surface-modified perovskite layer. *The Journal of Physical Chemistry C*, 121(12), 6546-6553.

- Lobregas, M. O. S., & Camacho, D. H. (2019). Gel polymer electrolyte system based on starch grafted with ionic liquid: Synthesis, characterization and its application in dye-sensitized solar cell. *Electrochimica Acta*, 298, 219-228.
- Luo, P., Niu, H., Zheng, G., Bai, X., Zhang, M., & Wang, W. (2009). From salmon pink to blue natural sensitizers for solar cells: *Canna indica* L., *Salvia splendens*, cowberry and *Solanum nigrum* L. *Spectrochimica Acta Part A: Molecular and Biomolecular Spectroscopy*, 74(4), 936-942.
- Mahadevi, P., & Sumathi, S. (2020). Mini review on the performance of Schiff base and their metal complexes as photosensitizers in dye-sensitized solar cells. *Synthetic Communications*, 50(15), 2237-2249.
- Manafi, P., Nazockdast, H., Karimi, M., Sadighi, M., & Magagnin, L. (2021). A study on the microstructural development of gel polymer electrolytes and different imidazolium-based ionic liquids for dye-sensitized solar cells. *Journal of Power Sources*, 481, Article#228622.
- Mashmoul, M., Azlan, A., Khaza'ai, H., Mohd Yusof, B. N., & Mohd Noor, S. (2013). Saffron: a natural potent antioxidant as a promising anti-obesity drug. *Antioxidants*, 2(4), 293-308.
- Mathew, S., Yella, A., Gao, P., Humphry-Baker, R., Curchod, B. F., Ashari-Astani, N., ... & Grätzel, M. (2014). Dye-sensitized solar cells with 13% efficiency achieved through the molecular engineering of porphyrin sensitizers. *Nature Chemistry*, 6(3), 242-247.
- Maurya, I. C., Singh, S., Gupta, A. K., Srivastava, P., & Bahadur, L. (2018). Dye-sensitized solar cells employing extracts from four *Cassia* flowers as natural sensitizers: Studies on dye ingredient effect on photovoltaic performance. *Journal of Electronic Materials*, 47(1), 225-232.
- Maurya, I. C., Singh, S., Srivastava, P., Maiti, B., & Bahadur, L. (2019). Natural dye extract from *Cassia fistula* and its application in dye-sensitized solar cell: Experimental and density functional theory studies. *Optical Materials*, 90, 273-280.
- Maurya, I. C., Srivastava, P., & Bahadur, L. (2016). Dye-sensitized solar cell using extract from petals of male flowers *Luffa cylindrica* L. as a natural sensitizer. *Optical Materials*, 52, 150-156.
- Mbaba, M., Golding, T. M., & Smith, G. S. (2020). Recent advances in the biological investigation of organometallic platinum-group metal (Ir, Ru, Rh, Os, Pd, Pt) complexes as antimalarial agents. *Molecules*, 25(22), 5276.
- Mehmood, U., Ahmad, S. H. A., Al-Ahmed, A., Hakeem, A. S., Dafalla, H., & Laref, A. (2020). Synthesis and characterization of cerium oxide impregnated titanium oxide photoanodes for efficient dye-sensitized solar cells. *IEEE Journal of Photovoltaics*, 10(5), 1365-1370.
- Mehmood, U., Rahman, S. U., Harrabi, K., Hussein, I. A., & Reddy, B. V. S. (2014). Recent advances in dye sensitized solar cells. *Advances in Materials Science and Engineering*, 2014.

- Miao, L., Song, Z., Zhu, D., Li, L., Gan, L., & Liu, M. (2021). Ionic liquids for supercapacitive energy storage: a mini-review. *Energy & Fuels*, 35(10), 8443-8455.
- Middleton, E., Kandaswami, C., & Theoharides, T. C. (2000). The effects of plant flavonoids on mammalian cells: implications for inflammation, heart disease, and cancer. *Pharmacological Reviews*, 52(4), 673-751.
- Miles, T. D., & Schilder, A. C. (2013). Host defences associated with fruit infection by *Colletotrichum* species with an emphasis on anthracnose of blueberries. *Plant Health Progress*, 14(1), Article# 30.
- Mohamed, B. B., Sulaiman, A. A., & Dahab, A. A. (2012). Roselle (*Hibiscus sabdariffa* L.) in Sudan, cultivation and their uses. *Bulletin of Environment, Pharmacology and Life Sciences*, 1(6), 48-54.
- Mohammed, M. K. (2020). 21.4% efficiency of perovskite solar cells using BMImI additive in the lead iodide precursor based on carbon nanotubes/TiO<sub>2</sub> electron transfer layer. *Ceramics International*, 46(17), 27647-27654.
- Moharam, M. M., El Shazly, A. N., Anand, K. V., Rayan, D. E., Mohammed, M. K., Rashad, M. M., & Shalan, A. E. (2021). Semiconductors as effective electrodes for dye sensitized solar cell applications. *Topics in Current Chemistry*, 379(3), 1-17.
- Mozaffari, S. A., Ranjbar, M., Kouhestanian, E., Amoli, H. S., & Armanmehr, M. H. (2015). An investigation on the effect of electrodeposited nanostructured ZnO on the electron transfer process efficiency of TiO<sub>2</sub> based DSSC. *Materials Science in Semiconductor Processing*, 40, 285-292.
- Mrinalini, M., Islavath, N., Prasanthkumar, S., & Giribabu, L. (2019). Stipulating low production cost solar cells all set to retail...!. *The Chemical Record*, 19(2-3), 661-674.
- Muin, M. A. A., Zakaria, N. S., & Zaini, S. N. A. (2022). Optimization of thin polystyrene waste embedded multiwall carbon nanotubes (MWCNT) film for solid electrolyte of flexible dye-sensitized solar cell (DSSC). *Materials Today: Proceedings*.
- Mulati, D. M., Timonah, N. S., & Bjorn, W. (2012). The absorption spectra of natural dyes and their suitability as a sensitizer in organic solar cell application. *Journal of Agriculture, Science and Technology*, 14(1), 45-61.
- Muna Muzahim Abbas, M. R. (2020). Solid state reaction synthesis and characterization of aluminum doped titanium dioxide nanomaterials. *Journal of Southwest Jiaotong University*, 55(2).
- Nastasi, B., Markovska, N., Puksec, T., Duić, N., & Foley, A. (2022). Renewable and sustainable energy challenges to face for the achievement of sustainable development goals. *Renewable and Sustainable Energy Reviews*, 157, Article#112071.
- Nazeeruddin, M. K., Bessho, T., Cevey, L., Ito, S., Klein, C., De Angelis, F., ... & Grätzel, M. (2007). A high molar extinction coefficient charge transfer sensitizer and its

application in dye-sensitized solar cell. *Journal of Photochemistry and Photobiology A: Chemistry*, 185(2-3), 331-337.

- Nazeeruddin, M. K., De Angelis, F., Fantacci, S., Selloni, A., Viscardi, G., Liska, P., ... & Grätzel, M. (2005). Combined experimental and DFT-TDDFT computational study of photoelectrochemical cell ruthenium sensitizers. *Journal of the American Chemical Society*, 127(48), 16835-16847.
- Nguyen, P. T., & Do Nguyen, N. P. (2018). 4, 4'-dinonyl-2, 2'-bipyridine as an alternative electrolyte additive for improving the thermal stability of ruthenium dyes in dye-sensitized solar cells. *Journal of Physics and Chemistry of Solids*, 122, 234-238.
- Nguyen, T. T., Patel, M., Kim, S., Mir, R. A., Yi, J., Dao, V. A., & Kim, J. (2021). Transparent photovoltaic cells and self-powered photodetectors by TiO<sub>2</sub>/NiO heterojunction. *Journal of Power Sources*, 481, Article#228865.
- Ning, Z., Fu, Y., & Tian, H. (2010). Improvement of dye-sensitized solar cells: what we know and what we need to know. *Energy & Environmental Science*, 3(9), 1170-1181.
- Nkele, A. C., Chime, U. K., Asogwa, L., Nwanya, A. C., Nwankwo, U., Ukoba, K., ... & Ezema, F. I. (2020). A study on titanium dioxide nanoparticles synthesized from titanium isopropoxide under SILAR-induced gel method: transition from anatase to rutile structure. *Inorganic Chemistry Communications*, 112, Article#107705.
- Noor, M. M., Buraidah, M. H., Careem, M. A., Majid, S. R., & Arof, A. K. (2014). An optimized poly (vinylidene fluoride-hexafluoropropylene)-NaI gel polymer electrolyte and its application in natural dye sensitized solar cells. *Electrochimica Acta*, 121, 159-167.
- Nurliyana, R., Syed Zahir, I., Mustapha Suleiman, K., Aisyah, M. R., & Kamarul Rahim, K. (2010). Antioxidant study of pulps and peels of dragon fruits: a comparative study. *International Food Research Journal*, 17(2).
- O'regan, B., & Grätzel, M. (1991). A low-cost, high-efficiency solar cell based on dye-sensitized colloidal TiO<sub>2</sub> films. *Nature*, 353(6346), 737-740.
- O'Regan, B., and Grätzel M. (2018). "A low-cost, high-efficiency solar cell based on dye-sensitized colloidal TiO<sub>2</sub> films." *In Renewable Energy*, 208-13. Routledge.
- Pan, Z. W., Dai, Z. R., & Wang, Z. L. (2001). Nanobelts of semiconducting oxides. *Science*, 291(5510), 1947-1949.
- Park, J., Lee, P., & Ko, M. J. (2019). Design and fabrication of long-term stable dye-sensitized solar cells: Effect of water contents in electrolytes on the performance. *International Journal of Precision Engineering and Manufacturing-Green Technology*, 6(1), 125-131.
- Patel, N. G., Patel, P. D., & Vaishnav, V. S. (2003). Indium tin oxide (ITO) thin film gas sensor for detection of methanol at room temperature. *Sensors and Actuators B: Chemical*, 96(1-2), 180-189.

- Patrocínio, A. O. D. T., Mizoguchi, S. K., Paterno, L. G., Garcia, C. G., & Iha, N. M. (2009). Efficient and low-cost devices for solar energy conversion: Efficiency and stability of some natural-dye-sensitized solar cells. *Synthetic Metals*, *159*(21-22), 2342-2344.
- Patrocínio, A. O. D. T., Paterno, L. G., & Iha, N. M. (2010). Role of polyelectrolyte for layer-by-layer compact TiO<sub>2</sub> films in efficiency enhanced dye-sensitized solar cells. *The Journal of Physical Chemistry C*, *114*(41), 17954-17959.
- Perrin, A., Myers, D., Fucke, K., Musa, O. M., & Steed, J. W. (2014). N-Alkyl pyrrolidone ether podands as versatile alkali metal ion chelants. *Dalton Transactions*, *43*(8), 3153-3161.
- Pirashanthan, A., Thanihaichelvan, M., Mariappan, K., Velauthapillai, D., Ravirajan, P., & Shivatharsiny, Y. (2021). Synthesis of a carboxylic acid-based ruthenium sensitizer and its applicability towards Dye-Sensitized Solar Cells. *Solar Energy*, *225*, 399-406.
- Polo, A. S., & Iha, N. Y. M. (2006). Blue sensitizers for solar cells: natural dyes from Calafate and Jaboticaba. *Solar Energy Materials and Solar Cells*, *90*(13), 1936-1944.
- Prima, E. C., Hidayat, N. N., Yulianto, B., & Dipojono, H. K. (2017). A combined spectroscopic and TDDFT study of natural dyes extracted from fruit peels of *Citrus reticulata* and *Musa acuminata* for dye-sensitized solar cells. *Spectrochimica Acta Part A: Molecular and Biomolecular Spectroscopy*, *171*, 112-125.
- Ramamoorthy, R., Radha, N., Maheswari, G., Anandan, S., Manoharan, S., & Victor Williams, R. (2016). Betalain and anthocyanin dye-sensitized solar cells. *Journal of Applied Electrochemistry*, *46*(9), 929-941.
- Rebecca, O. P. S., Boyce, A. N., & Chandran, S. (2010). Pigment identification and antioxidant properties of red dragon fruit (*Hylocereus polyrhizus*). *African Journal of Biotechnology*, *9*(10), 1450-1454.
- Rho, W. Y., Jeon, H., Kim, H. S., Chung, W. J., Suh, J. S., & Jun, B. H. (2015). Recent progress in dye-sensitized solar cells for improving efficiency: TiO<sub>2</sub> nanotube arrays in active layer. *Journal of Nanomaterials*, 2015.
- Richhariya, G., Kumar, A., Tekasakul, P., & Gupta, B. (2017). Natural dyes for dye sensitized solar cell: A review. *Renewable and Sustainable Energy Reviews*, *69*, 705-718.
- Ruhane, T. A., Islam, M. T., Rahaman, M. S., Bhuiyan, M. M. H., Islam, J. M., Newaz, M. K., ... & Khan, M. A. (2017). Photo current enhancement of natural dye sensitized solar cell by optimizing dye extraction and its loading period. *Optik*, *149*, 174-183.
- Ruzainah, A. J., Ahmad, R., Nor, Z., & Vasudevan, R. (2009). Proximate analysis of dragon fruit (*Hylocereus polyrhizus*). *American Journal of Applied Sciences*, *6*(7), 1341-1346.

- Saidi, N. M., Farhana, N. K., Ramesh, S., & Ramesh, K. (2021). Influence of different concentrations of 4-tert-butyl-pyridine in a gel polymer electrolyte towards improved performance of Dye-Sensitized Solar Cells (DSSC). *Solar Energy*, 216, 111-119.
- Saikia, D., Han, C. C., & Chen-Yang, Y. W. (2008). Influence of polymer concentration and dyes on photovoltaic performance of dye-sensitized solar cell with P (VdF-HFP)-based gel polymer electrolyte. *Journal of Power Sources*, 185(1), 570-576.
- Sánchez, A. M., Carmona, M., Zalacain, A., Carot, J. M., Jabaloyes, J. M., & Alonso, G. L. (2008). Rapid determination of crocetin esters and picrocrocin from saffron spice (*Crocus sativus* L.) using UV-visible spectrophotometry for quality control. *Journal of Agricultural and Food Chemistry*, 56(9), 3167-3175.
- Sanda, M. D., Badu, M., Awudza, J., & Boadi, N. (2021). Development of TiO<sub>2</sub>-based dye-sensitized solar cells using natural dyes extracted from some plant-based materials. *Chemistry International*, 7(1), 9-20.
- Sangiorgi, N., Bondoni, R., Sangiorgi, A., Aversa, L., Tatti, R., Verucchi, R., ... & Sanson, A. (2021). Titanium-doped hydroxyapatites photoanodes for dye-sensitized solar cells. *Ceramics International*, 47(7), 9701-9710.
- Sanjay, P., Deepa, K., Madhavan, J., & Senthil, S. (2018). Optical, spectral and photovoltaic characterization of natural dyes extracted from leaves of *Peltophorum pterocarpum* and *Acalypha amentacea* used as sensitizers for ZnO based dye sensitized solar cells. *Optical Materials*, 83, 192-199.
- Sarkar, A., Bera, S., & Chakraborty, A. K. (2020). CoNi<sub>2</sub>S<sub>4</sub>-reduced graphene oxide nanohybrid: An excellent counter electrode for Pt-free DSSC. *Solar Energy*, 208, 139-149.
- Sathyajothi, S., Jayavel, R., & Dhanemozhi, A. C. (2017). The fabrication of natural dye sensitized solar cell (Dssc) based on TiO<sub>2</sub> using henna and beetroot dye extracts. *Materials Today: Proceedings*, 4(2), 668-676.
- Scalzo, R., Todaro, A., & Rapisarda, P. (2012). Methods used to evaluate the peroxy (ROO<sup>•</sup>) radical scavenging capacities of four common antioxidants. *European Food Research and Technology*, 235(6), 1141-1148.
- Schwarz, M., Hillebrand, S., Habben, S., Degenhardt, A., & Winterhalter, P. (2003). Application of high-speed countercurrent chromatography to the large-scale isolation of anthocyanins. *Biochemical Engineering Journal*, 14(3), 179-189.
- Sclafani, A., Palmisano, L., & Schiavello, M. (1990). Influence of the preparation methods of titanium dioxide on the photocatalytic degradation of phenol in aqueous dispersion. *Journal of Physical Chemistry*, 94(2), 829-832.
- Selvanathan, V., Yahya, R., Alharbi, H. F., Alharthi, N. H., Alharthi, Y. S., Ruslan, M. H., ... & Akhtaruzzaman, M. (2020). Organosoluble starch derivative as quasi-solid electrolytes in DSSC: Unravelling the synergy between electrolyte rheology and photovoltaic properties. *Solar Energy*, 197, 144-153.

- Selvaraj, B., Shanmugam, G., Kamaraj, S., Gunasekeran, A., & Sambandam, A. (2021). Effect of 1-substituted 2-(Pyridin-2-yl)-1 H-benzo [d] imidazole ligand-coordinated copper and cobalt complex redox electrolytes on performance of Ru (II) dye-based dye-sensitized solar cells. *Inorganic Chemistry*, 60(3), 1937-1947.
- Semalti, P., & Sharma, S. N. (2020). Dye sensitized solar cells (DSSCs) electrolytes and natural photo-sensitizers: a review. *Journal of Nanoscience and Nanotechnology*, 20(6), 3647-3658.
- Senthil, T. S., Muthukumarasamy, N., Velauthapillai, D., Agilan, S., Thambidurai, M., & Balasundaraprabhu, R. (2011). Natural dye (cyanidin 3-O-glucoside) sensitized nanocrystalline TiO<sub>2</sub> solar cell fabricated using liquid electrolyte/quasi-solid-state polymer electrolyte. *Renewable Energy*, 36(9), 2484-2488.
- Shalini, S., Prasanna, S., Mallick, T. K., & Senthilarasu, S. (2015). Review on natural dye sensitized solar cells: Operation, materials and methods. *Renewable and Sustainable Energy Reviews*, 51, 1306-1325.
- Shamsuddin, L., Noor, I. M., Albinsson, I., Mellander, B. E., & Arof, A. K. (2017). Perovskite solar cells using polymer electrolytes. *Molecular Crystals and Liquid Crystals*, 655(1), 181-194.
- Sharma, G D, P Suresh, and John A Mikroyannidis. 2010. "Quasi solid state dye-sensitized solar cells with modified TiO<sub>2</sub> photoelectrodes and triphenylamine-based dye." *Electrochimica Acta* 55 (7): 2368–72.
- Sharma, K., Sharma, V., & Sharma, S. S. (2018). Dye-sensitized solar cells: Fundamentals and current status. *Nanoscale Research Letters*, 13(1), 1-46.
- Sharmoukh, W., Cong, J., Gao, J., Liu, P., Daniel, Q., & Kloo, L. (2018). Molecular engineering of D–D– $\pi$ –A-based organic sensitizers for enhanced dye-sensitized solar cell performance. *ACS Omega*, 3(4), 3819-3829.
- Shcherbakov, V. V., Artemkina, Y. M., Akimova, I. A., & Artemkina, I. M. (2021). Dielectric characteristics, electrical conductivity and solvation of ions in electrolyte solutions. *Materials*, 14(19), Article#5617.
- Shi, Y., Wang, X., Zhang, H., Li, B., Lu, H., Ma, T., & Hao, C. (2015). Effects of 4-tert-butylpyridine on perovskite formation and performance of solution-processed perovskite solar cells. *Journal of Materials Chemistry A*, 3(44), 22191-22198.
- Shi, Y., Zhu, C., Wang, L., Zhao, C., Li, W., Fung, K. K., ... & Wang, N. (2013). Ultrarapid sonochemical synthesis of ZnO hierarchical structures: from fundamental research to high efficiencies up to 6.42% for quasi-solid dye-sensitized solar cells. *Chemistry of Materials*, 25(6), 1000-1012.
- Silva, L., Sánchez, M., & Freeman, H. S. (2020). New tetrazole based dyes as efficient co-sensitizers for DSSCs: Structure-properties relationship. *Organic Electronics*, 87, Article#105964.
- Singh, P. K., Bhattacharya, B., & Khan, Z. H. (2018). Environment approachable dye sensitized solar cell using abundant natural pigment-based dyes with solid polymer electrolyte. *Optik*, 165, 186-194.

- Singh, P. K., Singh, R., Singh, V., Bhattacharya, B., & Khan, Z. H. (2018). New class of lead-free perovskite material for low-cost solar cell application. *Materials Research Bulletin*, 97, 572-577.
- Singh, R., Polu, A. R., Bhattacharya, B., Rhee, H. W., Varlikli, C., & Singh, P. K. (2016). Perspectives for solid biopolymer electrolytes in dye sensitized solar cell and battery application. *Renewable and Sustainable Energy Reviews*, 65, 1098-1117
- Singh, S., Singh, P. K., Kakroo, S., Hachim, D. M., Dhapola, P. S., & Khan, Z. H. (2021). Eco-friendly dye sensitized solar cell using natural dye with solid polymer electrolyte as hole transport material. *Materials Today: Proceedings*, 34, 760-766.
- Sinopoli, A., Calogero, G., & Bartolotta, A. (2019). Computational aspects of anthocyanidins and anthocyanins: A review. *Food Chemistry*, 297, 124898.
- Sirimanne, P. M., Senevirathna, M. K. I., Premalal, E. V. A., Pitigala, P. K. D. D. P., Sivakumar, V., & Tennakone, K. (2006). Utilization of natural pigment extracted from pomegranate fruits as sensitizer in solid-state solar cells. *Journal of Photochemistry and Photobiology A: Chemistry*, 177(2-3), 324-327.
- Sokolský, M., & Cirák, J. (2010). Dye-sensitized solar cells: materials and processes. *Acta Electrotechnica et Informatica*, 10(3), 78-81.
- Sonker, R. K., & Sabhajeet, S. R. (2018). ZnO nanoneedle structure-based dye-sensitized solar cell utilizing solid polymer electrolyte. *Materials Letters*, 223, 133-136.
- Strik, B. C. (2007). *Berry crops: Worldwide area and production systems*. Berry fruit value added products for health promotion, 1, 3-49.
- Su'Ait, M. S., Ahmad, A., Badri, K. H., Mohamed, N. S., Rahman, M. Y. A., Ricardo, C. A., & Scardi, P. (2014). The potential of polyurethane bio-based solid polymer electrolyte for photoelectrochemical cell application. *International Journal of Hydrogen Energy*, 39(6), 3005-3017.
- Suhaimi, S., Shahimin, M. M., Alahmed, Z. A., Chyský, J., & Reshak, A. H. (2015). Materials for enhanced dye-sensitized solar cell performance: Electrochemical application. *International Journal of Electrochemical Science*, 10(4), 2859-2871.
- Sun, W., Han, Y., Li, Z., Ge, K., & Zhang, J. (2016). Bone-targeted mesoporous silica nanocarrier anchored by zoledronate for cancer bone metastasis. *Langmuir*, 32(36), 9237-9244.
- Supriyanto, A., Nurosyid, F., & Ahliha, A. H. (2018, November). *Carotenoid pigment as sensitizers for applications of dye-sensitized solar cell (DSSC)*. In IOP Conference Series: Materials Science and Engineering (Vol. 432, No. 1, p. 012060). IOP Publishing.
- Supriyanto, E., Alviati, N., Kartikasari, H. A., Rohman, L., & Triyana, K. (2019, April). *Simulation of electron diffusion coefficient interpretation on the optimum thickness of TiO<sub>2</sub> photoanode in dye-sensitized solar cell (DSSC)*. In IOP Conference Series: Materials Science and Engineering (Vol. 515, No. 1, p. 012058). IOP Publishing.

- Suzuka, M., Hayashi, N., Sekiguchi, T., Sumioka, K., Takata, M., Hayo, N., ... & Nishide, H. (2016). A quasi-solid state DSSC with 10.1% efficiency through molecular design of the charge-separation and-transport. *Scientific Reports*, 6(1), 1-7.
- Syafinar, R., Gomesh, N., Irwanto, M., Fareq, M., & Irwan, Y. M. (2015). Cocktail dyes from blueberry and dragon fruit in the application for DSSC. *ARPJ Journal of Engineering and Applied Sciences*, 10(15), 6348-6353.
- Syairah, A., Khanmirzaei, M. H., Saidi, N. M., Farhana, N. K., Ramesh, S., & Ramesh, K. (2019). Effect of different imidazolium-based ionic liquids on gel polymer electrolytes for dye-sensitized solar cells. *Ionics*, 25(5), 2427-2435.
- Tang, H., Prasad, K., Sanjines, R., Schmid, P. E., & Levy, F. (1994). Electrical and optical properties of TiO<sub>2</sub> anatase thin films. *Journal of Applied Physics*, 75(4), 2042-2047.
- Tashakkori, F., Mohammadi Torkashvand, A., Ahmadi, A., & Esfandiari, M. (2021). Prediction of saffron yield based on soil properties using regression and artificial neural networks models in the vamenan region of golestan province. *Saffron Agronomy and Technology*, 9(2), 159-175.
- Taya, S. A., El-Agez, T. M., El-Ghamri, H. S., & Abdel-Latif, M. S. (2013). Dye-sensitized solar cells using fresh and dried natural dyes. *International Journal of Materials Science and Applications*, 2(2), 37-42.
- Taya, S. A., El-Ghamri, H. S., El-Agez, T. M., Abdel-Latif, M. S., & Batniji, A. (2015). Three fresh plant seeds as natural dye sensitizers for titanium dioxide-based dye sensitized solar cells. *British Journal of Applied Science & Technology*, 5, 380-386.
- Thambidurai, M., Muthukumarasamy, N., Velauthapillai, D., Sabari Arul, N., Agilan, S., & Balasundaraprabhu, R. (2011). Dye-sensitized ZnO nanorod based photoelectrochemical solar cells with natural dyes extracted from *Ixora coccinea*, Mulberry and Beetroot. *Journal of Materials Science: Materials in Electronics*, 22(11), 1662-1666.
- Tumen-Ulzii, G., Auffray, M., Matsushima, T., & Adachi, C. (2021). Unintentional passivation of 4-tertbutyl pyridine for improved efficiency and decreased operational stability of perovskite solar cells. *Applied Physics Letters*, 118(24), 241603.
- Ulucak, R., & Khan, S. U. D. (2020). Determinants of the ecological footprint: role of renewable energy, natural resources, and urbanization. *Sustainable Cities and Society*, 54, Article#101996.
- Vishveshvar, K., Krishnan, A., Haribabu, K., & Vishnuprasad, S. (2018). Green synthesis of copper oxide nanoparticles using *Ixora coccinea* plant leaves and its characterization. *BioNanoScience*, 8(2), 554-558.
- Vorontsov, A. V., Kabachkov, E. N., Balikhin, I. L., Kurkin, E. N., Troitskii, V. N., & Smirnotis, P. G. (2018). Correlation of surface area with photocatalytic activity of TiO<sub>2</sub>. *Journal of Advanced Oxidation Technologies*, 21(1), 127-137.

- Wang, C., Li, X., Wu, Y., & Tan, S. (2019). An efficient and thermally stable dye-sensitized solar cell based on a lamellar nanostructured thiolate/disulfide liquid crystal electrolyte and carbon/PEDOT composite nanoparticle electrode. *RSC Advances*, *9*(61), 35924-35930.
- Wang, P., Zakeeruddin, S. M., Moser, J. E., Humphry-Baker, R., Comte, P., Aranyos, V., ... & Grätzel, M. (2004). Stable new sensitizer with improved light harvesting for nanocrystalline dye-sensitized solar cells. *Advanced Materials*, *16*(20), 1806-1811.
- Wendel, M., Kumorkiewicz, A., Wybraniec, S., Ziółek, M., & Burdziński, G. (2017). Impact of S1→S0 internal conversion in betalain-based dye sensitized solar cells. *Dyes and Pigments*, *141*, 306-315.
- Wongcharee, K., Meeyoo, V., & Chavadej, S. (2007). Dye-sensitized solar cell using natural dyes extracted from rosella and blue pea flowers. *Solar Energy Materials and Solar Cells*, *91*(7), 566-571.
- Wu, K., Zhao, Q., Chen, L., Liu, Z., Ruan, B., & Wu, M. (2019). Effect of transition-metal ion doping on electrocatalytic activities of graphene/polyaniline-M<sup>2+</sup> (Mn<sup>2+</sup>, Co<sup>2+</sup>, Ni<sup>2+</sup>, and Cu<sup>2+</sup>) composite materials as Pt-Free counter electrode in dye-sensitized solar cells. *Polymer-Plastics Technology and Materials*, *58*(1), 40-46.
- Wu, Y. H., Shi, X. Q., Ding, X. H., Ren, Y. K., Hayat, T., Alsaedi, A., ... & Dai, S. Y. (2018). Incorporating 4-tert-butylpyridine in an antisolvent: a facile approach to obtain highly efficient and stable perovskite solar cells. *ACS Applied Materials & Interfaces*, *10*(4), 3602-3608.
- Wunderlich, W., Oekermann, T., Miao, L., Hue, N. T., Tanemura, S., & Tanemura, M. (2004). Electronic properties of nano-porous TiO<sub>2</sub>- and ZnO thin films-comparison of simulations and experiments. *Journal of Ceramic Processing & Research*, *5*(4), 343-354.
- Wybraniec, S., Stalica, P., Jerz, G., Klose, B., Gebers, N., Winterhalter, P., ... & Mizrahi, Y. (2009). Separation of polar betalain pigments from cacti fruits of *Hylocereus polyrhizus* by ion-pair high-speed counter current chromatography. *Journal of Chromatography A*, *1216*(41), 6890-6899.
- Xie, X., Zhu, D., Zhang, W., Huai, W., Wang, K., Huang, X., ... & Fan, H. (2017). Microwave-assisted aqueous two-phase extraction coupled with high performance liquid chromatography for simultaneous extraction and determination of four flavonoids in *Crotalaria sessiliflora* L. *Industrial Crops and Products*, *95*, 632-642.
- Xu, H. R., Zhou, H., Zhu, G., Chen, J., & Liao, C. (2006). Synthesis of tin-doped indium oxide nanoparticles by an ion-exchange and hydrothermal process. *Materials Letters*, *60*(7), 983-985.
- Yamazaki, E., Murayama, M., Nishikawa, N., Hashimoto, N., Shoyama, M., & Kurita, O. (2007). Utilization of natural carotenoids as photosensitizers for dye-sensitized solar cells. *Solar Energy*, *81*(4), 512-516.

- Yang, C., He, G., He, Y., & Ma, P. (2008). Densities and viscosities of N, N-dimethylformamide+ N-methyl-2-pyrrolidinone and+ dimethyl sulfoxide in the temperature range (303.15 to 353.15) K. *Journal of Chemical & Engineering Data*, 53(7), 1639-1642.
- Yen, Y. S., Chen, Y. C., Hsu, Y. C., Chou, H. H., Lin, J. T., & Yin, D. J. (2011). Heteroleptic ruthenium sensitizers that contain an ancillary bipyridine ligand tethered with hydrocarbon chains for efficient dye-sensitized solar cells. *Chemistry—A European Journal*, 17(24), 6781-6788.
- Yu, Z., Vlachopoulos, N., Gorlov, M., & Kloo, L. (2011). Liquid electrolytes for dye-sensitized solar cells. *Dalton Transactions*, 40(40), 10289-10303.
- Yusuf, S. N. F., Azzahari, A. D., Yahya, R., Majid, S. R., Careem, M. A., & Arof, A. K. (2016). From crab shell to solar cell: A gel polymer electrolyte based on N-phthaloylchitosan and its application in dye-sensitized solar cells. *RSC Advances*, 6(33), 27714-27724.
- Zareena, A. V., Variyar, P. S., Gholap, A. S., & Bongirwar, D. R. (2001). Chemical investigation of gamma-irradiated saffron (*Crocus sativus* L.). *Journal of Agricultural and Food Chemistry*, 49(2), 687-691.
- Zdyb, A., & Krawczyk, S. (2019). Natural flavonoids as potential photosensitizers for dye-sensitized solar cells. *Ecological Chemistry and Engineering*, 26(1), 29-36.
- Zeng, K., Tong, Z., Ma, L., Zhu, W. H., Wu, W., & Xie, Y. (2020). Molecular engineering strategies for fabricating efficient porphyrin-based dye-sensitized solar cells. *Energy & Environmental Science*, 13(6), 1617-1657.
- Zhang, Q., Gao, L., & Guo, J. (2000). Effects of calcination on the photocatalytic properties of nanosized TiO<sub>2</sub> powders prepared by TiCl<sub>4</sub> hydrolysis. *Applied Catalysis B: Environmental*, 26(3), 207-215.
- Zhang, X., Wang, C. X., Li, F. Y., & Xia, Y. Y. (2008). A quasi-solid-state dye-sensitized solar cell based on porous polymer electrolyte membrane. *Journal of Photochemistry and Photobiology A: Chemistry*, 194(1), 31-36.